Emergent Quantum Mechanics

A student's guide

Robert Brady

Ross Anderson

DRAFT for feedback
Version: March 10, 2014

Preface

This monograph is a student's introduction to two experimental systems – droplets of oil bouncing on the vibrating surface of the same liquid, and resonances in superfluids – whose equations of motion are analogous to the established equations of relativistic quantum mechanics. In fact, they share the same equations, with the speed c in the experiments being the speed of sound or surface waves instead of light. Such experiments are at the heart of two new fields of study: emergent quantum mechanics, often shortened to 'EMQM,' and analogue gravity.

Here we explain in simple terms why bouncing droplets exhibit the symmetries of special relativity; they experience an inverse square force of attraction or repulsion which obeys Maxwell's equations; their wave fields obey the same equations as in quantum mechanics; and two droplets orbiting around one another exhibit spin-half symmetry. This two-dimensional system has a three-dimensional version: resonances in superfluid helium, called rotons, which can be understood using a natural extension of the equations that emerge in the droplet experiments. The field of analogue gravity is founded on the observation that resonances in a superfluid have the symmetries of general relativity.

These experimental systems can help understand the natural phenomena which they mimic. Repeatedly in historical times, hydrodynamic models were advanced for electrodynamic, relativistic and then quantum mechanical phenomena. They all amounted to pulsating or oscillating structures in a fluid. They were not pursued because transverse waves, which seemed to be needed to mimic light waves, were wrongly assumed to be impossible in a fluid. Transverse waves had not yet been observed in superfluids.

This approach differs from string theory and loop quantum gravity in that it makes definite predictions in the analogue acoustic systems, which can be tested experimentally. It has the advantage that the mathematics is accessible to undergraduates.

The material is aimed at mathematicians, physicists, chemists and engineers. Each chapter covers a topic at a level that should be accessible to undergraduates. The exercises and dialogues are an integral part, and should be read even if you don't do them. There is also 'Track 2' material which is aimed at graduate students and the more ambitious undergraduates.

Robert Brady, Ross Anderson
Cambridge, March 2014

About the authors

Robert Brady is a research fellow at Cambridge University Computer Laboratory. In his PhD he predicted the gyroscopic effect in charged quantum systems and demonstrated it experimentally in superconductors. He founded a company that develops software to model risk and was a fellow at Trinity College Cambridge. His research includes scale-free systems and thermodynamic models of software dependability.

Ross Anderson is Professor of Security Engineering at Cambridge University Computer Laboratory. He is a Fellow of the Royal Society, the Royal Academy of Engineering and the Institute of Physics. He has made contributions to a number of fields including cryptography, semiconductor testing, the economics of dependability and the analysis of authentication protocols.

Acknowledgements: We are very grateful to Yves Couder, Emmanuel Fort and Antonin Eddi not just for discussions but for access to their raw data on bouncing droplets and permission to use it here. We are also grateful to Robin Ball, Michael Berry, John Bush, Graziano Brady, Basil Hiley, Keith Moffatt, Valeriy Sbitnev and to seminar participants at Warwick and Cambridge for comments, criticism and feedback.

Contents

Chapter 1

Periodic fluid motion

[water waves] that are easily seen by everyone and which are usually used as an example of waves in elementary courses ... are the worst possible example ... they have all the complications that waves can have

Richard Feynman

This chapter introduces the elementary equations of periodic fluid motion which are required to understand the experiments in the later chapters.

Figure 1.1: *North Pacific storm waves. (Courtesy National Oceanic and Atmospheric Administration)*

One of the experimental systems, a droplet of oil bouncing on the surface of the same liquid, is largely unaffected by viscosity because the droplet always rides on a cushion of air, and the other, superfluid ^{4}helium, has no viscosity at all, and so it is not necessary for us to include viscosity in the equations.

1.1 Euler's equation

The equation of motion for a fluid without viscosity was first published in 1757 by Leonhard Euler, a Swiss mathematician.

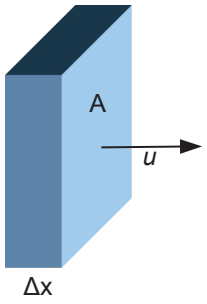

Figure 1.2: *A fluid element discussed in the text*

Consider a fluid element of thickness Δx and area A, as shown in figure 1.2. If the pressure P varies in the x direction, the pressure on the two surfaces will differ by $\Delta x\, \partial P/\partial x$ and the net force on the element will be $F = -A\Delta x\, \partial P/\partial x$. The mass of the element is $m = \rho A \Delta x$, where ρ is the density, and so from Newton's second law the element must accelerate at $a = F/m$, or

$$\left.\frac{du}{dt}\right|_{x=ut} = -\frac{1}{\rho}\frac{\partial P}{\partial x}$$

The left hand side is the acceleration which would be measured by a probe that moves with the element, often written in the shorter notation Du/Dt. Extended to three dimensions, this is Euler's equation

$$\frac{D\mathbf{u}}{Dt} = -\frac{1}{\rho}\nabla P \tag{1.1}$$

where $\mathbf{u}$ means the vector (u_x, u_y, u_z) and ∇ means $(\partial/\partial x, \partial/\partial y, \partial/\partial z)$.

In general, we will study the solutions to Euler's equation in a **barotropic** fluid, whose density is a function only of the pressure, $\rho = \rho(P)$.

1.2 Circulation

Figure 1.3 illustrates a liquid flowing past a boundary. The flow is parallel to the boundary and its speed increases with distance from it.

If you were to walk anticlockwise around the dotted line shown in the figure, you would always be facing the flow or walking perpendicular to it. You would never be facing away from it since the flow speed vanishes very close to the boundary. To quantify this asymmetry, we define the **circulation** by

$$\Gamma = \frac{1}{2\pi}\oint \mathbf{u}.d\mathbf{l} \tag{1.2}$$

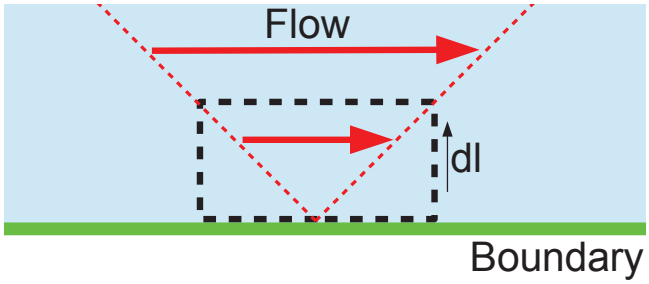

Figure 1.3: *Steady shear flow near a boundary. The dotted line shows a path of integration* $d\mathbf{l}$.

where $d\mathbf{l}$ is a closed path wholly immersed in the fluid.

If the circulation vanishes on any closed path in a region, the flow is said to be **irrotational**.

Exercise 1.1 This exercise is about a vortex such as you might see when draining a bath.

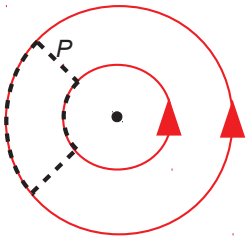

An idealisation of the flow is shown in red in the figure. It speed at distance r from the centre is $u = \Gamma/r$, where Γ is constant.

(a) By choosing a closed circular path of integration at fixed radius r, show that the circulation is Γ

(b) By choosing another closed path such as P in the figure, show that the flow is irrotational except very near the centre.

(c) Use your results to show that the circulation of the vortex does not depend on the path of integration as long as it encloses the centre.

1.3 Kelvin's circulation theorem

In 1869, Sir William Thompson (who was later Lord Kelvin) proved what is now called Kelvin's circulation theorem, which states that circulation is conserved in a barotropic fluid without viscosity. The invariance of Γ with time follows from

its definition,

$$\begin{aligned} 2\pi \frac{D\Gamma}{Dt} &= \oint \frac{D\mathbf{u}}{Dt}.d\mathbf{l} + \oint \mathbf{u}.\frac{Dd\mathbf{l}}{Dt} \\ &= -\oint \left(\frac{1}{\rho}\nabla P\right).d\mathbf{l} + \oint \mathbf{u}.\left.\frac{d(d\mathbf{l})}{dt}\right|_{d\mathbf{l}=d\mathbf{l}_o+td\mathbf{u}} \\ &= -\oint \left(\frac{1}{\rho}\nabla P\right).d\mathbf{l} + \oint \mathbf{u}.d\mathbf{u} \\ &= 0 \end{aligned}$$

where we have substituted Euler's equation. The second term on the right hand side equates to $\frac{1}{2}\oint d(u^2)$, which vanishes since u^2 has the same value at both ends of the loop, which are one and the same point. To see that the other term vanishes, we use the property that the fluid is barotropic, so the density, being a function of the excess pressure P, can be expanded as

$$\frac{1}{\rho} = \frac{1}{\rho_o}\left(1 + a_1 P + a_2 P^2 + ..\right) \tag{1.3}$$

where P is measured relative to the ambient pressure and the a_i are constants. Substituting we get

$$\begin{aligned} \oint \left(\frac{1}{\rho}\nabla P\right).d\mathbf{l} &= \frac{1}{\rho_o}\oint \left(1 + a_1 P + a_2 P^2 + ..\right)\nabla P.\mathbf{dl} \\ &= \frac{1}{\rho_o}\oint \left[\nabla P.d\mathbf{l} + \tfrac{1}{2}a_1\nabla(P^2).d\mathbf{l} + \tfrac{1}{3}a_2\nabla(P^3).d\mathbf{l} + ..\right] \\ &= 0 \end{aligned}$$

Each term is proportional to the change in P^n around the loop, which vanishes.

1.4 Potential flow of waves

If a fluid is initially stationary then it has no circulation and Kelvin's circulation theorem tells us it must remain so when a periodic wave passes through it. It follows that the wave itself must be irrotational.

Irrotational flow is also called **potential flow** because it can be written

$$\mathbf{u} = \nabla\phi$$

where ϕ is called the **velocity potential**. It follows automatically that the flow is irrotational

$$\oint \mathbf{u}.d\mathbf{l} = \oint \nabla\phi.d\mathbf{l} = 0$$

The second expression is the change in ϕ around a loop, which vanishes.

1.5 Alternative forms for Euler's equation

Euler's equation can also be written using ordinary partial derivatives rather than the derivative D/Dt which moves with the fluid. Using the chain rule of partial differentiation,

$$\begin{aligned}\frac{D\mathbf{u}}{Dt} &= \left.\frac{d\mathbf{u}}{dt}\right|_{\mathbf{x}=\mathbf{u}t} \\ &= \frac{\partial \mathbf{u}}{\partial t} + \frac{dx}{dt}\frac{\partial \mathbf{u}}{\partial x} + \frac{dy}{dt}\frac{\partial \mathbf{u}}{\partial y} + \frac{dz}{dt}\frac{\partial \mathbf{u}}{\partial z} \\ &= \frac{\partial \mathbf{u}}{\partial t} + u_x\frac{\partial \mathbf{u}}{\partial x} + u_y\frac{\partial \mathbf{u}}{\partial y} + u_z\frac{\partial \mathbf{u}}{\partial z} \end{aligned} \tag{1.4}$$

In vector notation, this is Euler's equation in its alternative form [1]:

$$\frac{\partial \mathbf{u}}{\partial t} + (\mathbf{u}.\nabla)\mathbf{u} = -\frac{1}{\rho}\nabla P \tag{1.5}$$

In the case of potential flow, each component of $\mathbf{u}$, say u_i where i can mean any of x, y or z, can be written in the form $u_i = \partial\phi/\partial x_i$. The last line of (1.4) becomes

$$\begin{aligned}\frac{Du_i}{Dt} &= \frac{\partial u_i}{\partial t} + u_x\frac{\partial u_i}{\partial x} + u_y\frac{\partial u_i}{\partial y} + u_z\frac{\partial u_i}{\partial z} \\ &= \frac{\partial u_i}{\partial t} + \frac{\partial \phi}{\partial x}\frac{\partial^2\phi}{\partial x \partial x_i} + \frac{\partial \phi}{\partial y}\frac{\partial^2\phi}{\partial y \partial x_i} + \frac{\partial \phi}{\partial z}\frac{\partial^2\phi}{\partial x \partial x_i} \\ &= \frac{\partial u_i}{\partial t} + \tfrac{1}{2}\frac{\partial}{\partial x_i}\left(\frac{\partial \phi}{\partial x}\right)^2 + \tfrac{1}{2}\frac{\partial}{\partial x_i}\left(\frac{\partial \phi}{\partial y}\right)^2 + \tfrac{1}{2}\frac{\partial}{\partial x_i}\left(\frac{\partial \phi}{\partial z}\right)^2 \\ &= \frac{\partial u_i}{\partial t} + \tfrac{1}{2}\frac{\partial}{\partial x_i}(u^2)\end{aligned}$$

In vector notion, this is **Euler's equation for potential flow**

$$\frac{\partial \mathbf{u}}{\partial t} + \tfrac{1}{2}\nabla(u^2) = -\frac{1}{\rho}\nabla P \tag{1.6}$$

This is the form of the equation which we will use for periodic waves.

1.6 Expectation values

Suppose we are not able to measure the periodic motion of a fluid directly. The frequency of oscillation may be too high or the wavelength too short, or the experimental apparatus might not be designed to measure oscillations at all. It is still possible to detect the oscillations indirectly, using natural phenomena which build up over multiple cycles. One such phenomenon was discussed by George Forbes in 1881, when he wrote in *Nature* [2]

> It has long been known that if a tuning fork be struck and held near to a light object like a balloon it attracts it. This is an old experiment ... Among others, Sir William Thomson gave the theory in the Philosophical Magazine in 1867.

The balloon is attracted to the source of sound because the average pressure of the air is reduced there. To see why, it suffices to integrate Euler's equation for potential flow (1.6) over a period τ

$$\frac{1}{\tau}\int_0^\tau \frac{\partial \mathbf{u}}{\partial t}\,dt \quad + \quad \frac{1}{\tau}\int_0^\tau \tfrac{1}{2}\nabla(u^2)\,dt \quad = \quad -\frac{1}{\tau}\int_0^\tau \frac{1}{\rho}\nabla P\,dt \qquad (1.7)$$

The integral in first term on the left hand side is the change in $\mathbf{u}$ over a period, which vanishes since the motion is periodic. If the amplitude of the motion is small then we can approximate the density ρ to a constant and integrate, giving

$$< P > \quad \approx \quad -\tfrac{1}{2}\rho < u^2 > \quad + \quad constant$$

where <..> is shorthand for the mean value over one or more a complete cycles. We will call such a quantity an **expectation value**. In the historical experiment discussed by Forbes, the oscillation near the tuning fork can be detected through the reduced expectation pressure, which attracts the balloon.

Exercise 1.2 The density ρ of an inviscid fluid is related to its excess pressure P by

$$\frac{1}{\rho} \quad = \quad \frac{1}{\rho_o}(1 + a_1 P + a_2 P^2 + a_3 P^3 + ..)$$

where the a_i are constants.

By substituting this expansion into Euler's equation for potential flow and averaging over a period, obtain an exact expression for the expectation value $< u^2 >$ as an expansion in $< P >, < P^2 >, < P^3 >$ and so on.

This reduced expectation pressure is related to a phenomenon which dates back to Daniel Bernoulli in 1738, called the Bernoulli effect, in which the pressure of a fluid decreases with its flow speed [3].

1.7 Expectation velocity of a fluid

When a periodic wave passes through a region, it does not change the expectation velocity $< \mathbf{u} >$ of the fluid. The proof uses a similar line of reasoning to Kelvin's circulation theorem in section 1.3, where the integration is over a wavelength rather than over a closed loop.

The time derivative of the fluid velocity, averaged over a wavelength λ, is

$$\begin{aligned}\frac{\partial}{\partial t}<\mathbf{u}> &= \frac{\partial}{\partial t}\left(\frac{1}{\lambda}\int_0^\lambda \mathbf{u}.d\mathbf{l}\right)\\ &= \frac{1}{\lambda}\int_0^\lambda \frac{\partial \mathbf{u}}{\partial t}.d\mathbf{l}\\ &= -\frac{1}{\lambda}\int_0^\lambda \tfrac{1}{2}\nabla(u^2).d\mathbf{l} - \frac{1}{\lambda}\int_0^\lambda \frac{1}{\rho}\nabla P.d\mathbf{l}\\ &= 0\end{aligned}$$

where we have substituted Euler's equation for potential flow (1.6). The first term is proportional to the change in u^2 over a wavelength, which vanishes since the motion is periodic. To see that the second term vanishes when the fluid is barotropic, substitute the Taylor expansion of $1/\rho$, which we saw in (1.3), giving

$$\begin{aligned}\frac{1}{\lambda}\int_0^\lambda \frac{1}{\rho}\nabla P\, d\mathbf{l} &= \frac{1}{\rho_o\lambda}\int_o^\lambda (1 + a_1P + a_2P^2 + ..)\,\nabla P.\mathbf{dl}\\ &= \frac{1}{\rho_o\lambda}\int_o^\lambda \nabla P.d\mathbf{l} + \tfrac{1}{2}a_1\nabla(P^2).d\mathbf{l} + \tfrac{1}{3}a_2\nabla(P^3).d\mathbf{l} + ..\\ &= 0\end{aligned}$$

Each term is proportional to the change in P^n over a wavelength, which vanishes since the motion is periodic.

It follows that if the fluid was stationary before the arrival of the wave, then the expectation value of the fluid speed remains zero when the wave passes over, and so $<\mathbf{u}> = 0$ for the wave.

1.8 Continuity equation

When the density of a barotropic fluid varies, due to its compressibility, the conservation of mass gives us a relationship called the **continuity equation**.

Consider a fluid element of area A and width Δx, with flow u in the x direction (figure 1.2). In the following argument, the boundaries of the region do not move with the fluid but are considered to be fixed. The mass flowing through each surface is $A\rho u$ and the net mass flowing into the region is the difference between the flows on each surface,

$$\frac{\partial m}{\partial t} = -A\Delta x\frac{\partial(\rho u)}{\partial x}$$

The mass inside the region is $m = \rho A\Delta x$. Substituting gives

$$\frac{\partial \rho}{\partial t} = -\frac{\partial(\rho u)}{\partial x}$$

and extending to three dimensions, this is the continuity equation

$$\frac{\partial \rho}{\partial t} = -\nabla.(\rho\mathbf{u}) \tag{1.8}$$

1.9 Sound waves

We now obtain the equation of motion for sound waves in a barotropic fluid, which is a good approximation at small amplitude. We have seen that a wave propagating into a region of stationary fluid does not have any circulation, and hence it has no shear flow, and so it seems a reasonable approximation to neglect viscosity, even if the fluid has some.

In a barotropic fluid the density is a function of pressure and can be written

$$\rho = \rho_o(1 + b_1 P + b_2 P^2 + ..)$$

where P is measured relative to the ambient pressure and b_i are constants. Substituting into the continuity equation (1.8) gives

$$\frac{\partial \rho}{\partial t} = -\rho_o \nabla.\mathbf{u} - \rho_o \nabla.([b_1 P + b_2 P^2 + ..]\,\mathbf{u})$$

We will neglect the second term on the right hand side since P is small for low amplitude motion. Differentiating gives

$$\begin{aligned} \frac{\partial^2 \rho}{\partial t^2} &= -\rho_o \nabla\left(\frac{\partial \mathbf{u}}{\partial t}\right) \\ &= \rho_o \nabla\left(\frac{1}{\rho}\nabla P\right) + \tfrac{1}{2}\nabla^2(u^2) \end{aligned} \tag{1.9}$$

where we have substituted Euler's equation for potential flow (1.6). Again, we will neglect the second term on the right hand side since u^2 is small.

Treating $1/\rho$ as a function of P and using a Taylor expansion about the ambient pressure gives

$$\frac{1}{\rho} = \frac{1}{\rho_o}(1 + a_1 P + a_2 P^2 + ..)$$

Substituting into (1.9) gives

$$\frac{\partial^2 \rho}{\partial t^2} - \nabla^2 P = \nabla.[(a_1 P + a_2 P^2 + ..)\nabla P]$$

Again, the right hand side can be neglected for low amplitude motion. Defining

$$c^2 = \frac{dP}{d\rho}$$

so that $\nabla^2 \rho = c^2 \nabla^2 P$, we get the **wave equation**

$$\frac{1}{c^2}\frac{\partial^2 \rho}{\partial t^2} - \nabla^2 \rho = 0 \tag{1.10}$$

The next exercise reviews the basics of the solutions to the wave equation.

Exercise 1.3 When a sound wave propagates through the air, its density ρ is given by

$$\frac{\rho - \rho_o}{\rho_o} \;=\; A\cos(kx - \omega t)$$

where ρ_o the mean density, and A is the amplitude of the wave. By considering the wave at the point $x = 0$, or otherwise, show that its frequency is

$$f \;=\; \frac{\omega}{2\pi}$$

and by considering it at $t = 0$ show that its wavelength is

$$\lambda \;=\; \frac{2\pi}{k}$$

The compressions and rarefactions of the wave propagate at a speed v_ϕ called the 'phase velocity'. By substituting $\rho = \rho_o(1 + A)$ for the densest part of a compression, or otherwise, show that it propagates at speed

$$v_\phi \;=\; \frac{\omega}{k} \;=\; f\lambda$$

Show by direct substitution into (1.10) that ρ is a solution to the wave equation when $\omega = c\,|k|$. Hence or otherwise show that it propagates at speed $v_\phi = \pm c$.

There is a wall at $x = 0$. Near it, there is a standing wave ρ_s where

$$\frac{\rho_s - \rho_o}{\rho_o} \;=\; A\cos(-\omega t)\cos(kx)$$

The minus sign is to conform to convention and has no other significance. Show that ρ_s is another solution to the wave equation.

Show that this standing wave is a sum of of two propagating waves, one travelling towards the wall and the other away from it, that is,

$$2\,\frac{\rho_s - \rho_o}{\rho_o} \;=\; A\cos(kx - \omega t) \;+\; A\cos(-kx - \omega t)$$

Hint. Look up a trigonomic identity for $\cos A \cos B$.

1.10 Surface waves

The waves on the surface of a liquid also obey the wave equation to a good approximation when viscosity and the wave height are small. However, the wave speed depends on the wavelength of the waves. This can be shown by considering a wave of a single wavelength. Suppose the height h of the surface is in the simple form

$$h \;=\; f(t)\,\cos(kx) \tag{1.11}$$

where $f(t)$ is a function of time to be determined.

The gravitational potential energy of this wave is just the energy required to raise or lower a small column of liquid relative to the ambient level, integrated over the surface

$$PE_g \;=\; \tfrac{1}{2}\rho g \int h^2\, dx\, dy \;=\; \tfrac{1}{2}\rho g f^2 \int \cos^2(kx) dx dy$$

where ρ is the density of the liquid and g the acceleration due to gravity.

The wave also increases the surface area. From Pythagoras's theorem for a right angled triangle, the area of the surface is

$$\int \left[1 + \left(\frac{\partial h}{\partial x}\right)^2\right]^{\frac{1}{2}} dxdy \;\approx\; \int \left[1 + \frac{1}{2}\left(\frac{\partial h}{\partial x}\right)^2\right] dxdy$$

Multiplying by the surface tension σ, the stretching of the surface contributes potential energy of

$$PE_\sigma \;\approx\; \tfrac{1}{2}\sigma k^2 f^2 \int \sin^2(kx)\, dxdy$$

It follows that the total potential energy of the wave is

$$PE \;=\; Af^2 \tag{1.12}$$

where $A \approx \frac{1}{2}\rho g \int \cos^2(kx)\, dxdy + \frac{1}{2}\sigma k^2 \int \sin^2(kx)\, dxdy$.

If the surface is large, then the total potential energy of any one component is independent of the other components. Writing subscripts 1 and 2 for the two components, at any given time the total potential energy is proportional to

$$PE \;\propto\; \int \left[A_1 \cos(k_1 x) + A_2 \cos(k_2 x)\right]^2 dx \;\propto\; A_1^2 + A_2^2$$

The cross terms vanish as long as the integration is over a whole number of wavelengths of the combined wave.

Likewise the kinetic energy is driven by the motion of the surface and it is everywhere proportional to the square of the fluid speed,

$$KE \;=\; B\left(\frac{df}{dt}\right)^2 \tag{1.13}$$

where B is proportional to the density, and geometric factors have also been rolled up into it. The value of B depends on the detailed flow patterns. For example, in deep oil the motion will extend vertically beneath the wave by of order a wavelength, but in shallow oil the flows are constrained to be more concentrated. For more detail about the flow patterns in the various regimes, see a textbook on fluid mechanics such as Tom Faber's *fluid dynamics for physicists* [1].

Equations (1.12) and (1.13) are the same as those for a harmonic oscillator, such as a pendulum. If a bob of mass m is at angle $\theta(t)$ from vertical, then

the potential energy is $mgl(1-\cos(\theta)) \approx \frac{1}{2}mgl\theta^2$ where l is the length, and the kinetic energy is $\frac{1}{2}m(l\ d\theta/dt)^2$. The sum of these must be constant, which is satisfied when $\theta \propto \cos(\omega t)$ with $\omega = \sqrt{g/l}$, as may be seen by direct substitution. The waves have $f(t)$ in place of $\theta(t)$ and the same condition gives

$$h \quad \propto \quad \cos(-\omega t)\cos(kx) \tag{1.14}$$

where $\omega = \sqrt{A/B}$. The minus sign is conventional and has no physical significance. By direct substitution, (1.14) obeys the wave equation when

$$c \quad = \quad \frac{\omega}{k}$$

The speed $c = \omega/k = \sqrt{A/(Bk^2)}$ usually depends on depth and frequency, but both of these were kept constant in any given experiment.

1.11 Interactions between waves

The wave equation is linear, which means that any two waves do not interact with each other when they have low amplitude.

Exercise 1.4 Two water waves have heights $h_1(x,t)$ and $h_2(x,t)$. They each obey the wave equation (1.10).

Show by direct substitution that their sum also obeys the wave equation.

When the motion has greater amplitude, the nonlinear terms we neglected when deriving the wave equation will perturb this symmetry and cause two waves to interact. Figure 1.4 shows what happens when two waves cross.

Figure 1.4: *The interaction between shallow water waves. (Courtesy Douglas Baldwin, University of Colorado)*

The waves experience a local advance or retardation so they bend into temporary alignment near the centre. However the interaction does not seem to have much of a lasting effect. For example, by observing a wave, it is hard to

tell whether or not another wave has crossed its path at some time in the past. It is as if the interactions average out over a wavelength.

To understand why this is the case, consider one source of perturbation: the non-linear term $\nabla(u^2)$ in Euler's equation for potential flow (1.6). Suppose the two waves, A and B, have flow speeds $\mathbf{a}$ and $\mathbf{b}$, so that $\mathbf{u} = \mathbf{a} + \mathbf{b}$ for the combined flow pattern. The perturbation is

$$\nabla(u^2) \quad = \quad \nabla(a^2) \; + \; \nabla(b^2) \; + \; 2\nabla(\mathbf{a}.\mathbf{b})$$

The first two terms on the right hand side do not depend on the interactions between the waves; it is the final term that is of interest here.

Let us suppose for simplicity that one wave in the photograph, say A, propagates in the y direction and wave B, which perturbs it, propagates at an angle. Figure 1.5 shows an idealisation of their wavefronts; it includes a second wavefront of B to indicate a complete cycle.

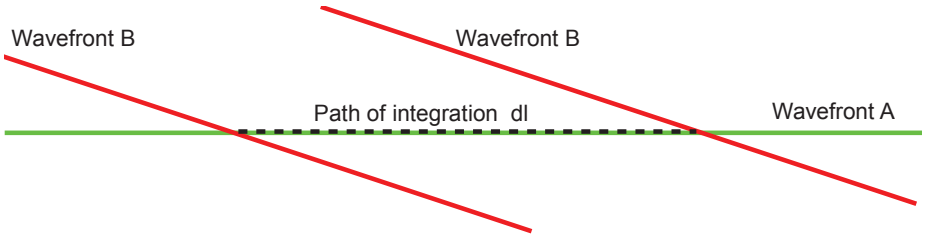

Figure 1.5: *Idealisation of the waves photographed in figure 1.4.*

The flow due to A is in the y direction, and so we do not need to consider any components of velocity in the x direction when calculating the perturbation. The perturbation term expands to

$$2\nabla(a_y b_y) \quad = \quad 2a_y \nabla b_y \; + \; 2b_y \nabla a_y$$

We will calculate the expectation value of the perturbation by integrating along a path shown in the figure. This is a reasonable estimate of the net effect of the perturbation on any given part of wave A because the waves roll past one another over time. This path is also convenient for calculation because the parameters of A can be treated as constant and taken out of the integration. The expectation value of the perturbation is thus

$$\begin{aligned} < 2\nabla(a_y b_y) > \quad &= \quad \frac{2a_y}{\lambda} \int_0^\lambda (\nabla b_y).d\mathbf{l} \; + \; \frac{2\nabla a_y}{\lambda}. \int_0^\lambda b_y \, d\mathbf{l} \\ &= \quad 0 \end{aligned}$$

The first term on the right hand side is proportional to the change in b_y over a complete cycle of wave B, which vanishes because the wave is periodic, and the second term vanishes because of the conservation of expectation fluid velocity discussed in the section 1.7.

1.12 Fourier's theorem

We have seen that we can treat components with different wavevectors **k** independently of one another, to a good approximation, if the motion is of low amplitude, or, even if the amplitude is greater, if our instruments are only capable of measuring expectation values. In the terminology of the field, the waves are 'orthogonal'.

This approximate, but nevertheless rather good, symmetry enables us to simplify the treatment of waves using a mathematical theorem first proved by Joseph Fourier in 1822. Suppose for simplicity that a wave varies only in the x direction, so the density of the fluid is $\rho(x)$ at any given time. Fourier defined his transformation by

$$\widehat{\rho}(k) \quad = \quad \int_{-\infty}^{\infty} \rho(x)\, e^{-ikx}\, dx$$

where k is real and is called the wavevector, and $\widehat{\rho}(k)$ is a complex-valued function of k called the Fourier transform.

Under a wide range of conditions (which are wide enough to apply to the waves we are interested in), Fourier proved that we can recover the original density of the fluid as follows

$$\rho(x) \quad = \quad \frac{1}{2\pi} \int_{-\infty}^{\infty} \widehat{\rho}(k)\, e^{ikx}\, dk$$

For any given value of k, the integrand $\widehat{\rho}(k)e^{ikx}$ has the simple properties of a wave which we saw in section 1.9. For example, if $\widehat{\rho}(k)$ is real then the integrand is proportional to $\cos(kx)+i\sin(kx)$. Both components are solutions to the wave equation which oscillate at angular frequency $\omega = ck$, as may be verified, for example, by substituting $\rho = \cos(kx)\cos(\omega t)$ into (1.10).

Fourier's theorem shows that any solution to the wave equation, however complicated, can be treated as a sum of these simple solutions. The orthogonality allows us to neglect the interactions between these components to a very good approximation, provided our measuring instruments are restricted to measuring expectation values.

You may be familiar with the Fourier transformation from music. The pressure of the sound waves reaching your ear is likely to be a complicated function of time. Your ear and brain tend to analyse it as a sum of Fourier components which you interpret as tones. For example, if a piano is played at middle C you will perceive it as a tone, which is easier to analyse and understand than a wave pattern.

It is common to simplify the treatment still further by not paying much attention to the complex phase of $\widehat{\rho}(k)$. This neglect might introduce an imaginary part to $\rho(x)$ after the inverse transformation, but, if necessary, it can be corrected for by multiplying by a suitable factor, such as $e^{i\theta}$, or, more commonly, by discarding the imaginary part at the end of the calculation.

1.13 Scale invariance

Given a solution to Euler's equation, we can immediately write down another solution using the symmetry that the equation is **scale invariant**, that is, if a flow field $\mathbf{u}(\mathbf{x}, t)$ is a solution then so is $\mathbf{u}(\alpha\mathbf{x}, \alpha t)$ where α is a scale factor.

This symmetry may be familiar in sound waves, where doubling the frequency halves the period and wavelength. It is used in acoustic scale models. Suppose you are singing in a bathroom at, say, middle C, which is 261.6 Hz. The wave pattern, including reflections from the walls, might be rather complicated. Using the scale symmetry of Euler's equation, you could obtain the wave pattern from a half-scale model. The scale model of your body must sing at the C above middle C, $523.2Hz$.

The proof is as follows. Consider the transformation

$$(\mathbf{x}',\, t') \;=\; (\alpha\mathbf{x},\, \alpha t) \tag{1.15}$$

where α is some scale factor. The chain rule of partial differentiation gives

$$\frac{\partial}{\partial t} \;=\; \frac{\partial t'}{\partial t}\frac{\partial}{\partial t'} \;=\; \alpha\,\frac{\partial}{\partial t'}$$

Likewise we get $\nabla = \alpha\nabla'$ where ∇' means $(\partial/\partial x',\, \partial/\partial y',\, \partial/\partial z')$.

The scale transformation leaves all velocities unaffected at the corresponding positions in the two solutions. For example, in the x direction

$$u' \;=\; \frac{dx'}{dt'} \;=\; \frac{dx}{dt} \;=\; u$$

Substituting these relationships gives

$$\frac{D\mathbf{u}}{Dt'} \;+\; \frac{1}{\rho}\,\nabla' P \;=\; \frac{1}{\alpha}\left(\frac{D\mathbf{u}}{Dt} \;+\; \frac{1}{\rho}\,\nabla P\right)$$

If $\mathbf{u}(\mathbf{x}, t)$ is a solution to Euler's equation then the right hand side must vanish. Equating the left hand size to zero shows that $\mathbf{u}(\mathbf{x}', t')$ is also a solution.

In a barotropic fluid the pressure-density relationship, $P = P(\rho)$, does not depend on position or time and so it does not break the scale symmetry. The symmetry might be disturbed if lossy processes are involved, such as thermal conductivity, but we will only be interested in lossless fluids.

Exercise 1.5 By direct substitution of the scale transformation (1.15), show that

$$\frac{1}{c^2}\frac{\partial^2 h}{\partial t^2} - \frac{\partial^2 h}{\partial x^2} - \frac{\partial^2 h}{\partial y^2} \;=\; \alpha^2\left(\frac{1}{c^2}\frac{\partial^2 h}{\partial t'^2} - \frac{\partial^2 h}{\partial x'^2} - \frac{\partial^2 h}{\partial y'^2}\right)$$

Use your result to show that if $h(x, y, t)$ obeys the wave equation, so does $h(\alpha x, \alpha y, \alpha t)$.

1.14 Acoustic Lorentz covariance

If we are given a periodic solution to Euler's equation in a barotropic fluid, we can immediately write down another solution which is moving relative to the fluid. This uses a symmetry called **Lorentz covariance**, which states that if $h(x, y, t)$ is a solution then so is $h(x', y', t')$ where

$$\begin{aligned} x' &= \gamma\,(x - vt) \\ y' &= y \\ t' &= \gamma\left(t - \frac{vx}{c^2}\right) \\ \gamma &= \frac{1}{\sqrt{1 - \frac{v^2}{c^2}}} \end{aligned} \tag{1.16}$$

This is the same Lorentz transformation that is used in electromagnetism and other areas of physics, but with an acoustic value for the characteristic speed c. It is also used in aerodynamics and acoustics; see for example [4]. The proof is as follows.

Applying the chain rule of partial differentiation to the Lorentz transformation (1.16), we get

$$\begin{aligned} \frac{\partial}{\partial x} &= \frac{\partial x'}{\partial x}\frac{\partial}{\partial x'} + \frac{\partial t'}{\partial x}\frac{\partial}{\partial t'} \\ &= \gamma\left(\frac{\partial}{\partial x'} - \frac{v}{c^2}\frac{\partial}{\partial t'}\right) \end{aligned}$$

and applying it a second time gives

$$\frac{\partial^2 h}{\partial x^2} = \gamma^2\left(\frac{v^2}{c^2}\,\frac{1}{c^2}\frac{\partial^2 h}{\partial t'^2} + \frac{\partial^2 h}{\partial x'^2} - \frac{2v}{c^2}\,\frac{\partial^2 h}{\partial x'\partial t'}\right) \tag{1.17}$$

Likewise, for t,

$$\begin{aligned} \frac{\partial}{\partial t} &= \frac{\partial x'}{\partial t}\frac{\partial}{\partial x'} + \frac{\partial t'}{\partial t}\frac{\partial}{\partial t'} \\ &= \gamma\left(\frac{\partial}{\partial t'} - v\frac{\partial}{\partial x'}\right) \\ \frac{1}{c^2}\frac{\partial^2 h}{\partial t^2} &= \gamma^2\left(\frac{1}{c^2}\,\frac{\partial^2 h}{\partial t'^2} + \frac{v^2}{c^2}\,\frac{\partial^2 h}{\partial x'^2} - \frac{2v}{c^2}\,\frac{\partial^2 h}{\partial x'\partial t'}\right) \end{aligned} \tag{1.18}$$

Subtracting (1.17) from (1.18) and using $\gamma^2(1 - v^2/c^2) = 1$ gives

$$\frac{1}{c^2}\frac{\partial^2 h}{\partial t^2} - \frac{\partial^2 h}{\partial x^2} - \frac{\partial^2 h}{\partial y^2} = \frac{1}{c^2}\frac{\partial^2 h}{\partial t'^2} - \frac{\partial^2 h}{\partial x'^2} - \frac{\partial^2 h}{\partial y'^2}$$

If $h(x, y, t)$ is a solution to the wave equation, the left hand side vanishes and therefore, by equating the right hand side to zero, $h(x', y', t')$ is also a solution.

This proves the Lorentz covariance for small amplitude motion. At larger amplitude, the Lorentz symmetry will be perturbed by the nonlinear terms in

the equation of motion. In particular, the solution with primed coordinates is moving relative to the fluid as constant speed $\mathbf{v}$, so that the fluid velocity $\mathbf{u}$ becomes $\mathbf{u}' = \mathbf{u}+\mathbf{v}$. This perturbs the quadratic term $\nabla(u^2)$ in Euler's equation for potential flow (1.6),

$$\nabla(u'^2) \quad = \quad \nabla(\mathbf{u}+\mathbf{v})^2 \quad = \quad \nabla(u^2) + 2\nabla(\mathbf{u}.\mathbf{v})$$

The perturbation is in the second term on the right hand side. Taking $\mathbf{v}$ to be in the x direction without loss of generality, its spatial expectation value is

$$< 2\nabla(\mathbf{u}.\mathbf{v}) > \quad = \quad 2v_x \frac{1}{\lambda} \int_0^\lambda \frac{\partial u_x}{\partial x}\, dx \quad = \quad 0$$

The expression vanishes because u_x has the same value at points a wavelength apart. Thus, the expectation value of this perturbation vanishes, and so it will be difficult or impossible for an apparatus that is only capable of measuring expectation values to detect it.

Exercise 1.6 We saw in section 1.9 that there is another perturbation to the wave equation that depends on $\mathbf{u}$, namely

$$\rho_o \nabla.([b_1 P + b_2 P^2 + ..]\, \mathbf{u})$$

By taking an average over a wavelength, show that the expectation value of this term is unchanged by the transformation $\mathbf{u}' = \mathbf{u} + \mathbf{v}$ where $\mathbf{v}$ is constant.

It follows that the solutions to Euler's equation in a barotropic fluid are Lorentz covariant when the motion is low amplitude. This symmetry is perturbed at greater amplitude but the perturbations average to zero over a wavelength, and so it will be difficult or impossible for an apparatus that is only capable of measuring expectation values to detect any deviation from the Lorentz symmetry.

1.15 Momentum of a wave

We now show that the momentum p of a wave is related to its energy E through

$$p \quad = \quad \frac{E}{c} \tag{1.19}$$

where c is the wave speed.

Figure 1.6 shows the horizontal flow speed for a wave propagating in the $+x$ direction. The flow near the submerged line A does not contribute to the momentum, since it is symmetrical. The expectation velocity $< \mathbf{u} >$ vanishes on this line (section 1.7).

But the elevations carry extra fluid. If you take a line of integration which is not completely submerged, such as B, the elevations dominate and the integral

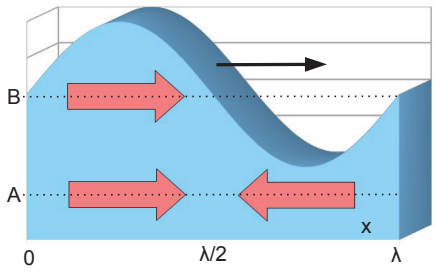

Figure 1.6: *In a simple propagating wave, the horizontal flow speed (red arrows) is proportional to the wave height. The flow is symmetrical on the submerged line A, so there is no net momentum when measured on this line. But the crest carries extra fluid, so the wave has momentum due to its forward motion.*

$\int \mathbf{u}.d\mathbf{l}$ does not vanish. The wave has net momentum,

$$\overline{\mathbf{p}} \quad \propto \quad \int_o^\lambda h\, \mathbf{u}.d\mathbf{l} \;>\; 0$$

since the mass of an element is proportional to the height. This does not violate Kelvin's circulation theorem since the path of integration is not wholly submerged.

The proof of equation (1.19) is as follows.

If the wave height is given by

$$h \quad = \quad A\cos(\omega t - kx) \tag{1.20}$$

then substituting into (1.1) and integrating gives

$$u \quad = \quad \pm\frac{k}{\omega}\, gh \quad = \quad \pm\frac{g}{c}\, h \tag{1.21}$$

where the sign depends on the direction of propagation and will be dropped for simplicity.

Consider a small vertical column of fluid whose area is $dxdy$. Its potential energy is the energy required to raise its height by h above the ambient level against the force of gravity, namely

$$E_p \quad = \quad \frac{1}{2}\int \rho g h^2\, dxdy$$

The potential energy of motion is equal to the kinetic energy when averaged over a cycle. Substituting (1.20) and averaging over a cycle, the total is

$$E \quad = \quad \frac{1}{2}\int \rho g A^2\, dxdy \tag{1.22}$$

The momentum of the column in the x direction is $p = \rho u(h + h_o)dxdy$. Substituting (1.21) gives

$$p \quad = \quad \frac{1}{c}\int \rho h(h + h_o)\, dxdy$$

Substituting (1.20) and averaging over a cycle, the second term vanishes leaving

$$p \;=\; \frac{1}{2c}\int \rho g A^2 \, dxdy \;=\; \frac{E}{c}$$

where we have substituted (1.22). See [1] for an alternative derivation.

1.16 Longitudinal and transverse motion

It was believed for many years that a fluid can only support **longitudinal** waves, which have their fluid velocity parallel to the direction of propagation. Any component of motion in the **Transverse** direction, perpendicular to the direction of travel (not counting vertical motion in the case of waves on the surface of a liquid), was thought impossible. The proof assumes that the fluid is initially stationary, as follows.

When a wave propagates into a region of stationary fluid, it cannot introduce any circulation into the region, from Kelvin's theorem, and so the wave cannot have any circulation, which excludes shear flow and transverse motion. Some may prefer the less rigorous, but more intuitive, argument that an ordinary fluid has no resilience under shear, and so it cannot supply the restoring forces that seem to be needed for transverse motion.

This proof assumes that the fluid was initially stationary. It does not apply if the fluid is rotating, since a wave propagating towards the centre will have a transverse component of velocity because of the Coriolis forces. Likewise it does not apply when there are pre-existing shear flows.

An example of such a wave was photographed in 1980 by Michael Berry and colleagues. They drained water from a tank, carefully refilling it so as not to disturb the flow. This created a region of shear flow, in the form of a vortex. They then sent waves into the region [5]. Figure 1.7 is a photograph of a light pattern made by the waves.

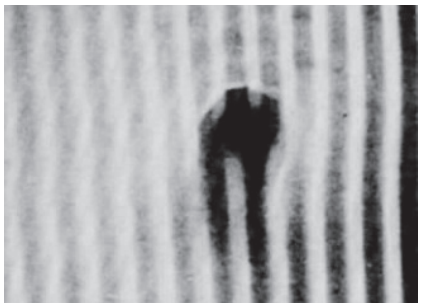

Figure 1.7: *Water waves near a vortex. (Courtesy Michael Berry [5])*

If the vortex has circulation Γ then its tangential flow speed is $u = \Gamma/r$ (see the exercise in section 1.2). On the x axis, the velocity in the y direction is

$$u_y \;=\; \frac{\Gamma}{x}$$

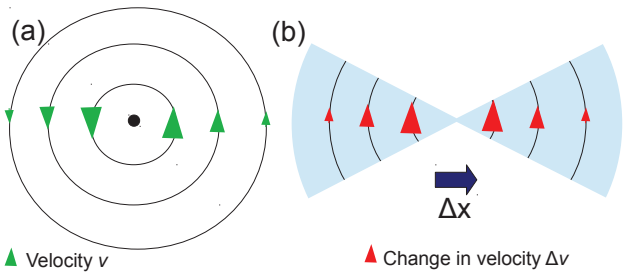

Figure 1.8: *(a) The fluid flow near a vortex (b) When it is displaced in the $+x$ direction, the net effect is to increase the fluid velocity in the $+y$ direction everywhere except very near the centre (the figure is schematic only).*

which constitutes shear flow.

Suppose the fluid is displaced by Δx, as shown in figure 1.8. In the region $|x| > \Delta x$, the y component of velocity becomes

$$u_y' \;=\; u_y \;-\; \frac{\partial u_y}{\partial x}\,\Delta x \;=\; u_y \;+\; \frac{\Gamma}{x^2}\,\Delta x \tag{1.23}$$

The wave in the photograph will cause a displacement $\Delta x = A\cos(kx - \omega t)$. Substituting into (1.23), they have an oscillatory transverse component

$$u_y' \;=\; u_y \;+\; \frac{A\Gamma}{x^2}\,\cos(kx - \omega t)$$

As measured by a stationary observer, circulation is not, in general, conserved when the wave passes, that is, $\partial\Gamma/\partial t \neq 0$. This does not violate Kelvin's circulation theorem, which states that $D\Gamma/Dt = 0$, where the path used to measure the circulation must move with the fluid.

A related example of transverse motion is when an ordinary sound wave in a compressible fluid encounters shear flow. We predict the unusual property that their direction of polarisation is not carried by the wave, but is determined by the orientation of the shear flows through which it propagates. More generally, if the shear flow is itself oscillatory, the polarisation might also depend on the phase orientation between the wave and the flows.

We would expect this phenomenon in superfluid ^{4}helium. When it is cooled below 2.172 Kelvin at atmospheric pressure, liquid ^{4}helium becomes a superfluid, which behaves in many respects like a compressible fluid with no viscosity. Ordinary sound waves (called 'first sound') propagate at approximately 230 m s^{-1}, and shear flow continues indefinitely in it, as evidenced by the fact that vortices do not decay. We are not aware of attempts to measure the polarisation of sound waves in superfluid ^{4}helium to date.

Another example of a transverse wave in a fluid dates to 1957 and the Soviet physicist Lev Davidovich Landau. He predicted that one of the low temperature phases of superfluid ^{3}helium might exhibit transverse sound waves, where the restoring forces for shear waves are supplied by the collective action of the particles in the fluid. This phenomenon was later observed experimentally [6,7].

The fluid has additional terms in Euler's equation which are outside the scope of this monograph.

1.17 Summary

In this chapter we derived the basic equations for periodic motion a barotropic fluid.

If, for any reason, it is not practical to measure the oscillations of a wave, for example if its frequency is too high for the instruments available, then the only measurements that remain are those which are averaged over one or more complete periods or a wavelengths. These are called 'expectation values' and we saw an example of their use in an experiment from the 19th century where a balloon is attracted towards a tuning fork.

We saw that the periodic solutions to Euler's equation possess three symmetries. Firstly, they are 'scale invariant', a symmetry which relates larger and smaller solutions. Secondly, solutions with different wavevectors are orthogonal to one another. And thirdly, they possess a symmetry called 'Lorentz covariance' which relates solutions in a stationary fluid to the corresponding solutions in which the fluid is moving. The first symmetry is exact. The other two are good approximations at low amplitude, and, at greater amplitude, the perturbations to these symmetries average out over a cycle, making it difficult detect them using an apparatus that is only capable of measuring expectation values.

Finally we discussed transverse motion of waves in a fluid. Their direction of polarisation depends on the direction of shear in the fluid.

Chapter 2

Bouncing droplets

A man came crashing through the crowds carrying in his hands a cage in which the rightful owner of the music sat

Interruption at the Opera house by Brian Patten [8]

In 1978, Jearl Walker, writing in the *Amateur Scientist* department of *Scientific American*, wrote about the curious phenomenon in which water droplets glide across a water surface for several seconds before sinking into it [9]. The droplet rides on a thin cushion of air which cannot escape quickly due to its viscosity.

Walker went on to describe an experiment that can be performed at home, using an electric hair clipper to vibrate the side of a cake pan containing a solution of water and liquid detergent. This kept the droplets going for longer by making them bounce, which replenishes the air film.

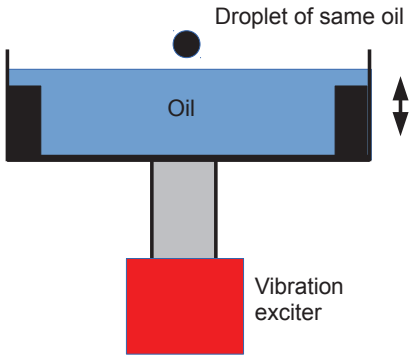

Figure 2.1: *Schematic of Couder's experimental apparatus. The shape of the container reduces unwanted waves from the edge by viscous damping.*

Bouncing droplets began to be explored more systematically in 2005, when Yves Couder, Suzie Protière, Emmanuel Fort and Arezki Badouad reported in the scientific journal *Nature* that droplets of oil can be made to bounce

indefinitely on the surface of the same oil when it is vibrated vertically [10]. The apparatus is illustrated in figure 2.1.

Today, researchers are interested in this phenomenon in its own right, and also because it is an association between a particle (the droplet) and a wave: a physical analogue for what happens in quantum mechanics. As we shall see in this monograph, this interplay between the particle-like and wave-like aspects of the motion yields many surprising results.

2.1 The bouncing motion

Figure 2.2 has six photographs of a bouncing droplet, and figure 2.3 illustrates the vertical motion as a function of time.

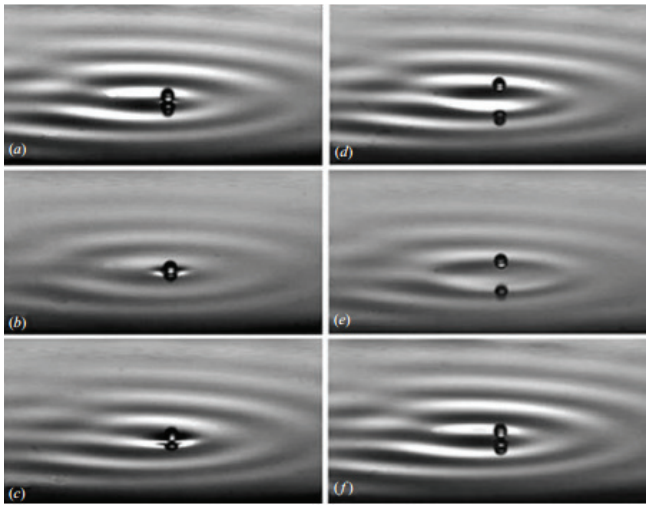

Figure 2.2: *A droplet of silicone oil bouncing on the surface of the same liquid which is vibrated vertically. (courtesy Suzie Protière, Arezki Boudaoud and Yves Couder [11])*

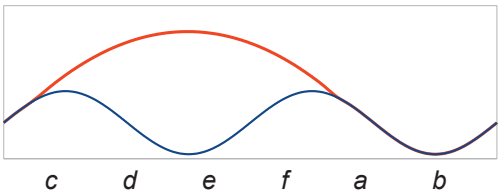

Figure 2.3: *The height of the droplet (red) and the surface (blue) as it oscillates vertically with time. In this simulation, the maximum forcing acceleration is 3.5g and surface waves are neglected. The labels cdefab refer to the photograph in figure 2.2.*

In these photographs, the droplet touches down every other cycle of the vertical vibration of the container. At lower forcing amplitudes there are less interesting modes of bouncing, where the droplet grazes off the peak near f in figure 2.3 or touches down every cycle.

These experiments have since been reproduced in laboratories around the world, such as by Jan Moláček and John Bush at MIT [12]. You can get started by running a free downloadable sine wave generator on your computer or mobile phone, and using it to drive a loudspeaker with a dish of oil glued to it. Such experiments are growing in popularity for student projects because they are so simple. A research version uses a vibration exciter which is carefully coupled to the oil tray so as to minimise horizontal motion; it has baffles to protect against winds; and it is carefully tuned, for example using crocodile clips, to reduce variations in the vertical motion around the container.

2.2 Surface waves

The horizontal motion of the droplet is guided by the surface waves. Like waves on a pond, the waves on the surface of the oil obey the standard wave equation to first order

$$\frac{1}{c^2}\frac{\partial^2 h}{\partial t^2} \; - \; \nabla^2 h \;\; = \;\; 0 \tag{2.1}$$

where h is the wave height. See section 1.10 for the proof. The parameter c is the wave speed. It usually depends on depth and frequency, but both of these were kept constant in any given experiment and so c can be treated as a constant.

2.3 Wave field near a stationary droplet

The waves near a stationary bouncing droplet are circularly symmetric, and the wave equation has a circularly symmetric solution,

$$h \;\; = \;\; h_o \; \cos(\omega_o t) \; J_0\left(\frac{\omega_o r}{c}\right) \tag{2.2}$$

where h_o is the maximum wave height and J_0 is a Bessel function of the first kind, which is drawn in figure 2.4. Compare this to the waves photographed in figure 2.2.

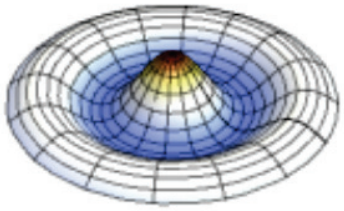

Figure 2.4: *The Bessel function $J_0(\omega_o r/c)$ at small radius*

The definition of J_0 and the proof that (2.2) obeys the wave equation are in the advanced material below.

† *Track 2* *This material may be skipped on a first reading*

In circular coordinates (r, θ), the wave equation (2.1) is

$$\frac{1}{c^2}\frac{\partial^2 h}{\partial t^2} - \frac{\partial^2 h}{\partial r^2} - \frac{1}{r}\frac{\partial h}{\partial r} - \frac{1}{r^2}\frac{\partial^2 h}{\partial \theta^2} = 0 \tag{2.3}$$

A Bessel function of the first kind, $J_m(z)$, is defined as a solution to Bessel's differential equation

$$z^2\,\frac{\partial^2 J_m}{\partial z^2} + z\,\frac{\partial J_m}{\partial z} + (z^2 - m^2)J_m = 0 \tag{2.4}$$

Using this definition with $m = 0$, it is readily verified by direct substitution that (2.2) is a solution to the wave equation in circular coordinates (2.3).

The photographs in figure 2.2 confirm that the waves are predominantly standing waves, as given by (2.2), rather than propagating waves. For example, the waves have only a small amplitude in photographs (b) and (e) but they are significantly larger at other points in the cycle. The reason for this is connected with the vertical vibration of the oil tray, as we now examine.

2.4 Parametric reinforcement

A child on a swing can go higher by moving her body up and down at twice the frequency of the swing. She does work when she accelerates her body upwards against the centrifugal force near the bottom of the swing. In physics such a processes is called **parametric excitation**.

The standing waves near a droplet are reinforced in a similar way by the vertical acceleration of the oil tray. See figure 2.5. When the oil tray is at its highest, it is accelerating downwards, typically with an acceleration of 3.5-4.5g. This reverses the effective direction of gravity, lifting the wave crests and enlarging the waves. As can be seen in the figure, the oil tray must oscillate at twice the frequency of the standing waves for the reinforcement to build up.

This can also be understood in terms of propagating waves as shown in figure 2.6. Like a pebble thrown into a pond, a droplet creates outgoing propagating waves when it lands. They are reinforced and reflected back when the oil tray is at its greatest height. The combination of outgoing and incoming waves forms the standing waves.

If the container is large enough, there will be multiple reflections which reverberate and reinforce one another. A similar reflection mechanism is used in the highest quality optical mirrors, which are called Bragg mirrors. Multiple layers of material with alternating high and low dielectric constant are laid on

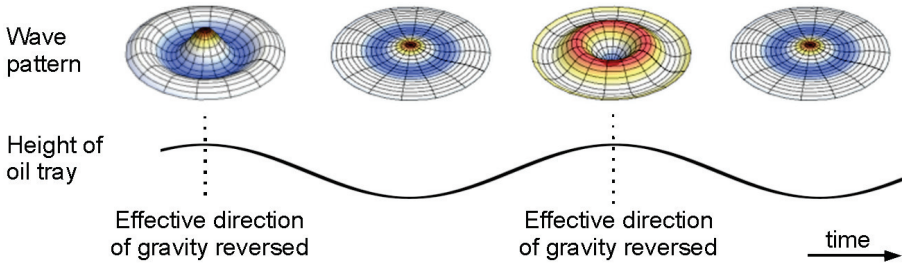

Figure 2.5: *Parametric reinforcement of the standing wave near a droplet. When the oil tray is at its greatest height it is accelerating downwards, reversing the effective direction of gravity. This lifts the wave crests and enlarges the waves.*

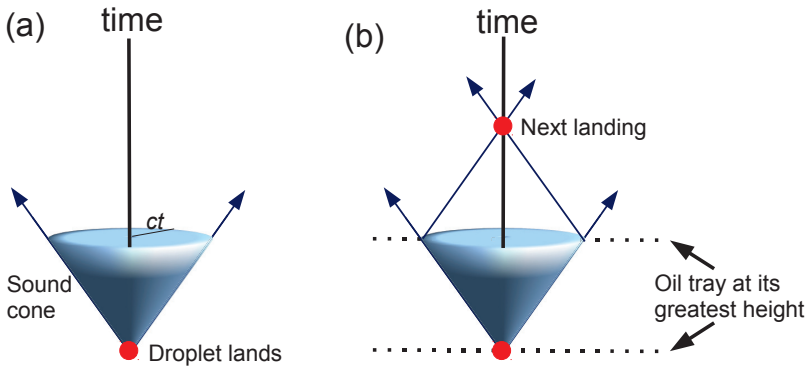

Figure 2.6: *Bragg reflection. (a) When a droplet lands it creates a trough in the surface which propagates outwards (marked 'sound cone'). (b) When the oil tray is at its greatest height it accelerates downwards. This reverses the effective direction of gravity, reinforcing the wave and forming an inward-directed trough that reaches the centre when the droplet next lands.*

top of one another. Light is reflected weakly at each interface. By choosing the geometry so that reflections reinforce, we can produce Bragg mirrors with up to 99.999% reflectivity.

When the parametric driving is large enough, each bounce of the droplet influences the next through this mechanism. The system behaves as if it had a memory of previous bounces; this is called the 'high memory' regime.

2.5 Wave speed

The speed c in (2.1) depends on frequency and depth, but these parameters were not varied during an experiment. It is more relevant that the wave speed is affected by the forcing acceleration, as follows.

Consider an isolated propagating wave. If it oscillates in-phase with the forcing acceleration (similar to figure 2.5) at one position, it will have the opposite phase a quarter of a wavelength away. Thus, any effect on the wave speed will

approximately cancel and the average phase velocity is largely unaffected.

But the standing wave (2.2) near the droplet is always in-phase with the forcing acceleration. Temporarily neglecting surface tension, the restoring force on the wave is proportional to $h\{g - a_m \cos(2\omega_o t)\}$ where a_m is the maximum acceleration, so the net change of momentum on a half-cycle is

$$\Delta p \quad \propto \quad \int_{-\frac{\pi}{2}}^{\frac{\pi}{2}} \cos(\omega_o t)\{g - a_m \cos(2\omega_o t)\} dt \quad \propto \quad g - \frac{a_m}{3}$$

Since $a_m > 3g$ in all the relevant experiments, the parametric driving outweighs the net restoring force of gravity and reverses it, leaving only surface tension to restore the waves. This substantially reduces the average speed c. These standing waves are the ones that interact with the droplet and determine its motion, so we will need a reduced value of c in the equations that follow. When higher order terms are included, surface tension is less effective in restoring larger waves, which are slowed a little more than small waves.

If the forcing acceleration is increased further, eventually it also overcomes the restoring force of surface tension. The average speed c approaches zero and the surface becomes unstable, which is experimentally undesirable. This instability is related to (but is not quite the same as) the Faraday instability as discussed in the advanced material below.

† *Track 2* *This material may be skipped on a first reading*

If the container is small, the waves from a droplet do not need to propagate very far before they reach the edge. There is a shallower region there (see figure 2.1) which is designed to damp the waves by inducing greater shear. In the absence of reflected waves, the instability must be local in origin. As the forcing acceleration is increased, eventually the net restoring force on the waves vanishes and the surface becomes unstable, as discussed above.

There is a related phenomenon, the Faraday instability, which is associated with reflected waves. In a large container, there are multiple layers of parametrically reflected waves, similar to figure 2.6, which build up because they are all coherent. Under these conditions, the surface may become unstable at a lower forcing acceleration than in a small container. The onset of instability is largely determined by the viscosity of the liquid [13].

In practice the container is of intermediate size and the damping at the edge is not perfect, and so both of these phenomena must be considered.

2.6 Quasiparticles or ‘ghost droplets’

Sometimes a droplet encounters an imperfection in the surface, such as a small air bubble, which causes it to merge with the liquid. In a high memory regime, the experimenters observed what they called a ‘ghost droplet,’ in which the oscillation continues for a significant time as if the droplet were still there (see figure 2.7). The motion continues as the energy cannot escape, being continually

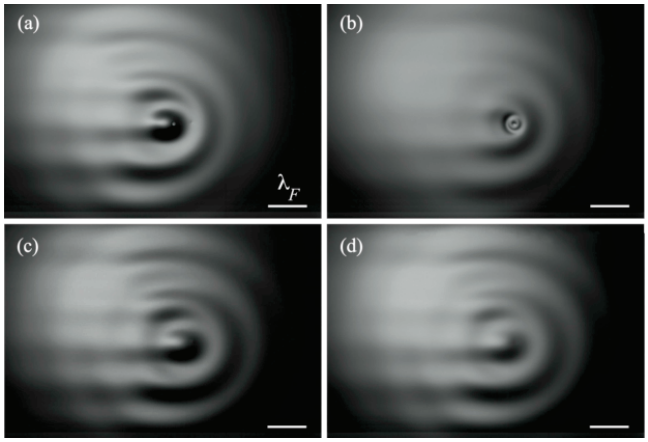

Figure 2.7: *Quasiparticle or 'ghost droplet'. A droplet (a) collides with a small floating bubble and coalesces (b). The continuing wave field is photographed 5 periods later (c) and 15 periods later (d). Courtesy Antonin Eddi, Eric Sultan, Julien Moukhtar, Emmanual Fort, Maurice Rossi and Yves Couder [14]*

reflected back to the centre by the parametric Bragg reflection shown in figure 2.6.

A ghost droplet behaves like a resonant association between a particle and a wave, even though there is no actual droplet there. It is a collective phenomenon of the fluid motion. We will call it a 'quasiparticle' after similar structures in condensed matter physics, such as holes in a semiconductor.

In the calculations that follow, we will find that quasiparticles are among the simplest and most tractable solutions. They occur in the high memory regime, where the effects of viscosity are nearly balanced by the driving acceleration and the wave equation can be used without viscosity. The Bragg reflection forms the boundary condition.

2.7 Summary

The famous experiments of Yves Couder, Suzie Protière, Emmanuel Fort and Arezki Badouad shows how a bouncing droplet can ride on a wave and the two can sustain each other in a mutual association. These 'Paris experiments' hold out the prospect of illuminating the underlying processes of quantum mechanics, which also manifest themselves as an association between a particle and a wave. This is one reason for the growing interest in the topic in laboratories around the world. The experiments have been extended by the original team and colleagues [10, 15, 16] and reproduced by others, including Jan Moláček and John Bush at MIT [12]. A portion of a television programme about it is available online on YouTube: see [17] or just search for 'Couder'. We'd strongly suggest you watch it!

Chapter 3

Walker

We accept the reality of the world with which we are presented

Christof in *The Truman Show*

The droplet photographed in figure 2.2 on page 28 advances to the right as it bounces. The researchers dubbed a moving droplet a "walker" and found they could control its speed by varying the amplitude of the vertical forcing acceleration, as shown in Figure 3.1.

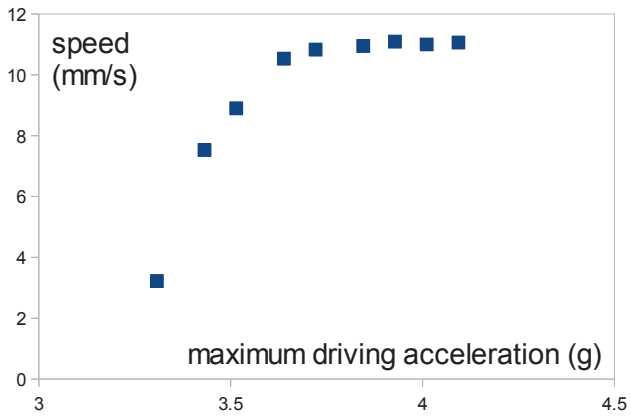

Figure 3.1: *The speed of a walker depends on the maximum vertical forcing acceleration, graphed as a multiple of the acceleration g due to gravity. (Data courtesy Antonin Eddi, published in [14])*

Figure 3.2 has three photographs of droplet moving at various speeds. At low speed, the droplet merely appears to be displaced slightly to the right of the associated wave field, but as the forcing amplitude and the droplet speed increase, the wave field supporting the droplet becomes more complex.

We will begin by deriving a simplified model of this motion using the symme-

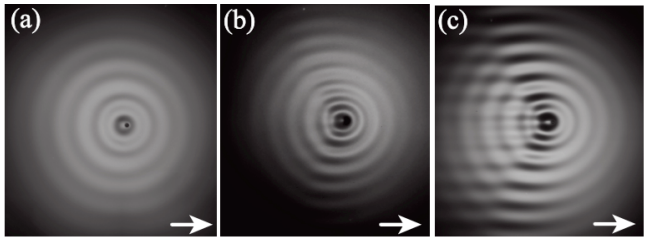

Figure 3.2: *A moving droplet. At low speed (left) it has been displaced from the centre; at higher speeds the wave field becomes more complex. (Courtesy Antonin Eddi, Eric Sultan, Julien Moukhtar, Emmanual Fort, Maurice Rossi and Yves Couder [14])*

tries of the wave equation, and testing its predictions against the experimental data.

3.1 The wave field near a walker

We saw in section 1.14 that if $f(x, y, t)$ is a solution to the wave equation, then there is always another solution, $f(x', y', t')$, which is moving relative to the fluid. The primed coordinates are given by an acoustic Lorentz transformation (1.16) which we repeat below

$$\begin{aligned} x' &= \gamma\,(x - vt) \\ y' &= y \\ t' &= \gamma\left(t - \frac{vx}{c^2}\right) \\ \gamma &= \frac{1}{\sqrt{1 - \frac{v^2}{c^2}}} \end{aligned}$$

Applying this to the wave field (2.2) near a stationary droplet gives a wave field that walks across the surface at speed v, namely

$$h = \cos(\omega_o t')\, J_0\left(\frac{\omega_o r'}{c}\right)$$

where $r'^2 = x'^2 + y'^2$. It is illustrated in Figure 3.3.

In the moving solution, all lengths in the direction of travel have contracted by the factor $1/\gamma$ (substitute $t = 0$ into the Lorentz transformation), while all time periods have dilated by the factor γ (substitute $x = vt$). This is mathematically the same as the Lorentz contraction and time dilation of special relativity, but with an acoustic value for the characteristic speed c.

This does not fully describe the wave field near a walker because its frequency of oscillation has been reduced by the Lorentz factor, and so it does not match the boundary conditions in this experiment, where the bouncing frequency is fixed. To obtain the full solution we must also use the scale symmetry of Euler's equation.

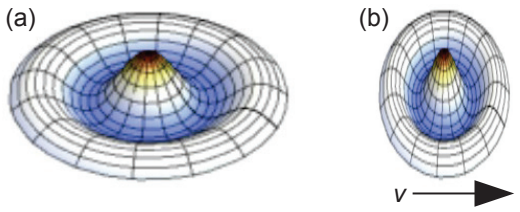

Figure 3.3: *(a) The wave field near a stationary droplet* $\cos(\omega_o t)J_0(\omega_o r/c)$ *(b) The Lorentz-boosted wave field* $\cos(\omega_o t')J_0(\omega_o r'/c)$ *moves at speed* v.

Given that $h(x', y', t')$ is a solution to the wave equation, then $h(\alpha x', \alpha y', \alpha t')$ is also a solution where α is a scale factor (see section 1.13 for the proof). The wave field near a walker is obtained by choosing $\alpha = \gamma$, giving

$$\begin{aligned} x'' &= \gamma^2(x - vt) \\ y'' &= \gamma\, y \\ t'' &= \gamma^2\left(t - \frac{vx}{c^2}\right) \end{aligned}$$

Applying this coordinate transformation to the stationary wave field in (2.2) gives

$$h = h_o \cos\left(\omega_o t - \frac{\gamma^2\omega_o v}{c^2}\Delta x\right) J_0\left(\frac{\omega_o}{c}r''\right) \tag{3.1}$$

where $\Delta x = x - vt$. This is a reasonable approximation for the wave field of a walker because it obeys the wave equation, it advances across the surface at speed v, and it oscillates at constant frequency, matching the boundary conditions imposed by the walking droplet.

3.2 The speed of a walker

We saw in section 2.4 that a stationary droplet lands in a depression due to previous bounces. In that stationary case, the wave field is given by (3.1) with $v = 0$, and for simplicity we will assume the droplet lands when $\omega_o t = \pi, 3\pi, 5\pi$ etc. Any variation from this landing time will merely change the origin of the analysis to follow.

As the forcing acceleration is increased, the droplet is thrown higher and lands later in the cycle (see figure 2.3). Suppose the delay in its landing time is T. Substituting into (3.1) with $y = 0$ gives

$$h = -h_o \cos\left(\omega_o T - \frac{\gamma^2\omega_o v}{c^2}\Delta x\right) J_o\left(\frac{\gamma^2\omega_o}{c}\Delta x\right)$$

and differentiating gives

$$\begin{aligned} \left.\frac{\partial h}{\partial x}\right|_{\Delta x=0} &= -h_o\,\frac{\gamma^2\,\omega_o}{c}\,\left(\frac{v}{c}\,\sin(\omega_o T)\right) \\ \left.\frac{\partial^2 h}{\partial x^2}\right|_{\Delta x=0} &= h_o\,\frac{\gamma^4\,\omega_o^2}{c^2}\,\left(\frac{v^2}{c^2}\cos(\omega_o T) + \frac{1}{2}\right) \end{aligned} \tag{3.2}$$

This shows that the surface has a negative slope in the x direction when the droplet lands, which can be thought of as the ultimate cause of the motion.

The droplet does not reach its terminal speed. It is always on a cushion of air, so the terminal speed is relatively high. Its speed is limited by the speed at which the entire wave field advances. In fact, the droplet and the wave field are constrained to advance together since they must always be in alignment.

The sloping surface displaces the droplet from the centre of the wave field, as seen in the photographs in figure 3.2. It will settle near $\partial h/\partial x = 0$. Defining $x_d = \Delta x$ at this point, we have $\partial h/\partial x|_{\Delta x=0} \approx -x_d\, \partial^2 h/\partial x^2$ and, from (3.2),

$$\gamma^2 \omega_o \left(\frac{v^2}{c^2} + \frac{1}{2} \right) x_d \quad = \quad vT$$

where we have approximated $\sin(\omega_o T) = \omega_o T$ and $\cos(\omega_o T) = 1$. Subsequent waves will always be generated at this displaced position, with the net result that the wave field moves at speed $v \propto x_d$ to first order, and

$$\gamma^2 \left(\frac{v^2}{c^2} + \frac{1}{2} \right) \quad \propto \quad T \tag{3.3}$$

3.3 Comparison with experiment

The test for such a simplified model can only come from the experimental data. Figure 3.4 plots the same data as figure 3.1 on new axes. We obtained the landing time T from the intersection between the trajectory of the droplet, for which $d^2h/dt^2 = -g$, and the vertical motion of the oil tray. Figure 2.3 shows this graphically in the case where the maximum forcing acceleration was 3.5g. We took the characteristic speed c of the standing waves near the droplet to be 11.95 mm/s, which is 8% larger than the maximum speed measured. The plot shows that the linear relationship we derive between T and $\gamma^2(v^2/c^2 + \frac{1}{2})$ is remarkably accurate out to an acoustic Lorentz factor of $\gamma = 2.6$.

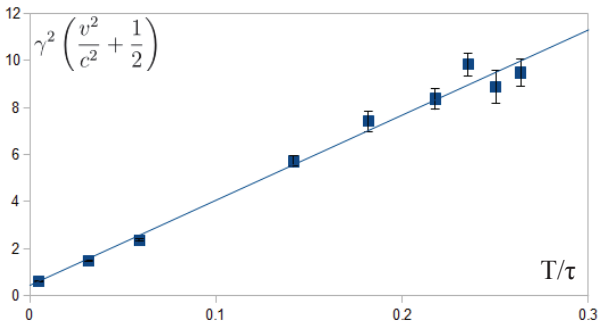

Figure 3.4: *The data in figure 3.1 plotted on new axes. T is the landing time and τ is the bouncing period. The straight line is a best fit to the experimental data. The final point has an acoustic Lorentz factor of $\gamma = 2.6$.*

There is further information in detailed velocimetry studies, reported by Eddi, Sultan, Moukhtar, Fort and Couder in [14]. Figure 3.5 is the wave field measured near a walker at high forcing amplitude. The echoes of successive bounces of the droplet can be seen in the peaks marked A, B and C. We can obtain an approximation to the wave field by treating these three peaks as the centres of three wave fields given by (3.1). The three waves reinforce nearly perpendicular to the direction of motion, as can be seen from the taller waves there. They interfere destructively at an angle behind them, producing the lines with nearly zero amplitude resembling a wake.

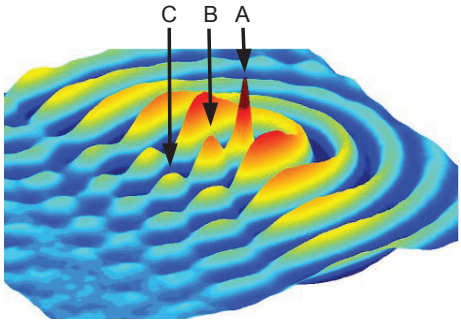

Figure 3.5: *The wave field near a walker at large forcing amplitude. Courtesy Antonin Eddi, Eric Sultan, Julien Moukhtar, Emmanual Fort, Maurice Rossi and Yves Couder [14]*

We saw in section 2.5 that taller waves have a reduced wave speed due to the parametric forcing. This reduced speed compresses the wave pattern perpendicular to the direction of motion. At the same time, the wave pattern is elongated parallel to the direction of travel because the source (A, B, C) is elongated. However, there is a counteracting effect. The Lorentz contraction in (3.1) compresses the wave field in the direction of motion. As we can see in figure 3.6, the resulting waves are roughly circular. See [14, 18] for further studies of the wave field.

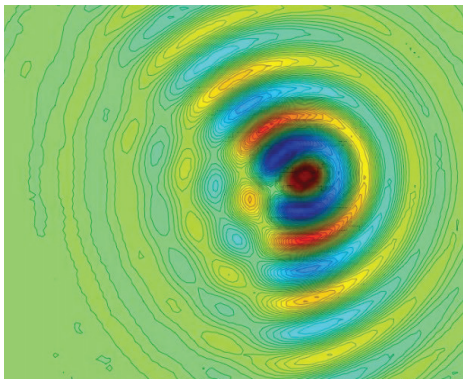

Figure 3.6: *Contours of the waves in figure 3.5.*

3.4 Summary

The wave equation for the waves on the surface of a liquid is Lorentz covariant with an acoustic value for the speed c, and experimental measurements confirm that the wave field of a walking droplet is Lorentz covariant to a good approximation, out to a Lorentz factor of $\gamma = 2.6$. In the experiments for which data are available, the bouncing frequency was constrained to be constant, which caused the wave field also to be reduced in size.

Chapter 4

Discovering absolute rest

I would suggest that almost the only hypothesis that can reconcile this opposition is that the length of material bodies changes, according as they are moving through the ether or across it.

George Francis Fitzgerald in 1889 [19]

Bouncing droplets can be assembled into crystal-like clusters as shown in figure 4.1. The droplets that bounce in-phase with one another are approximately an integral number of wavelengths apart, so each bounces in a depression due to the waves from its neighbours. It is possible to construct a wide range of different structures. For example, the droplets in the photograph have been arranged with some bouncing antiphase, namely those at the centre and at interstitial positions.

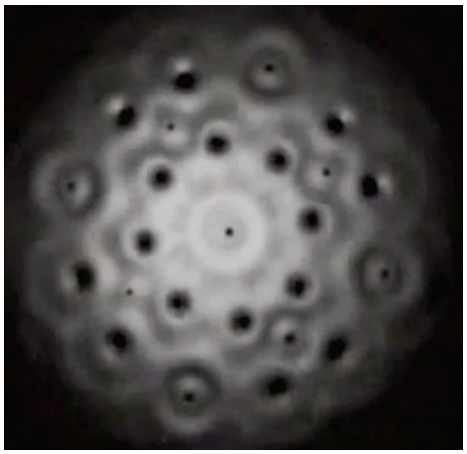

Figure 4.1: *Photograph of a crystal of bouncing droplets (Courtesy Yves Couder)*

In this chapter we will examine whether or not it is possible to construct an apparatus using bouncing droplets which is capable of discovering its own velocity relative to the oil.

4.1 Symmetry with respect to absolute rest

We saw in section 1.14 that oscillatory solutions to Euler's equation are Lorentz covariant with an acoustic value for the characteristic speed c. This symmetry is exact with low amplitude motion, where the equations of motion reduce to the wave equation which is symmetric under Lorentz transformation. It is also a very good approximation with larger amplitude motion (provided measurements are restricted to expectations values) because the perturbations due to Euler's equation average to zero over a cycle.

It follows that any structure fashioned out of bouncing droplets and propagating waves, such as the crystal in figure 4.1 or anything else we may care to make, must also be Lorentz covariant. In particular, it will suffer a Lorentz contraction in the direction of motion when it is moving relative to the oil

We now show that any such structure has the symmetry that it is incapable of discovering 'absolute rest', by which we mean measuring whether or not it is stationary relative to the oil, through any 'intrinsic measurement,' by which we mean any quantity that depends only on local interactions.

Let $h(x, y, t)$ be a solution to Euler's equation. An example is the wave field photographed in figure 4.1, or any other structure we may care to build from bouncing droplets and waves propagating on the surface of the oil. From the Lorentz covariance (section 1.14), every such system must have a twin, $h(x', y', t')$, which has received a velocity boost by an acoustic Lorentz transformation and which is also a solution of the wave equation. Some may prefer to add a scale enlargement, which does not affect the proof.

We will treat $h(x, y, t)$ as divided into two sub-systems, $S1$ and $S2$, and introduce an 'intrinsic measurement' which relies on one or more local interactions between $S1$ and $S2$. These interactions will be a result of the nonlinear terms, as discussed in section 1.11, and it must take place at a single position and time, $(x_1, y_1, t_1) = (x_2, y_2, t_2)$. By applying a Lorentz transformation, precisely the same interaction will occur in its moving twin at an equivalent position and time $(x'_1, y'_1, t'_1) = (x'_2, y'_2, t'_2)$. Therefore all local interactions, and hence all intrinsic measurements, will be the same in the two systems and it is not possible to discover absolute rest from them.

4.2 Attempt to discover absolute rest

To illustrate this symmetry, consider how we might try to discover absolute rest using an apparatus fashioned out of bouncing droplets. The apparatus consists of the crystal photographed in figure 4.1. We will suddenly disturb the central droplet. It might be magnetised and a magnet moved near it, or, more crudely, a small puff of air might be used. A disturbance in the wave field will propagate outwards in all directions at speed c relative to the oil, until it is reflected from the edge of the crystal.

If the crystal is at rest relative to the oil then it is easy to see that the wavelets will return to the central position at the same time and with the same phase, from the symmetry of the crystal. This phase alignment constitutes our

measurement.

Now suppose that the crystal is, in fact, moving relative to the oil. This might be achieved experimentally using a flow of oil. If we had expected to discover this motion by measuring a change in the interference between the returning waves, we would observe a null result, from the symmetry we proved above.

Another way to calculate the same result is to assume (counterfactually) that the dimensions of the crystal do not depend on its velocity through the medium. Since the disturbance moves at speed c relative to the oil, not relative to the crystal, we would expect the waves returning from different directions to have different phases when they recombine. However, the crystal suffers a Lorentz contraction in the direction of motion relative to the perpendicular direction, which exactly corrects for this and produces the null result. You are invited to prove this in the next exercise.

Exercise 4.1 This exercise is about the time for waves, which propagate at constant speed c relative to the oil, to go from the centre of the crystal photographed in figure 4.1 to the edge and back again.

If the radius of the crystal is r_o and it is stationary with respect to the oil, show that the time for the waves to return to the centre is

$$t_o \quad = \quad \frac{2\,r_o}{c}$$

The crystal is now made to advance at constant speed v relative to the oil, where $|v| < c$, and the experiment is repeated. Neglecting any scale enlargement, show that the perpendicular waves (i.e. those whose component of velocity in the direction of motion is v) travel a total distance

$$r_\perp \quad = \quad 2\sqrt{r_o^2 + v^2 t_1^2}$$

where t_1 is the time for them to propagate to the edge of the moving crystal. By equating this expression to $2ct_1$, show that they return after time

$$t_\perp \quad = \quad \gamma\, t_o$$

where $\gamma = (1 - v^2/c^2)^{-\frac{1}{2}}$. Suggest a simpler way to derive this result using the Lorentz symmetry of the wave equation.

Alice does not know that the crystal suffers a Lorentz contraction in its direction of motion. Show that she would expect a wave travelling in the same direction as the crystal to go from the centre to the edge in time $r_o/(c - v)$. By adding the time for the return path, show that she will expect the reflected wave to return after time

$$t_{||} \quad = \quad \gamma^2\, t_o \qquad\qquad (wrong)$$

Why might Alice expect to discover the velocity of the crystal relative to the oil by measuring the interference between the returning waves?

Alice did not take account of the crystal's Lorentz contraction in the direction of motion. Correct her mistake and show that her experiment will yield a null result.

What effect, if any, does a scale enlargement have on your conclusions?

There are a number of practical difficulties to overcome in realising this experiment. The crystal may tend to rotate rather than move with a linear velocity; and a large surface is required to accommodate the motion, which poses practical difficulties in keeping the excitation constant over a large area. The null result will be perturbed by viscosity, which is not Lorentz covariant. Whilst this is mitigated by the parametric forcing, it is at the cost of different wave components having different characteristic speed c (section 2.5). If these difficulties prove significant they might be corrected for mathematically or the experiment might be conducted in computer simulation.

4.3 Resonances in a lossless fluid

We saw in section 1.9 that the air obeys the wave equation to first order. One solution to this equation is

$$\frac{\rho}{\rho_o} \;=\; 1 \;+\; A\,\cos(\omega_o t)\,j_0\left(\frac{\omega_o r}{c}\right) \tag{4.1}$$

where ρ is the density of the air, ρ_o its mean density, j_0 is a spherical Bessel function of the first kind, and $A < 1$. This solution is similar to the wave field of a bouncing droplet, but in three dimensions. Compare it with equation (2.2), which has a circular Bessel function in place of a spherical one.

These resonances are likely to decay away quickly due to viscosity. There are two possible solutions to this experimental difficulty. Firstly, a mechanism might be used to pump energy back into them. In chapter 7 we will see experiments like this which were conducted in the 19th century. Secondly, of interest here, we could use a compressible fluid that does not have any viscosity at all.

When it is cooled below 2.172 Kelvin at atmospheric pressure, liquid ^{4}helium becomes a superfluid, which behaves in many respects like a compressible fluid, such as the air, with zero viscosity. The speed of ordinary sound waves (called 'first sound') is approximately 230 m s^{-1}. Acoustic solutions such as (4.1) will be excited by thermal motion.

In chapter 11 we will examine these solutions and their boundary conditions in more detail. It turns out that there are multiple families of resonances, with various conservation rules, which we will compare with the so-called rotons which are observed in superfluids. When excited by thermal motion, we will see that these resonances make a significant contribution to the specific heat and the thermal conductivity of the superfluid, which are known otherwise to be abnormally large.

We saw (section 1.14) that periodic solutions to Euler's equation are Lorentz covariant with respect to expectation values. If they can be clustered into groups, like droplet crystals, then the clusters will be Lorentz covariant as well.

It follows that any hypothetical experimental apparatus fashioned out of them will suffer a Lorentz contraction in the direction of motion and will be difficult or impossible for it to detect its own velocity relative to the medium through any expectation value.

4.4 d'Alembert's paradox

The foregoing symmetry aplies when the relevant motion has low amplitude so it obeys the wave equation, or, if it has larger amplitude, the frequency of oscillation is too high for the measuring apparatus to detect, so it is limited to measuring expectation values. It means it will be difficult or impossible for any apparatus fashioned out of resonances or other pulsations in an inviscid barotropic fluid to discover its own velocity relative to the fluid through any expectation value.

There is an alternative way to demonstrate this, using a result in fluid mechanics which was proved in 1752 by Jean le Rond d'Alembert, a French mathematician. He showed that a solid object moving at constant velocity through an incompressible fluid of infinite extent without viscosity experiences no drag. His proof was called **d'Alembert's paradox** because it seemed to fly in the face of common experience. Everyday fluids have at least some viscosity, so moving objects experience drag that increases with velocity and quickly becomes evident unless the speed is very small. But d'Alembert's demonstration only applies if there is no viscosity.

A simple demonstration of d'Alembert's paradox follows from the conservation of energy. The kinetic energy in the pattern of fluid flow is $\int \frac{1}{2}\rho u^2 dx^3$ where ρ is the density of the fluid and u the flow speed. There is only one irrotational flow pattern near a solid object of a given shape (d'Alembert did not consider turbulent motion, which does not arise without viscosity), and so the kinetic energy must be constant and there can be no drag [1]. In particular, it is not possible to detect the velocity of the fluid through drag forces.

It is straightforward to extend this demonstration to oscillatory systems such as bouncing droplets and resonances in a superfluid. When measured at a fixed point in the cycle, such as when the droplet is at its maximum height or the resonance is at its greatest extent, the wave pattern is the same except in so far as it has translated with the droplet. It follows that the energy is constant and there can be no net drag when considered over a full cycle.

4.5 Summary

We have seen that bouncing droplets cluster into crystals which are Lorentz covariant to a good approximation, with an acoustic value for the characteristic speed c. If perturbations such as viscosity can be neglected, we saw that it is diffucult or impossible for such a structure to discover its own velocity relative to the fluid using local expectation values.

More generally, we saw that resonances in a lossless fluid such as superfluid

^{4}helium possess the same symmetry provided that only 'expectation values' (those taken over a complete cycle) are measured.

4.6 Dialogue

Three friends meet on a regular basis to discuss the experiments in this monograph. Alice describes the conventional models of physics; Bob applies Alice's models to bouncing droplets and superfluids; and Carol advances an alternative interpretation.

On the first day of their dialogue, the friends are discussing the observation that material bodies change their dimensions as they move.

(a) Alice says that material bodies change their dimensions as their speed is varied relative to an observer. She concludes that the fabric of space and time has been compressed.

(b) Bob says that crystals of bouncing droplets change their dimensions as their speed is varied relative to the fluid. He concludes that the fabric of space and time has been compressed.

(c) Carol says both bodies are resonances obeying the wave equation in a fluid, and so their dimensions must change by the amount that is observed. The fabric of space and time is not compressed since this would cause additional distortion, contrary to observation.

Each of these approaches can be made consistent with all the relevant experiments. Argue in favour of each one in turn.

Chapter 5

Inverse square force

Outside of physics we know nothing of action at a distance

Albert Einstein [20]

When a walker approaches the edge of the container, it does not actually touch the edge but is deflected away. The stroboscopic photograph in figure 5.1 shows a droplet travelling three times round a rectangular dish. In this experiment, the walls of the dish were vertical, without the region of reduced depth near the edge in other experiments. This photograph yield data which gives a deep insight into one of the hydrodynamic forces between bouncing droplets.

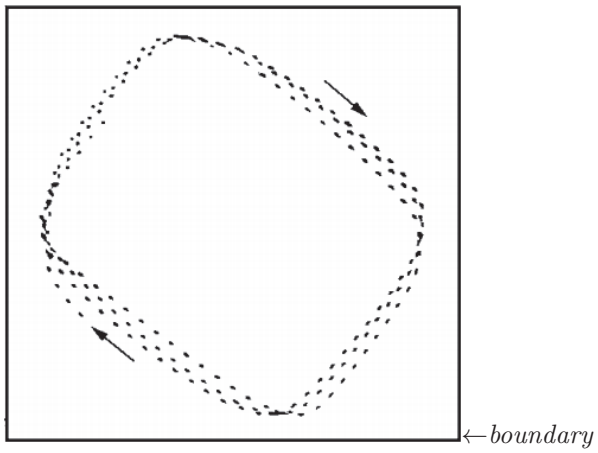

Figure 5.1: *Stroboscopic photograph of a droplet's path (dots) deflected near the walls of the container (solid). (Courtesy Suzie Protière, Arezki Badaoud and Yves Couder) [11]*

5.1 Velocity normal to the boundary

The velocity normal to the boundary, $V_\perp$, can be measured from the photograph in figure 5.1, using the fact that an equal time passes between each stroboscopic image. Figure 5.2 plots $V_\perp^2$ as a function of the inverse distance $\frac{1}{r}$ from the boundary.

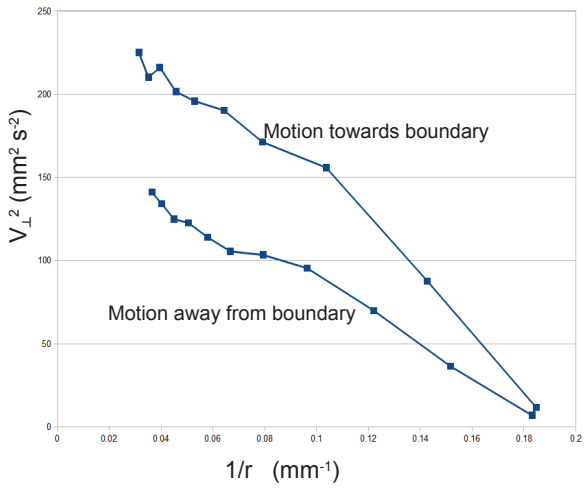

Figure 5.2: *The square of the velocity normal to the boundary, $V_\perp^2$, as a function of inverse distance from the boundary. The data are extracted from the stroboscopic images near the bottom of figure 5.1.*

Exercise 5.1 Figure 5.2 was obtained by measuring the stroboscopic images near the bottom of figure 5.1. The apparatus is 10cm across and the walker velocity is 18mm/s. By measuring a blow-up of a different part of the same figure, produce your own graph of the square of the normal component of velocity against inverse radius.

For each branch in figure 5.2, the data near the boundary (towards the right of the graph) fall very nearly on a straight line, before deviating at greater distances. This straight line can be written

$$V_\perp^2 \;=\; V_o^2 \;-\; \frac{B}{r} \tag{5.1}$$

where the slope of the graph is $-B$ and it depends on the branch.

Extrapolating to $1/r = 0$ from the collinear points to the right of the upper branch, $V_o \approx$ 18mm/s, which is the same as the speed of the droplet to the accuracy of measurement. The lower branch has $V_o \approx 14$mm/s. We will examine this reduced value later in this chapter, along with the reason for the deviation from the straight line when the droplet is further from the boundary.

These experimental results show there is an inverse square force of repulsion when the droplet is near the boundary. This can be seen by multiplying equation (5.1) by $\frac{1}{2}m$ where m is a constant mass. The left hand side is the kinetic energy and the right hand side the change in potential energy under an inverse square force.

Exercise 5.2 Obtain equation (5.1) directly by integrating Newton's second law of motion $F = ma$ with an inverse square force.

Hint $a = \frac{dV}{dt} = \frac{dV}{dr}\frac{dr}{dt} = V\frac{dV}{dr} = \frac{1}{2}d(V^2)/dr.$

5.2 Inverse square force in bubble experiments

Figure 5.3: *Degassing oil by applying ultrasonic vibration. The process takes about 5 seconds. (courtesy Hielscher Ultrasonics GmbH)*

The phenomenon responsible for the repulsion from the boundary is called the secondary Bjerknes force. It is used to remove unwanted bubbles of gas from oils and other liquids using ultrasonic vibration, as in figure 5.3. Ultrasonic pressure waves cause nearby bubbles to expand and contract in phase with one another, inducing oscillatory radial flows in the liquid. Near the mirror plane equidistant from the two, the flows reinforce as illustrated in figure 5.4. The increased velocity results in a reduced Bernoulli pressure on the mirror plane, and a force of attraction between the bubbles which merge and rise to the surface.

You can experience the same attractive force by putting your hand in a high-speed hand-dryer such as in figure 5.5. The air flow near your hand is similar to one half of figure 5.4, with your hand in place of the mirror plane. As long as you do not physically block the flow, you will feel your hand attracted towards the nearest nozzle due to the reduced Bernoulli pressure.

The exact same mechanism causes a bouncing droplet to avoid the boundary of the dish. The boundary has the same effect as an imaginary image droplet on the other side, at the same distance, and bouncing antiphase. Each droplet drives radial three dimensional flows in the liquid, which are similar to those near the bubbles in the degasser – except that the bouncing droplets are antiphase, so the force is one of repulsion rather than attraction.

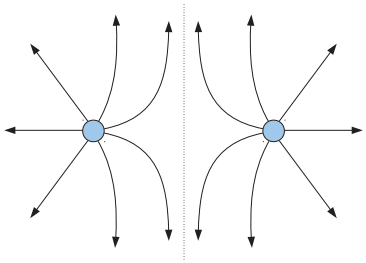

Figure 5.4: *Schematic of the flow from two sources. The flows reinforce near the mirror plane, resulting in a reduced Bernoulli pressure which causes the sources to be attracted to one another.*

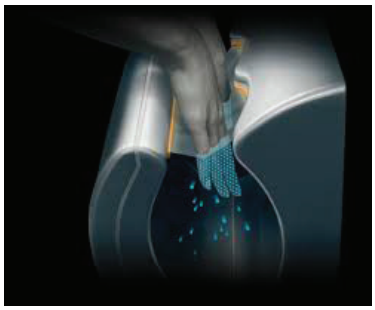

Figure 5.5: *A high-speed hand-dryer (copyright image reproduced by kind permission of Dyson Research Limited)*

5.3 Magnitude of the force

In figure 5.6, a vacuum cleaner nozzle ingests volume Q_1 of air per unit time. If the exhaust is at a large distance and the flow is spherically symmetric, the air speed at radius r will be $U = Q_1/(4\pi r^2)$. A second nozzle at this radius, with volume Q_2 per unit time, will ingest momentum along with the moving air particles

$$\frac{dp}{dt} \quad = \quad \rho_o U Q_2 \quad = \quad -\rho_o \frac{Q_1 Q_2}{4\pi r^2} \tag{5.2}$$

and so it will experience an inverse square force of attraction towards the other nozzle.

The direction of flow, and hence of the force, will be reversed if one of them is set to blow; then the force will be reversed for both hoses, by conservation of momentum (we assume the flow remains spherically symmetric, which might be achieved using a baffle on the end of the hose). More generally, oscillatory motion results in an attractive force if it is in-phase, and a repulsion if it is antiphase. The magnitude of the force is given by (5.2) averaged over a cycle.

In the droplet experiments, the force in (5.2) must be doubled due to the hemispherical geometry but halved to average over a cycle, leaving its magnitude unchanged.

Suppose a droplet of volume V bounces at frequency f. It will induce a

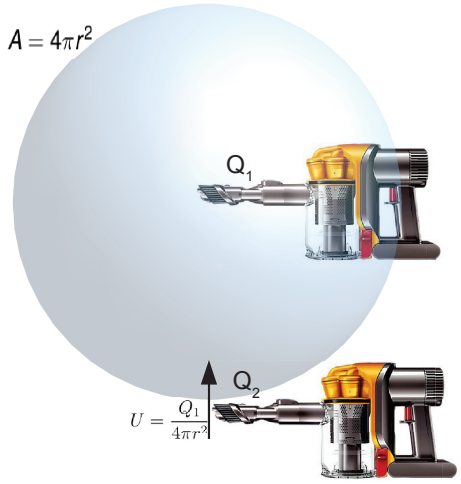

Figure 5.6: *The flow near two vacuum cleaner nozzles. (copyright images of Dyson machines reproduced by kind permission of Dyson Research Limited)*

flow fV directly, which will be enhanced by secondary flows due to entrained fluid and the resonance, giving $Q = \beta fV$ where β is a factor into which we will also incorporate the effects of higher harmonics. Substituting into (5.2) and remembering to invert the sign, the acceleration of a droplet is

$$a \;=\; -\frac{F}{\rho_o V} \;=\; \frac{V\beta^2 f^2}{4\pi r^2}$$

Using $f = 25$Hz and a droplet radius of 0.35mm (a typical value; the size was not reported in this run), the acceleration measured in the upper branch of figure 5.2 gives an apparently reasonable $\beta \approx 5$.

5.4 The force expressed in conventional form

An inverse square force can always be written in the form

$$F \;=\; \alpha\,\frac{\hbar c}{r^2} \tag{5.3}$$

where α is a dimensionless constant and $\hbar$ is a constant with the dimensions of energy $\times$ time.

Suppose the radius of a bubble is given by

$$r_b \;=\; r_o(1 + A\sin\omega t)$$

We will simplify the calculation by assuming that A is small. The flow speed at the surface is

$$v_s \;=\; \frac{dr_b}{dt} \;=\; A\; r_o\omega\cos(\omega t)$$

Multiplying by the area, the flow is $Q = 4\pi r_o^2 v_s$. Substituting into (5.2) gives

$$\begin{aligned} F &= 4\pi\rho_o r_o^3 . r_o^3 A^2\omega^2 \cos^2(\omega t)\frac{1}{r^2} \\ &= 3m_d . r_o^3 A^2\omega^2 \frac{1}{2r^2} \end{aligned}$$

where m_d is the displaced mass of the bubble and we have replaced $\cos^2(\omega t)$ by its average value, $\frac{1}{2}$.

This can be rearranged into the conventional form (5.3) using the fact that the inertial mass of the bubble, due to the motion of the displaced fluid around it, is approximately $m = \frac{1}{2}m_d$ [1]. Thus

$$\begin{aligned} \alpha &= 3A^2 \left(\frac{r_o\omega}{c}\right)^3 \\ \hbar &= \frac{mc^2}{\omega} \end{aligned} \tag{5.4}$$

The dimensionless constant α depends on whether the bubbles are resonant or not. Consider the resonant case. Neglecting geometric factors (which are of order 1), the bubble radius will vary from a small value to $2r_o$, giving $A \approx 1$. The maximum surface speed $r_o\omega$ will also increase, but it cannot much exceed the speed of sound in the fluid since the pressure would reduce to zero due to the Bernoulli effect. Therefore, if the bubbles are resonant then both A and the ratio $r_o\omega_o/c$ will be of order 1, and so α is also of order 1.

5.5 Constant of the motion

To the extent that viscosity can be neglected, so the Lorentz symmetry is not perturbed, $\hbar$ in (5.4) is a constant of the motion. This follows from its dimensions, energy × time, which are Lorentz invariant as illustrated in the next exercise.

Exercise 5.3 A body of mass m has energy mc^2 when stationary, and kinetic energy $\frac{1}{2}mv^2$ when at speed $v \ll c$. Show that its total energy is

$$E \approx mc^2\left(1 + \frac{v^2}{2c^2}\right)$$

An oscillator of period T_o is set in motion at speed $v \ll c$. By applying the Lorentz transformation (1.16) with $x = 0$ show that its period, when measured at a fixed position, is

$$T = \frac{T_o}{\gamma} \approx \frac{T_o}{1 + \frac{v^2}{2c^2}}$$

By considering a series of infinitesimal velocity boosts, show that $E \times T$ is a constant of the motion at all speeds.

Another way to see that $\bar{b}$ is a constant of the motion is to consider the wave field of an acoustic resonance which remains stationary in a moving fluid. The inertial mass m of the resonance is proportional to its volume, so the Lorentz contraction multiplies it by $1/\gamma$, whilst its angular frequency ω is multiplied by the same factor, so $\bar{b} \propto m/\omega$ is independent of velocity.

Experimentally, the fit with the inverse square force in (5.3) confirms that $\bar{b}$ is constant, and in particular it does not depend on position, direction, or the perpendicular component of velocity. However the speed $|v| = (v_{\perp}^2 + v_{||}^2)^{\frac{1}{2}}$ of the droplet was kept constant by the experimental conditions and so it is not possible to verify from the data that $\bar{b}$ is independent of speed. One way to test for this might be to vary the forcing amplitude and frequency, but this would introduce experimental difficulties since the variation is known to affect the proximity to the Faraday instability, particularly near a boundary. A better test might be to make the droplet out of a ferrofluid and de-weight it magnetically so it lands later in the cycle and travels faster. The factor $(1 - v^2/c^2)^{\frac{1}{2}}$ from the scale enlargement in (3.1) could be corrected for as in chapter 3. In such a test, of course, the mass of the droplet itself must be treated separately from the inertial mass of the wave field.

5.6 Comparing the force between electrons

In (5.4), the constant of motion $\bar{b}$ is defined in exactly the same way as Planck's reduced constant

$$\hbar = \frac{mc^2}{\omega}$$

where m is the mass of an electron and ω its angular frequency. The expressions differ, of course, in that the speed c has an acoustic value in the droplet experiments.

Further, equations (5.3) and (5.4) for the force between droplets are also in exactly the same form as those for the electrostatic force between electrons, which is given by

$$F = \alpha \frac{\hbar c}{r^2}$$
$$\alpha \approx \frac{1}{137.036}$$

The dimensionless quantity α is called the 'fine structure constant' and it is used to gauge the strength of the electromagnetic interaction.

In addition to having an acoustic value for the speed c, the force between droplets differs from the force between electrons in two respects. Firstly, they appear to have opposite signs, since like droplets (those that bounce in phase with one another) attract and unlike ones (which bounce antiphase) repel, whereas like electrical charges repel and unlike one attract. Secondly, the mechanical force between droplets is about two orders of magnitude stronger than the force between electrons on a comparable basis, since the fine structure constant for the force between droplets is $\alpha \sim 1$.

This suggests a limitation of these simple bouncing droplets as an analogy with quantum mechanics, namely that spherically-symmetric solutions are not a good model for the electron. In chapter 10 we will see that pairs of droplets can orbit around one another. There is an inverse square force between them which has the opposite sign and a reduced fine structure constant.

5.7 The effect of fluid depth

The above analysis assumed the droplet is closer to the boundary than the depth of hte oil. When the droplet's distance from the boundary exceeds the depth, the flows can no longer remain three-dimensional because they are restricted by the bottom of the oil tray, and they become more two-dimensional. This reduces the force of repulsion, as shown in the next exercise.

Exercise 5.4 The force was calculated in section 5.3 for three dimensional motion.

By a similar analysis where the flow is confined to a two-dimensional region, show that the flow speed is $U = \frac{Q_2}{2\pi r}$. Hence or otherwise show that the force is proportional to $1/r$ and the potential energy of the interaction is proportional to $\log r$.

By comparing the slopes of the graphs of $1/r$ and $\log r$, show that the force is reduced in the latter case.

The depth of the liquid in this experiment was not reported, but it was typically 5mm in similar experiments. In figure 5.2, we see that the deviations from the straight line begin after about 10mm, as we might expect.

5.8 Maxwell's equations

When the droplets or bubbles are stationary, we saw that there is an inverse square force between them. This obeys the same equations as the electrostatic field near a charged particle, since both are inverse square.

These equations can be extended to the case of moving droplets by noting that the solutions are acoustically Lorentz covariant to a reasonable approximation. So we need equations that are Lorentz covariant and that reduce to the equations of electrostatics when stationary.

These conditions are met by Maxwell's equations with an acoustic value of c. In fact, they are unique in that Maxwell's equations (more strictly, equations that are equivalent to them when they are averaged over a cycle) are the only ones that satisfy them. Suppose the contrary, that there existed a different set of Lorentz covariant equations that produce the same electric field with the same boundary conditions. The only difference between the two solutions can be in the magnetic field. But a Lorentz transformation turns a pure magnetic field into one with an electrical component, and so the electrical fields differ in the new reference frame. This is a contradiction.

† *Track 2* *This material may be skipped on a first reading*

Here we assume familiarity with the electromagnetic four-potential representation of Maxwell's equations, which we review very briefly before considering how to apply it to the force between the droplets.

Maxwell's equations can be written as

$$\left(\frac{1}{c^2}\frac{\partial^2}{\partial t^2} - \nabla^2\right) A^\alpha \;=\; \mu_o J^\alpha \tag{5.5}$$

The electromagnetic four-potential $A^\alpha = (\phi/c, \mathbf{A})$ comprises the electrostatic potential ϕ and the magnetic vector potential $\mathbf{A}$, and the four-current $J^\alpha = (c\rho, \mathbf{J})$ contains the charge density ρ and the current density $\mathbf{J}$.

In a static situation, the time dependence and the current $\mathbf{J}$ both vanish, so Maxwell's equations reduce to

$$-\nabla^2\phi \;=\; \frac{\rho}{\epsilon_o} \tag{5.6}$$

where $\mu_o\epsilon_o c^2 = 1$. In the case of a single charge Q the solution to this equation is

$$\phi \;=\; -\frac{Q}{4\pi\epsilon_o r}$$

and a particle of charge q experiences an inverse square force,

$$F \;=\; q\nabla\phi \;=\; \frac{Qq}{4\pi\epsilon_o r^2}$$

The interaction between droplets maps on to this formalism because it is also a Lorentz covariant inverse square force. Consequently, the interaction between stationary droplets can be described using the same equations as those of electrostatics, with an appropriate choice of constants.

Note that (5.6) has omitted any time dependence, so it is not valid when the droplets are in motion. To reinstate the time dependence, the term on the left hand side must be extended to a Lorentz covariant form,

$$\left(\frac{1}{c^2}\frac{\partial^2}{\partial t^2} - \nabla^2\right) \phi \;=\; \frac{\rho}{\epsilon_o}$$

Further, a moving droplet forms a current which obeys the continuity equation

$$\frac{\partial\rho}{\partial t} \;+\; \nabla.\mathbf{J} \;=\; 0$$

This is only possible if the current $\mathbf{J}$ also obeys the same equation. Therefore the interaction between the droplets obeys Maxwell's equations (5.5).

5.9 Magnetic component of the force

We now turn to the lower branch of figure 5.2.

A walker's speed is fixed by the driving amplitude as discussed above. As the walker's velocity normal to the boundary slows down and reverses in the experiment, it must accelerate parallel to the wall to maintain constant speed. This velocity boost is observed in the experiment. The researchers estimated the angle of incidence (relative to the normal to the boundary) at about 38°, and of reflection at about 53°.

In addition to the force of repulsion between the droplets, which obeys the same equations as those of electrostatics, there is a force of attraction when they are moving at a common velocity v parallel to the boundary. This obeys the equations of magnetism. It is like the magnetic force of attraction between two electrons moving at a common velocity parallel to one another. The magnetic force reduces the total force by a factor $1 - v^2/c^2$, as shown in the next exercise.

Exercise 5.5 A long straight wire carries electrical charge ρ per unit length. Show that the electric field at radius r from it has magnitude

$$E = \frac{\rho}{2\pi\epsilon_o r}$$

The wire is set moving at velocity v parallel to its length. Show that the moving charges constitute a current $I = \rho v$ which generates a magnetic field of magnitude

$$B = \frac{\mu_o \rho v}{2\pi r}$$

A second wire, identical to the first, is placed parallel to it and moves at the same velocity. Write down expressions for the electrostatic force F_e and the magnetic force F_m that it experiences per unit length.

By using the identity $\mu_o \epsilon_o c^2 = 1$, show that their ratio is

$$\frac{F_m}{F_e} = -\frac{v^2}{c^2} \tag{5.7}$$

and therefore the total force has been reduced by a factor $1 - v^2/c^2$.

(*Harder*) By using Maxwell's equations in the four-potential representation (5.5), write down an expression for the ratio of the electrostatic potential to the magnetic vector potential due to a charge that is moving at velocity v. Hence or otherwise show that the ratio of forces in the above experiment is given by (5.7), irrespective of the shape of the wires.

This reduced force accounts for the reduced slope of the lower graph in figure 5.2. We will take the approximation that the upper branch in figure 5.2 has no velocity perpendicular to the direction of travel, but by the time the droplet has reached the lower branch it has been accelerated to the full perpendicular speed, $v = 18$ mm s^{-1} by the tangential force. The force is proportional to the slope of the graph, whose ratio is 14/18. Equating these two gives $v = 0.47c$,

which suggests the droplets were moving at about half the relevant wave speed near the droplets.

5.10 Propagating waves

Since the force between bouncing droplets obeys Maxwell's equations with an acoustic value of c, and Maxwell's equations tell us that propagating waves will be emitted when a source is accelerated, it follows that a droplet will send out propagating waves into the medium if it is disturbed. These waves are modulations of the standing waves surrounding the source. We discussed similar waves in the droplet crystal experiment (section 4.2) but we are not aware of attempts to test for them experimentally to date.

To the extent that nonlinearities such as the parametric forcing can be neglected, these wave will have momentum

$$p = \frac{E}{c}$$

where E is the energy they transport. The proof follows by treating the wave as a sum of propagating Fourier components. Each component has momentum $p = E/c$ where E is the energy transported by the component (section 1.15). The energy and momentum must both be counted as positive or negative according to the direction of travel, and so it follows that the sum of these components must have the same energy-momentum relationship. For example, suppose two components propagate in opposite directions with energies E_1 and E_2. The total energy transported is $E = E_1 - E_2$ and the total momentum is $p = p_1 - p_2 = (E_1 - E_2)/c = E/c$.

These waves are analogous to light waves in that they obey Maxwell's equations and have the same energy-momentum relationship.

5.11 Summary

We have seen that droplets experience an inverse square force of attraction or repulsion whose sign depends on their relative phases. The force obeys Maxwell's equations with an acoustic value for the speed c. An analogue of the magnetic force was observed in the experiment.

The fine structure constant of the interaction is order 1, which is two orders of magnitude larger than that of the electromagnetic interaction, and it is associated with a constant of motion, $\hbar$, which is defined in the same way as Planck's constant, again with an acoustic value for the speed c.

When a droplet is suddenly disturbed we predict it will emit propagating waves which obey Maxwell's equations and have the same energy-momentum relationship as light waves. However, we are not aware of attempts to measure them experimentally.

5.12 Dialogue

On day 2 of their dialogue, Alice, Bob and Carol are discussing the concept of action-at-a distance.

(a) Alice says there is an inverse square force between electrons, even when they do not touch. This action at a distance shows the failure of mechanistic theories which seek to reduce all interactions to local collisions.

(b) Bob says there is an inverse square force between bouncing droplets, even when they do not touch. This action at a distance shows the failure of mechanistic theories which seek to reduce all interactions to local collisions.

(c) Carol says the forces are all transmitted by local collisions in a fluid.

Each of these approaches can be made consistent with all the relevant experiments. Argue in favour of each one in turn.

Chapter 6

Diffraction

Entia non praeter necessitatem multiplicandur.

William of Ockham

We saw that a droplet is repelled from a barrier. When the barrier has one or more slits in it, some droplets pass through as we can see in figure 6.1.

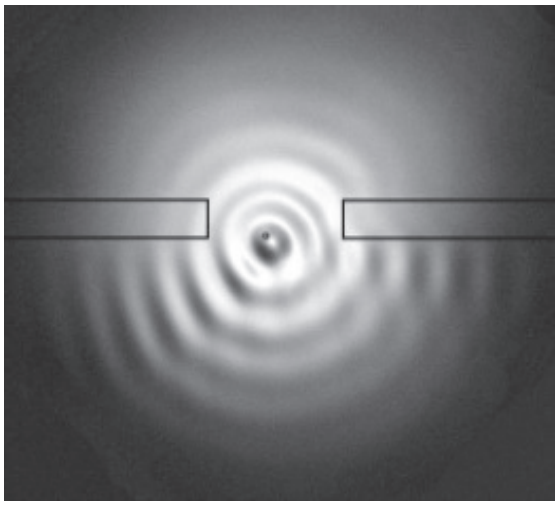

Figure 6.1: *A droplet passing through an aperture in a submerged barrier.*

When the Paris team measured which direction they went, they found almost the same diffraction patterns as you see for light waves, water waves or quantum mechanical particles, as in figure 6.2. Diffraction is only observed in the high memory regime. In the low memory regime the waves from a droplet have little effect because they propagate away and are lost to viscosity.

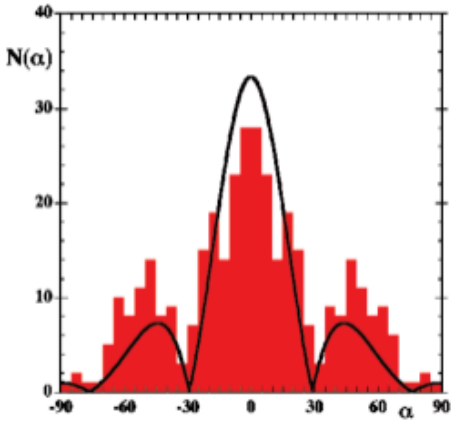

Figure 6.2: *Histogram showing the number N of droplets (out of 125) that emerge at angle α to the normal at large distance. The solid line is a single-slit diffraction pattern. Courtesy Yves Couder and Emmanuel Fort [15].*

6.1 Wavelength

We saw (equation 2.2) that the surface height h near a stationary droplet has two component factors which we will now write ψ and χ where

$$\begin{aligned} h &= \psi\,\chi \\ \psi &= \cos(-\omega_o t) \\ \chi &= -h_o\,J_0(k_r r) \end{aligned} \tag{6.1}$$

The forcing frequency and amplitude, and hence the walker velocity $|v|$, were kept constant in these diffraction experiments. The variation was in v_x and v_y, and so the wave field of the moving droplet can be obtained by an acoustic Lorentz transformation (1.16) in the x direction, L_x, followed by a transformation in the y direction L_y, so that $L = L_y L_x$. The scale enlargement in (3.1) can be treated as a constant and neglected since $|v|$ is constant.

We are interested in the wave field of a droplet that passes through the aperture in the x direction, perpendicular to the barrier. The component of velocity in the y direction has a mean of zero, but it perturbs the following analysis, as we will shortly see. Applying L_x to (6.1) gives

$$\begin{aligned} \psi &= \cos(-\omega_o t') \\ \chi &= -h_o\,J_0(k_r r') \end{aligned}$$

In this moving solution, the wave field χ advances with the droplet at speed v_x, and ψ has become a planar wave

$$\psi = \cos(kx - \omega t) \tag{6.2}$$

where the values of k and ω can be obtained by defining $S = -\omega_o t'$ and noting, from (1.16),

$$\begin{aligned} k &= \frac{\partial S}{\partial x} = \frac{\partial S}{\partial t'}\frac{\partial t'}{\partial x} = \frac{\gamma\omega_o}{c^2}\, v_x \\ \omega &= -\frac{\partial S}{\partial t} = -\frac{\partial S}{\partial t'}\frac{\partial t'}{\partial t} = \gamma\omega_o \end{aligned} \tag{6.3}$$

The wavelength of ψ is $\lambda = 2\pi/k$, or

$$\lambda = \frac{2\pi c^2}{\omega v_x} = \frac{b}{p} \tag{6.4}$$

where $p = mv_x$ is the momentum of the wave and $b = 2\pi\hbar$ where $\hbar = mc^2/\omega$.

We have already encountered $\hbar$ with the inverse square force. In section 5.5 we saw it is a constant of the motion. This suggests an experiment using a single droplet in which the value of $\hbar$ is inferred by two different methods: from the wavelength and from the inverse square force. The experimental constants might be eliminated by noting that the ratio of the two inferred values should be independent of the droplet size as long as second-order terms can be neglected. We are not aware of such experiments being conducted.

Equation (6.4) is the same as the de Broglie wavelength of a quantum mechanical particle with the constant of motion b in place of Planck's constant h. It can be extended to arbitrary axes. If the velocity is $\mathbf{v} = (v_x, v_y)$ then ψ in (6.2) becomes

$$\psi = \cos(\mathbf{k}.\mathbf{x} - \omega t) \tag{6.5}$$

where

$$\mathbf{p} = \hbar\mathbf{k} \tag{6.6}$$

and $\mathbf{p} = (p_x, p_y)$ is the momentum.

Exercise 6.1 By substituting $\lambda = 2\pi/|k|$ into $\mathbf{p}$=$\hbar$ $\mathbf{k}$, and choosing suitable axes, show the wavelength of the waves is the same as in (6.4).

6.2 The diffraction pattern

We now compare the histogram in figure 6.2 with the diffraction pattern of ψ through the aperture.

Exercise 6.2 Waves of wavelength λ propagate normally towards an aperture of width L. The diffraction pattern is plotted against angle θ.

By considering two small elements of the aperture that are a distance $\frac{1}{2}L$ apart, show that the wavelets from one of them have to travel an extra distance $\frac{1}{2}L\sin\theta$ compared to the other. Show that they interfere destructively, and hence that the diffraction pattern has a minimum, when $\lambda = L\sin\theta$.

The width of the aperture was 14.8 mm and, based on measuring the vertical distance from the barrier to the first node (measured near the corner to the right of the aperture), the wavelength of ψ near the aperture was $\lambda = 7.3$ mm. When waves of wavelength λ diffract through a single aperture of width L, the first minimum of amplitude is at angle θ where $\lambda = L \sin\theta$. The above measurements predict this will occur at $\theta = 30°$. The minimum in the experimental histogram occurs between 30° and 35°.

So we observe that the minimum in the histogram occurs where the waves of ψ interfere destructively. It is as if the droplet were repelled from these regions. This can be understood as follows. Bigger waves have deeper wave troughs, so a droplet bouncing in them will be physically lower than one bouncing elsewhere. Consequently it will be attracted towards them by the force of gravity. This deflects them away from the regions of destructive interference of ψ where the waves are smaller and the droplets cannot bounce as low.

Figure 6.2 superposes this theoretical diffraction pattern (solid line) on the experimental data. In comparison, more droplets are deflected at large angle than would be expected. Droplets that approach the aperture normally will produce the usual diffraction pattern, but droplets that are aimed, say, to the right of it will be accelerated parallel to the boundary (as we can see in figure 5.1). When they go through the aperture they will have momentum towards the left and will be more likely to end up at a large angle in that direction.

6.3 Double-slit diffraction

In another experiment, the droplet was made to diffract through two slits.

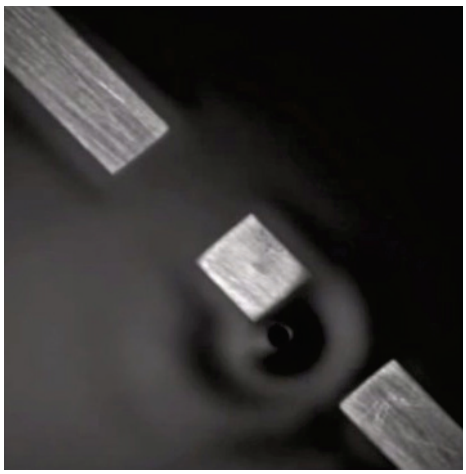

Figure 6.3: *Droplet passing through a double slit*

The histogram of the directions taken by the droplets after they had passed through one or other of the slits is shown in figure 6.4.

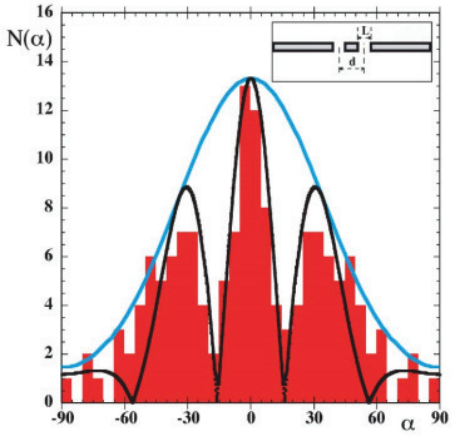

Figure 6.4: *Histgoram of the deflection angle for 75 droplets that have passed through one of two slits. The solid lines show a possible fit to a double-slit diffraction pattern. Courtesy Yves Couder and Emmanuel Fort [15].*

Exercise 6.3 Waves of wavelength λ propagate normally towards two slits which are distance L apart. After the waves have passed through, the diffraction pattern at angle θ to the normal is measured at large distance. Show that the waves from one slit have to travel an extra distance $L\sin\theta$ compared to the other.

Use your result to show that the diffraction pattern has a minimum where $\lambda = 2L\sin\theta$.

The distance between the slits was 14.3mm. Using the above parameters we would expect the first diffraction minimum to be at approximately 15°, which is what the researchers observed.

6.4 Classical approximation

Defining a quantity with the dimensions of energy

$$E = \hbar\omega$$

then, from (6.3),

$$\begin{aligned} \omega^2 - c^2k^2 &= \omega_o^2 \\ E^2 - p^2c^2 &= m_o^2c^4 \end{aligned}$$

where we have used $p^2 = \hbar^2k^2$ from (6.6) and the definition of $\hbar$ in (5.4). This is analogous to the relativistic equation of motion for a classical particle of rest mass m_o and energy E, which has the same form. The low-velocity approximation is

$$E = E_o\left(1 + \frac{p^2c^2}{E_o^2}\right)^{\frac{1}{2}} \approx E_o + \frac{p^2}{2m_o}$$

which is the Newtonian equation of motion.

In order to include the inverse square force between the wave fields which we have seen in the previous chapter, it suffices to add a term to the energy, namely

$$\hbar\omega \;=\; E \;=\; mc^2 \;-\; V \tag{6.7}$$

where V is the potential energy associated with the interaction.

These equations of motion are valid when coherent effects such as diffraction are not relevant.

6.5 Klein-Gordon equation

From (6.1), the factor ψ for a stationary particle obeys the equation

$$\frac{\partial^2\psi}{\partial t^2} \;=\; -\,\omega_o^2\psi \tag{6.8}$$

In order to extend this equation to the case of a droplet that is moving relative to the fluid, we need a Lorentz covariant equation with an acoustic value of c that reduces to (6.8) in the stationary case, namely

$$\frac{\partial^2\psi}{\partial t^2} \;-\; c^2\nabla^2\psi \;=\; \omega_o^2\psi \tag{6.9}$$

since the left hand side is Lorentz invariant.

Equation (6.9) is the same as the Klein-Gordon equation of quantum mechanics for a relativistic particle, with an acoustic value for the speed c.

6.6 Schrödinger equation

If the wave field for a stationary droplet (6.1) receives a Lorentz boost with velocity $v \ll c$ then we get $\psi = \cos(-\omega_o t') = \cos(vx\omega_o/c^2 - \omega_o t)$ where we have approximated $\gamma = 1$. Writing this in the form

$$\psi \;=\; R\cos(\theta - \omega_o t) \tag{6.10}$$

gives $\theta = vx\omega_o/c^2$. Extending to arbitrary axes gives the velocity of the droplet as determined by the local waves

$$\mathbf{v} \;=\; \frac{c^2}{\omega_o}\,\nabla\theta \tag{6.11}$$

The function in (6.10) can be analytically continued into the complex plane by defining

$$\psi_s \;=\; R\,e^{i\theta} \tag{6.12}$$

so that $\psi = \Re(e^{-i\omega_o t}\psi_s)$ where $\Re$ means the real part. Now, ψ obeys the Klein-Gordon equation (6.9), and we will seek a solution where both the real and

imaginary parts of $e^{-i\omega_o t}\psi_s$ obey this same equation, which is satisfied when

$$i\,\frac{\partial \psi_s}{\partial t} \;=\; -\,\frac{c^2}{2\omega_o}\,\nabla^2\psi_s \tag{6.13}$$

where we have neglected the term in $\partial^2\psi_s/\partial t^2$, which is small when the velocity is small.

Substituting (6.7) in the form $ƀ\omega_o = m_o c^2 - V$ gives

$$i\,ƀ\,\frac{\partial \psi_s}{\partial t} \;=\; \left(-\frac{ƀ^2}{2m_o}\nabla^2 + V\right)\psi_s \tag{6.14}$$

This is the same as the Schrödinger equation for the wavefunction of a quantum mechanical particle, with the constant of motion $ƀ$ in place of Planck's reduced constant $\hbar$.

6.7 Probability density

If the starting position of a droplet is not known precisely, and it is allowed to evolve over time, then there will be a range of final positions which we can calculate probabilistically. We will borrow part of the reasoning of David Bohm [21], who solved this problem in 1952. Madelung [22] and de Broglie [23] had independently derived similar equations in 1926 and 1927 respectively. They had all unknowingly written down the probabilistic equation for the motion of a bouncing droplet.

Substituting the definition $\psi_s = Re^{i\theta}$ (equation 6.12) back into (6.13), and taking the imaginary part when $\theta = 0$ gives

$$\frac{\partial R}{\partial t} \;=\; -\,\frac{c^2}{2\omega_o}\,(R\,\nabla^2\theta - 2\,\nabla R\,\nabla\theta)$$

which can be rearranged into

$$\frac{\partial R^2}{\partial t} \;+\; \nabla(R^2\;\mathbf{v}) \;=\; 0 \tag{6.15}$$

where $\mathbf{v}$ is the velocity of the droplet in (6.11).

This equation has a simple interpretation. When the velocity $\mathbf{v}$ of a compressible fluid, such as the air, varies with position, its density ρ obeys the continuity equation $\frac{\partial \rho}{\partial t} + \nabla(\rho\,\mathbf{v}) = 0$ (see the proof is in section 1.9). This is the same as (6.15) with R^2 replaced by ρ. Since the velocity of the droplets is $\mathbf{v}$, it follows that the probability density for the position of the droplet, averaged over nearby trajectories, must be $R^2 = |\psi_s|^2$ (provided the initial value of $|\psi_s|^2$ is appropriately calibrated, or 'normalised'). An analogous probability density $|\psi_s^2|$ is assumed as a postulate in the Copenhagen interpretation of quantum mechanics.

This is confirmed by the experimental results in figure 6.5. A droplet is repelled from a region of reduced depth for the reasons given in chapter 5.

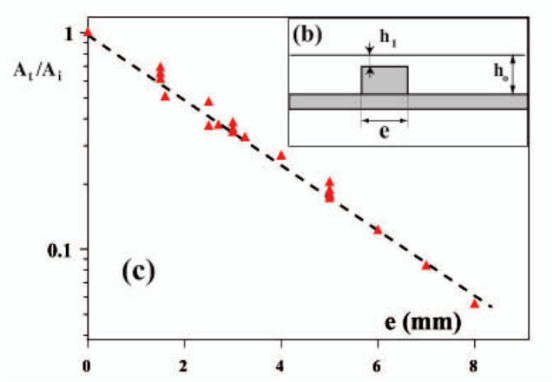

Figure 6.5: *Droplets encounter a region of reduced depth, which repels them. The x axis is the width of the barrier, and the y axis is the probability the droplet tunnels through the barrier, plotted on a logarithmic scale. Courtesy Antonin Eddi [24]*

When it reaches such a barrier, it is usually reflected but occasionally it passes through or 'tunnels'. The graph shows that the probability a droplet crosses the barrier reduces exponentially with its width. If you solve Schrödinger's equation with a barrier, you get the same exponential decay of $|\psi_s^2|$ with width, as shown in the next exercise.

Exercise 6.4 Consider a stationary solution to the Schrödinger-like equation (6.14), where $i\hbar\partial\psi_s/\partial t = E\psi_s$. In the region $0 < x < D$, there is a barrier where $V > E$.

The waves near $x = 0$ are given by $\psi_s = f(t)$, where $f(t)$ is a function of time with $|f|^2 = 1$. Show that $\psi_s = e^{-ax} f(t)$ inside the barrier where a is a constant. You are not required to evaluate a.

Just on the other side of the barrier, show that $\psi_s = e^{-aD} f(t)$ and $|\psi_s|^2 = e^{-2aD}$.

The foregoing calculation led Bohm to hypothesise the existence of a tiny particle which moves at the velocity $\mathbf{v}$ in (6.11), guided by waves that obey Schrödinger's equation (6.13), whose probability density is $|\psi_s^2|$. He had unknowingly obtained the equations of motion for a bouncing droplet at low velocity (but without the factor χ in (6.1)). His insight is remarkable. For him, this was purely an abstract exercise; he did not have the droplet model to inspire him to derive these equations from Euler's equation.

Based on these equations, Bohm showed the resulting mechanics to be indistinguishable from the Copenhagen interpretation of quantum mechanics. He subsequently found that Louis de Broglie had suggested a similar idea in 1927, and the model is now called the de Broglie-Bohm interpretation of quantum mechanics. He does not appear to have known about Madelung's related hydrodynamic interpretation of 1926.

6.8 Same equations, same solutions

Given that we have the same mathematics up to a constant factor, we might expect the calculations of quantum mechanics to carry over to other aspects of the droplet experiment.

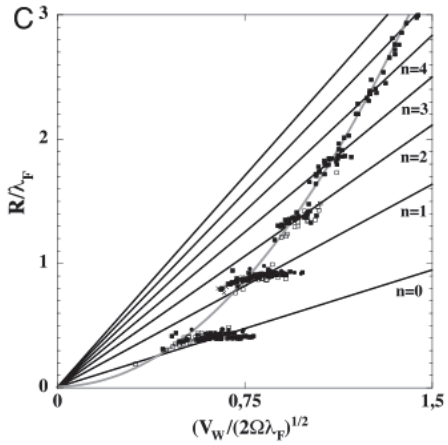

Figure 6.6: *A droplet in a rotating bath is attracted towards the centre, and exhibits quantized orbits. Courtesy Emmanual Fort [16]*

In figure 6.6, the experiment was conducted in a rotating bath, where the droplet was attracted towards the centre. They exhibited quantized orbits. See also later reports of self-organization into quantized eigenstates of a classical wave-driven particle [25].

6.9 Summary

In the approximation that viscosity can be neglected, we have seen that the wave field of a bouncing droplet has two component factors, ψ and χ. The former obeys the same equations of motion as the wavefunction of a relativistic quantum mechanical particle, with an acoustic value for the speed c and the constant of motion $\hbar$ in place of Planck's reduced constant $\hbar$. When its starting position is not known precisely, the motion of the droplet can be calculated probabilistically, with $|\psi|^2$ being the probability it arrives at a given position. These results are confirmed by experiments on single-slit diffraction, double-slit diffraction, tunnelling and quantised energy levels.

In the most common 'Copenhagen' interpretation of experiments in quantum mechanics, it is assumed that the wavefunction ψ is a complete description of the system. This is not true in the droplet experiments, where ψ is only one factor in the wave field near a droplet. We will turn to the factor χ in chapter 10.

6.10 Dialogue

Sensational new experimental results have recently been reported in the US by a team that claimed to reproduce quantum mechanical diffraction precisely, but in a completely classical system. They reproduced the double-slit droplet experiment, but in a dark room so it was not possible to photograph the droplets during their path (which they said mirrored quantum mechanics, where you cannot observe the exact path of a particle). The droplets were detected at the outer boundary and produced a double-slit diffraction pattern like figure 6.4.

On day 3 of their dialogue, Alice, Bob and Carol learn of these new results, and argue for the following propositions.

(a) Alice says an electron splits in two when it encounters two slits. One part goes through one slit, while the other goes through the other slit. They recombine at the exact moment they are detected, producing the diffraction pattern. There is a special faster-than-light process that prevents the two parts from being detected at the same time.

(b) Bob says a bouncing droplet splits into two when it encounters two slits. One part goes through one slit, while the other goes through the other slit. They recombine at the exact moment they are detected, producing the diffraction pattern. There is a special supersonic process that prevents the two parts from being detected at the same time.

(c) Carol says an electron and a bouncing droplet are both resonances that obey the wave equation in a fluid. They only go through one slit; the diffraction pattern is due to the interaction with the waves from the other slit.

Each of these approaches can be made consistent with all the relevant experiments. Argue in favour of each one in turn.

Chapter 7

Historical context

I have been judged vehemently suspected of heresy, namely of having held and believed that the sun is the centre of the world and motionless and the earth is not the centre and moves .... I abjure, curse, and detest the above-mentioned errors and heresies

Galileo Galilei

In the 19th Century, the Norwegian mathematician and physicist Carl Bjerknes studied the forces between pulsating bubbles in a bath of water. His experimental apparatus, drawn in figure 7.1, used pistons to create pressure waves and make the bubbles pulsate [26]. His work is part of a chain of ideas which we must examine in order to place the experiments we have discussed into their historical context.

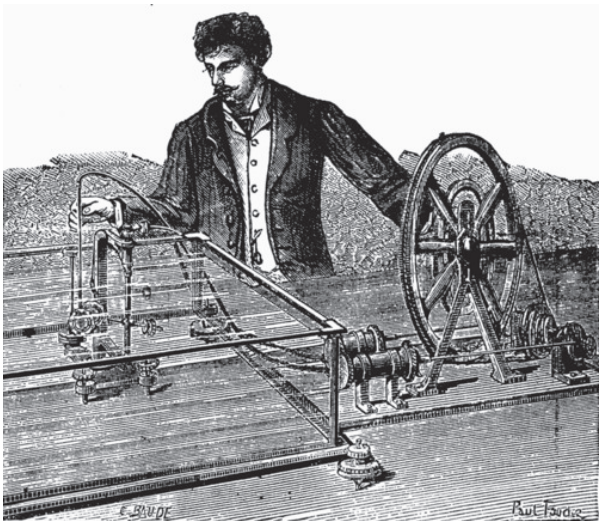

Figure 7.1: *Bjerknes's apparatus (from Scientific American in 1881)*

7.1 Pulsating bubbles

In 1875, Carl Bjerknes predicted that bubbles in a bath of water would attract one another with an inverse square force when they are made to pulsate in phase with each another, and repel with the same force when they are antiphase. He confirmed his theory experimentally in 1880. Figure 7.2 is a reproduction from the relevant papers.

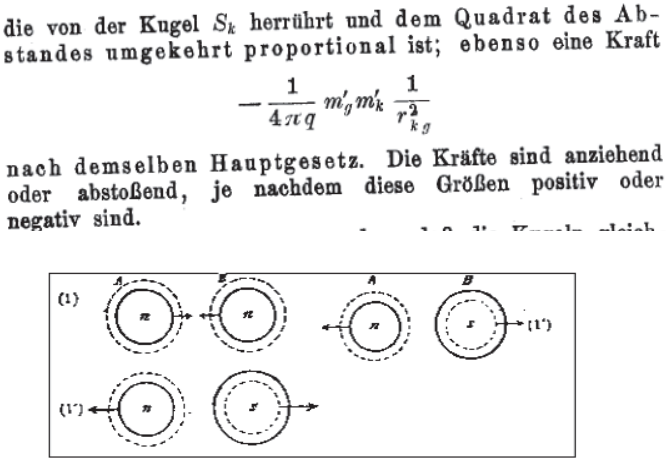

die von der Kugel S_k herrührt und dem Quadrat des Abstandes umgekehrt proportional ist; ebenso eine Kraft

$$-\frac{1}{4\pi q}\, m'_g m'_k \frac{1}{r^2_{kg}}$$

nach demselben Hauptgesetz. Die Kräfte sind anziehend oder abstoßend, je nachdem diese Größen positiv oder negativ sind.

Figure 7.2: *Reproduction of Bjerknes's prediction in 1875 of an inverse square force (top) and a figure from his experimental paper in 1880 (bottom) [26, p164].*

He had discovered the inverse square force which was measured more than a century later in the bouncing droplet experiments (chapter 5). Although Bjerknes correctly predicted that the force is inverse square, he did not discover that it obeys the full set of equation which Maxwell had advanced for electromagnetism, with an acoustic value of the speed c (section 5.8). The speed of sound in water was too large to have a measurable effect in his experiments, and his theory assumed the water was incompressible.

Nevertheless, he made a connection with electromagnetism. Maxwell's theory of electromagnetism lacked an explicit mechanism for transmitting the forces between charged particles, but Bjerknes's bubble experiments showed there are inverse square hydrodynamic forces acting at a distance between the bubbles (*Hydrodynamische Fernkräfte*), and they can be understood using purely local interactions in the fluid.

Furthermore, Maxwell had originally modelled a magnetic field in 1861 as a vortex in a lossless medium with rolling elements which resembled a fluid [27]. In the final version, his equations of electromagnetism were carefully expressed in abstract mathematical terms which did not require or exclude any particular substrate, fluid or otherwise, but Bjerknes's theory and experiments seemed to support the original, and seemingly more physical, formulation. This made some impact at the time. Writing in *Nature* in 1881, George Forbes wrote [2]

> From a scientific and purely theoretical point of view there is no

> object in the whole of the Electrical Exhibition at Paris of greater interest than the remarkable collection of apparatus exhibited by R. C[arl] A. Bjerknes of Christiana, and intended to show the fundamental phenomena of electricity and magnetism by the analogous ones of hydrodynamics.

7.2 Lorentz's model of the electron

These experiments were among the factors that led Hendrik Antoon Lorentz to model what he called 'electrons', as **covibrating particles**. He acknowledged the contribution of Bjerknes in his Nobel prize acceptance speech in 1902 [28]

> I am thinking in particular of the experiments of Prof. Bjerknes in Christiania on transmitted hydrodynamic forces and of his imitation of electrical phenomena with pulsating spheres.

Lorentz suggested three alternatives for the medium in which the particles vibrate: it might be an elastic medium, an incompressible frictionless fluid, or a jelly [28]. It seems that he did not examine a compressible frictionless fluid. Vibrations in such a fluid are Lorentz covariant (sections 1.14 and 4.3) and there is a force between them that obeys Maxwell's equations where the speed c is the speed of waves in the fluid (section 5.8).

Lorentz inferred what is today called the Lorentz transformation, not from the properties of vibrations in a compressible fluid, but from the results of an experiment conducted in 1881 by Albert Michelson and Edward Morley. Michelson and Morley had sent light waves in different directions from a central position and reflected them back to the starting point. We saw an analogous experiment with a crystal of bouncing droplets in section 4.2. Thinking, wrongly, that the dimensions of their apparatus were unaffected by its motion, they expected that the interference between the returning waves would discover the motion of the earth relative to the 'light medium' through which the waves were presumed to propagate, but they obtained a null result.

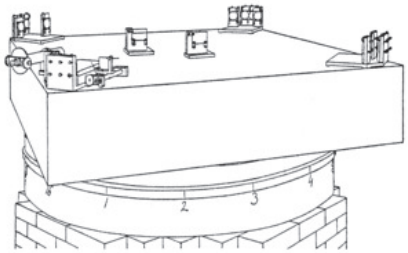

Figure 7.3: *The Michelson-Morley experiment floating on mercury*

The original drawings of their apparatus are reproduced in figures 7.3 and 7.4. Light from a source (marked f in the figure) encounters a beam splitter, b. The beams follow two paths at right angles to one another. They are reflected by mirrors d and e, and return along the same paths to recombine at b. The

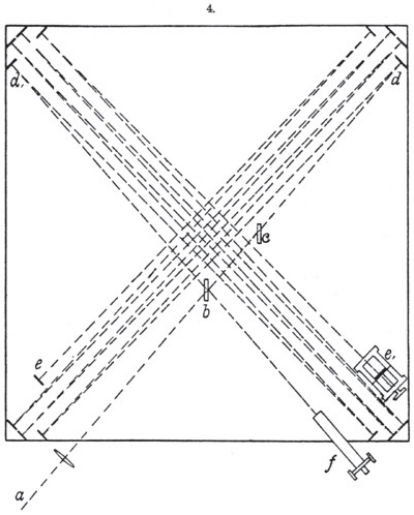

Figure 7.4: *The apparatus of Michelson and Morley [29]*

phase difference between the returning waves is viewed as an interference fringe at a.

The experimenters mounted their apparatus on a stone slab which they floated in a pool of mercury. If it had been moving with respect to the light medium, they expected to see the interference fringes change as it rotated, but they found no change at all. So they measured the interference at different times of the day and the year, when they presumed the velocity of the earth through the medium had different values, but still obtained a null result. More recent and accurate experiments have shown that the anisotropy in the apparent speed of light inferred from the measurements must be less than 10^{-17}.

In 1889 George Fitzgerald pointed out that, given reasonable-sounding assumptions, the molecular forces holding the apparatus together will be affected by the motion through their light medium, resulting in a change in its dimensions [19]. Three years later, in 1892, Lorentz independently came to the same conclusion and calculated the magnitude of the contraction by assuming the null result [30]. His result is the same as the contraction which we have seen is suffered by ordinary vibrations in a compressible frictionless fluid.

7.3 Properties of the light medium

When scientists considered the properties of the light medium of Michelson and Morley in the early 20th century, they discovered a number of constraints.

Firstly, they believed there was evidence for a medium of some sort, rather than none at all. Einstein gave the reason in a lecture in 1920. An experimenter who is far from any gravitational source can tell by intrinsic measurement, without looking outside, whether or not her laboratory is accelerating with respect to a nearby non-accelerating laboratory, for example by weighing objects. Be-

lieving that all interactions are local, Einstein concluded that the correlation between the two laboratories must be transmitted by a medium occupying the space between them [20].

Secondly, the medium cannot be a solid or semi-solid like a jelly. It was proved that these substances cannot be Lorentz covariant and so they are not consistent with Michelson and Morley's experimental result [20].

Thirdly, the medium cannot be a stationary fluid. We proved in section 1.16 that a stationary fluid cannot support propagating waves with any component of transverse motion. So the waves cannot be polarised and they do not behave like light waves.

It seems that the only remaining possibility is that the medium is a fluid which is not stationary. We saw in section 1.16 that when a wave propagates through a fluid with shear flows, it has a transverse component of velocity and it is polarised. In the coming chapters we will compare this possibility against measurements of the polarisation of light (section 8.9) and of oscillatory shear flows in bouncing droplets and superfluid helium (chapters 10 and 11).

A fluid with shear flows does not appear to have been considered historically, leaving only one way forward: simply not to consider the question, but to concentrate on equations that make definite testable predictions.

7.4 Two models of the Lorentz contraction

In 1905 a treatment was advanced which, like Maxwell's equations before it, was framed in abstract mathematical terms that did not require or exclude any particular substrate, fluid or otherwise. Albert Einstein's theory of special relativity obtained Lorentz's formulae from symmetry arguments similar to those in chapter 4. The paper begins by conjecturing a 'principle of relativity' based on assuming the experimental result of Michelson and Morley [31]. This principle states that no intrinsic measurement can detect absolute rest.

In the years that followed, Lorentz maintained his belief that the Lorentz contraction was caused by the moving medium perturbing the molecular forces in a material body, whilst Einstein thought the light medium was 'superfluous.' Neither could come up with a testable difference between their opinions. The droplet experiments tell us why: the two theories are mathematically equivalent to one another, provided the medium is a compressible frictionless fluid and the only measurements that are used are expectation values (chapter 4). The principle of relativity is a symmetry of Lorentz's model of the electron under these circumstances.

7.5 Successive re-discoveries

A discovery, or, it may be argued, the first of several re-discoveries of Lorentz's model of the electron, was made in 1926 when Madelung rearranged the equations of quantum mechanics into the same form as those for vibrations in a fluid [22]. Unaware of Madelung's work, de Broglie in 1927 and Bohm in 1952

separately and independently re-discovered similar equations [21,23]. In chapter 6 we used part of these historical calculations to predict the motion of bouncing droplets, finding good agreement with experiment.

Lorentz's model of the electron was once again seemingly re-discovered when it was noticed that vibrations in an ideal compressible fluid have the symmetries of general relativity. These observations have grown into an active field of study called **analogue gravity**: see the review article by Carlos Barceló, Stefano Liberati and Matt Visser [32].

Modern research in analogue gravity is usually regarded as having begun in 1981 when Bill Unruh's paper, 'Experimental black hole evaporation,' described an analogue model based on fluid flow, which he used to probe the Hawking radiation from 'real' general relativistic black holes [33]. In 2010, Oren Lahav, Amir Itah, Alex Blumkin, Carmit Gordon, Shahar Rinott, Alona Zayats and Jeff Steinhauer conducted experiments in a Bose-Einstein condensate and observed negative energy excitations in accordance with the predicted Hawking-Unruh radiation [34]. The book by Grisha Volovik, *The universe in a helium droplet*, builds on this field by suggesting pulsating particle-like solutions which resemble those of Lorentz [35].

7.6 Summary

In 1875 Carl Bjerknes predicted an inverse square force between pulsating bubbles in a tank of water, and confirmed his prediction experimentally in 1880. He envisaged these forces to be analogous to those of electromagnetism.

Bjerknes's experiments led Hendrik Lorentz to model electrons as covibrating particles. He discussed a number of possibilities for the medium in which the particles vibrate, but did not consider a compressible frictionless fluid. Vibrations in such a fluid are Lorentz covariant, and the force between them obeys Maxwell's full set of equations of electromagnetism.

Lorentz's model was rejected in the early 20th century because polarised waves cannot propagate in a stationary fluid. However they can propagate through a region of shear flow. We will examine polarisation due to shear flows in the forthcoming chapters.

Mathematical results which appear to point back to Lorentz's electron were subsequently discovered in quantum mechanics and in analogue gravity.

7.7 Dialogue

On day 4 of their dialogue, Alice, Bob and Carol are discussing the fact that Lorentz's 19th century model of the electron and bouncing droplets can both be treated as pulsation in a fluid medium.

(a) Alice says she can successfully predict the motion of light waves and of charged particles in a very wide range of circumstances. It suffices to as-

sume the postulates of mechanics, electrodynamics, special relativity and quantum mechanics. The light medium is superfluous.

(b) Bob says he can successfully predict the motion of surface waves and of bouncing droplets in a very wide range of circumstances. It suffices to assume the postulates of mechanics, electrodynamics, special relativity and quantum mechanics, with the characteristic speed c having an acoustic value. The equations of fluid mechanics are superfluous.

(c) Carol says she can successfully predict the motion of both systems from Euler's equation. The postulates of mechanics, electrodynamics, special relativity and quantum mechanics are superfluous.

Each of these approaches can be made consistent with all the relevant experiments. Argue in favour of each one in turn.

Chapter 8

Scale invariance

But on one supposition we should, in my opinion, absolutely hold fast: the real factual situation of the system $S2$ is independent of what is done with the system $S1$ which is spatially separated from the former.

Albert Einstein, cited by John Bell [36]

Fluid mechanical systems seem to exhibit non-local behaviour. For example, when two vortices are created together, say by stirring, Kelvin's circulation theorem (section 1.3) tells us they have opposite circulations, and, furthermore, if an external disturbance changes the circulation of one of them, it must change the other by the opposite amount at exactly the same time. This remains true even if their centres become separated by a large distance – which seems to demand instantaneous (non-local) interactions between the distant vortices.

In this chapter we will see that this non-local behaviour is, quite generally, a consequence of the scale invariance symmetry of fluid mechanics. Quantum mechanics has the same symmetry.

8.1 Self-similarity

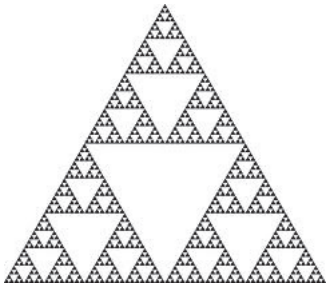

Figure 8.1: *A Sierpiński triangle*

Scale invariant systems are said to be **self-similar** because they contain

structures with a wide range of length scales. One example is the Sierpiński triangle in figure 8.1 which contains triangles of many different sizes.

The geometrical properties of self-similar systems can be counter-intuitive. For example, when the side L of a Sierpiński triangle is doubled, the number N of triangles is trebled, by inspection of the figure. It follows that $N \propto L^D$ where $D = \log(3)/\log(2) \approx 1.6$. The exponent D is called the **Hausdorff dimension**. Its value can seem counter-intuitive in comparison with ordinary systems in a plane, which are two-dimensional with $D = 2$.

Sierpiński's triangle began as a mathematical construct in 1915 [37]. In 1967, Benoit Mandelbrot showed its relevance to the physical world by studying the unusual geometrical properties of the coastline of Britain, which has crinkles at all relevant length scales [38]. This inspired the discovery of further self-similar systems. For example, the copper deposit when electrolysing copper sulfate solution sometimes appears black; it is self-similar with a Hausdorff dimension $D \approx 2.43$ [39]. More recently, structures with self-similar features such as the Mandelbrot set in figure 8.2 became popular for their beauty.

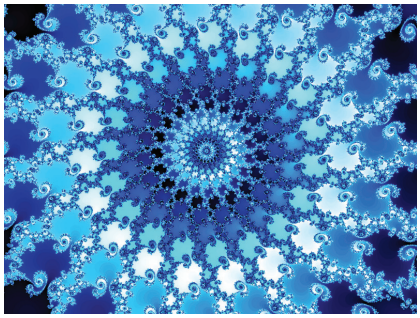

Figure 8.2: *A Mandelbrot set*

This is relevant to fluid motion because it, too, is scale invariant. As we saw in section 1.13, if $\mathbf{u}(\mathbf{x}, t)$ obeys Euler's equation, so does $\mathbf{u}(\alpha\mathbf{x}, \alpha t)$ where α is a scale factor.

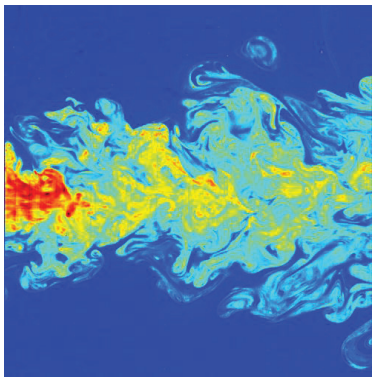

Figure 8.3: *Turbulence is a self-similar solution to Euler's equation. Courtesy C. Fukushima and J. Westerweel, Technical University of Delft, The Netherlands*

The turbulent motion in figure 8.3 obeys Euler's equation to a reasonable approximation. The eye can pick out components that are approximately similar (but not precisely the same) which span a wide range of length scales.

8.2 Drawing systems apart

There is another geometrical difference between ordinary systems and scale invariant systems, which is that they behave differently when they are drawn apart. This is illustrated in figure 8.4.

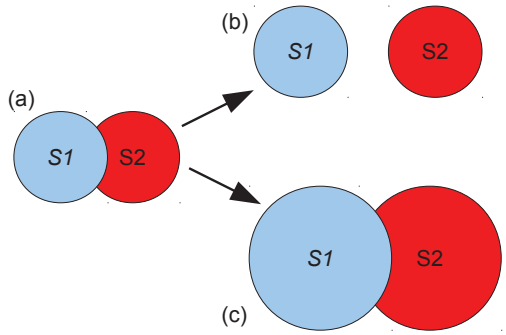

Figure 8.4: *(a) Two systems, S1 and S2, initially overlap. (b) Normally, the overlap reduces as they are drawn apart, so they become independent of one another. (c) But if they are scale invariant, the systems inflate as they separate. They remain in direct contact and do not become independent.*

Suppose two systems, $S1$ and $S2$, initially overlap, and are then drawn apart by some process. We would normally expect the systems to remain the same size, so their overlap reduces until eventually it is eliminated and the systems become independent of one another. This is illustrated in figure 8.4(a) and (b).

But scale invariant systems, including those in fluid mechanics, are different. See figure 8.4(c). Suppose two systems, $S1$ and $S2$, are scale invariant and the distance between their centres is d. If they are carefully drawn apart by the factor α, so the distance between their centres is now αd, then, from the scale invariance symmetry, there is a solution in which all distances and times have been inflated by the factor α. In the enlarged solution, $S1$ and $S2$ have grown in size by the factor α and the overlap between them remains unchanged. The systems remain in contact and do not become independent of one another.

8.3 Separation principle

There is a principle, due to Einstein, called the **separation principle** (*Trennungsprinzip*) which is usually cited as follows

> But on one supposition we should, in my opinion, absolutely hold fast: the real factual situation of the system $S2$ is independent of

> what is done with the system $S1$ which is spatially separated from the former.
>
> Albert Einstein, cited by John Bell [36]

John Howard gives an account of the history of this principle [40]. The separation principle applies, of course, to all systems, including scale invariant ones, when they are spatially separated. But when two scale invariant systems are created together and carefully drawn apart, we saw that they do not become spatially separated, and so it would be wrong to assume that the separation principle applies to them. It may be helpful to take a concrete example.

Consider two vortices, far from any boundary, which have been created together as in figure 8.5. To a good approximation the air obeys Euler's equation, which is scale invariant, and so, by the reasoning set out above, the vortices will inflate as they are drawn apart and they will not become independent of one another. The separation principle does not apply to them.

Figure 8.5: *A vortex pair. Courtesy National Center for Atmospheric Research*

Another way to arrive at the same conclusion is to follow the reasoning of John Kosterlitz and David Thouless, who showed in 1973 that there is an intimate pairing between vortices that were created together, which is independent of the distance between them as long as the fluid is below a critical temperature [41]. For simplicity they considered vortices that are trapped between between two large parallel plates, which we will take to be a distance W apart.

Suppose an isolated vortex could be created with circulation Γ so that its flow speed is $u = \Gamma/r$. The kinetic energy density is $\frac{1}{2}\rho u^2$ where ρ is the density of the fluid and the total is $\int \frac{1}{2}\rho u^2 . 2\pi r W dr$. This energy diverges logarithmically at large r, which shows that it is impossible to create an isolated vortex far from a boundary at low temperature, since it would be too costly energetically.

Indeed, vortices are not created in isolation. They are created in pairs of opposite circulation, as shown in figure 8.5. Their velocity fields are opposed at large distance, and so the total energy does not diverge as long as the correlation is maintained between them. Kosterlitz and Thouless went on to show that this intimate pairing is broken when the fluid is above a critical temperature, at which the so-called **Kosterlitz-Thouless phase transition** occurs (discussed further in section 11.15) but here we are only interested in low temperatures.

It follows that the circulations of the two vortices must remain precisely opposed since a large amount of energy would be required to make their circulations different. This remains true whatever their separation. This intimate pairing of their energy means that the separation principle does not apply to them.

A third way to picture this phenomenon is from Kelvin's circulation theorem (section 1.3). Kelvin proved that the vortices must always have opposite circulations, whatever their separation.

† *Track 2* *This material may be skipped on a first reading*

The scaling of the two vortices has an additional factor: amplitude.

In a more precise description of the vortices as they separate, all distances and times grow by the factor a and the amplitudes of all disturbances reduce by the same factor a. The net effect is that the flow speed due to each vortex remains $u = \Gamma/r$, independent of their separation.

Near the core of a vortex, the fluid velocity would diverge if there were no other effect. Here, viscosity and nonlinearities in the equation of state become relevant. A different solution emerges, which is observed in the eye of a hurricane [1]. The size of the core does not scale with the separation of the vortices because the processes involved are not scale invariant.

8.4 Paradox

When viewed from a certain perspective, the foregoing system seems to demand a type of instantaneous action at a distance. The paradox is as follows.

We have seen that when two scale invariant systems are created together, they thereafter remain 'entangled' in the sense that external events affect them simultaneously, even when their centres are spatially separated. For example, if some external event changes the circulation of one vortex, the circulation of its anti-vortex partner must change instantaneously. This might seem to suggest some non-local process that operates instantaneously over a distance, that is, faster than light. But faster-than-light processes are impossible. Indeed, there is a stronger constraint: in the fluid motion under consideration, there is no mechanism for transmitting information faster than the speed of sound.

The mistake in this paradox is illustrated in figure 8.4(c). It is not necessary to assume anything goes faster than light (or sound) since it is only the centres of the systems which are separated. The systems themselves remain in direct contact through their overlap.

Another way to see this is shown in figure 8.6. The apparent paradox of faster-than-light processes relies on the fallacy that a small disturbance, such as small paddles, can change the circulation of a large vortex instantaneously. As shown in the figure, if small paddles are set into rotation, they may affect the fluid nearby but they cannot affect the fluid at large distance instantaneously. This means they have no immediate effect on the circulation $\Gamma = \frac{1}{2\pi} \oint \mathbf{u}.d\mathbf{l}$

around them at large distance. In particular, a disturbance due to small paddles cannot instantaneously affect the circulation of an existing vortex which has been inflated by being separated from its anti-vortex partner.

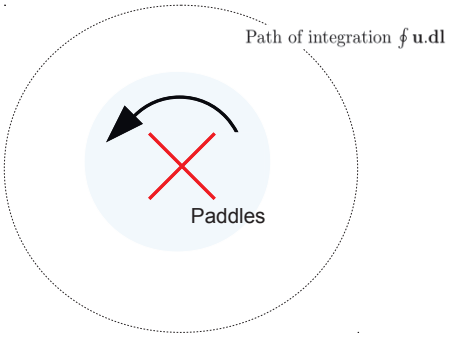

Figure 8.6: *Small rotating paddles can disturb the fluid nearby (blue shadow) but they do not immediately affect the fluid at large radius, and so they cannot immediately change the circulation* $\Gamma = \frac{1}{2\pi}\oint \mathbf{u}.d\mathbf{l}$ *at large radius.*

Yet another way to visualise this is by a thought-experiment in which we try (as we shall see, unsuccessfully) to manipulate a vortex $S1$ by changing its circulation without simultaneously affecting its co-created partner $S2$. In the thought experiment we will try to achieve this using paddles. We have seen that the system $S1$ extends over a large region, with its energy residing at large distance, and so the paddles must be large in order to couple to it effectively. In fact, they must be large in relation to the separation of the centres of $S1$ and its partner $S2$. Paddles this large will affect the circulation of $S2$, defeating the purpose of the thought experiment.

8.5 Scale invariance of quantum mechanics

The Klein-Gordon equation (6.9) for a quantum mechanical particle is also scale invariant. It inherits this symmetry from Euler's equation, from which we derived it in section 6.5. The scale symmetry can also be verified by direct substitution of a scale enlargement $(\mathbf{x}', t') = (\alpha\mathbf{x}, \alpha t)$, giving

$$\frac{\partial^2\psi}{\partial t'^2} - c^2\nabla'^2\psi + \omega_o'^2\psi = \frac{1}{\alpha^2}\left(\frac{\partial^2\psi}{\partial t^2} - c^2\nabla^2\psi + \omega_o^2\psi\right)$$

where $\omega_o' = \omega_o/\alpha$ from the scale enlargement. If $\psi(\mathbf{x}, t)$ obeys the Klein-Gordon equation then the right hand side vanishes. Equating the left hand side to zero shows that $\psi(\alpha\mathbf{x}, \alpha t)$ is also a solution.

This suggests that particles obeying the Klein-Gordon equation will be scale invariant. In particular, if two particles are created in a single process and then carefully drawn apart, without interacting with any external systems, then they do not become separated and the separation principle does not apply.

8.6 EPR paradox

In 1935, Albert Einstein, Boris Podolsky and Nathan Rosen ('EPR') considered just such a system [42]. They assumed

(a) Particles obey the equations and postulates of quantum mechanics,

(b) Particles which are created together and then carefully drawn apart become independent of one another.

We have just seen that these two assumptions are mutually inconsistent. If (a) is true, then particles obey the Klein-Gordon equation. From the scale invariance symmetry, we would expect its solutions to inflate in proportion to their separation when they are carefully drawn apart, as shown in figure 8.4. They consequently remain in direct contact and the separation principle does not apply. It follows that (b) is false.

The authors EPR reached the same conclusion, that (a) and (b) are mutually inconsistent, using a different method starting with the detailed postulates of quantum mechanics. This conclusion is now known as the **EPR paradox** because it can seem counter-intuitive. It was not until 1967 that Mandelbrot began to write about physical systems with counter-intuitive geometrical properties due to their scale invariance [38].

Thinking their result to be unphysical, Einstein, Podolsky and Rosen hypothesised that the equations of quantum mechanics be modified by adding new variables, called **hidden variables**, which would have the effect of making assumption (b) true. We can immediately observe that these hidden variables, were they to exist, would break the scale invariance symmetry of quantum mechanics.

8.7 Non-locality

In the terminology of the field, the hidden variables hypothesised by Einstein, Podolsky and Rosen are **local**, by which we mean they have the effect that any two systems will become independent of one another when drawn apart. Using this terminology, the known equations of inviscid fluid mechanics (as well as those of quantum mechanics) are **non-local** because they are scale invariant and their solutions do not become independent when carefully drawn apart.

If you assume the existence of local hidden variables in fluid mechanics, as defined above, then you can make a prediction about the circulations of vortices which does not agree with Kelvin's circulation theorem. If you were to test this prediction experimentally it would be violated and you would conclude that the hypothesis of local hidden variables can be excluded. You are invited to show this in the next exercise.

Exercise 8.1 This exercise is about the experiment in fluid mechanics discussed in section 8.3, in which two vortices are created with zero total circulation and they are drawn apart before their individual circulations are manipulated.

You are asked to assume the existence of local hidden variables in fluid mechanics, the effect of which is to cause the circulations of the vortices to become independent of one another when they are drawn apart.

(a) Assuming the hidden variables exist, predict what will happen after the vortices have been drawn apart if the circulation of one of them is suddenly disturbed by an external influence. How will this affect the total circulation of the two vortices?

(b) Show that your prediction is inconsistent with Kelvin's circulation theorem.

8.8 Bell's inequality

In 1964, John Bell proposed an experiment in quantum mechanics which is analogous in a number of respects to the experiment in exercise 8.1. He proposed an experiment in which two particles are created together with zero total spin (or angular momentum, see section 10.5) and they are drawn apart before their spins are measured. He devised a statistical measurement, which is now called **Bell's inequality**, to test for the existence of local hidden variables. If the equations of quantum mechanics are as originally formulated, Bell showed that his inequality would be violated in the experiment, so that local hidden variables could be excluded [36].

In its original form, Bell's inequality does not appear to have been tested directly (but see the experiments on a different system in the next section). However, in view of the success of quantum mechanics in predicting the behaviour of matter, it is generally believed that the inequality is violated, and therefore the local hidden variables which Einstein, Podolsky and Rosen had hypothesised can be excluded.

The geometrical properties of scale invariant systems were still not widely appreciated in 1964 when Bell's paper was published. Mandelbrot's first paper about scale invariance in physical systems was not until 1967 [38]. Unaware that local hidden variables, as defined above, can be excluded in all systems which are scale invariant, many scientists thought such exclusion was unique to quantum mechanics. Some believed it was evidence for faster-than-light processes, due to the paradox discussed in section 8.4. Others thought this explanation to be unsatisfactory since no signals have ever been observed to propagate faster than light, and a number of alternative mechanisms entered mainstream physics, including the hypothesis of backwards-in-time processes [43] and the creation of a new universe with each measurement [44]. There is an extensive literature on this topic, which has spawned a field of study called quantum computing. For further discussion see Bell's collected papers [45], the *dialogue* at the end of this

chapter, our more detailed mathematical treatment of this topic [46,47], and the alternative approaches of David Ferry, Verner Hofer and Joy Christian [48–51].

8.9 CHSH inequality

In 1969, John Clauser, Michael Horne, Abner Shimony and Richard Holt (collectively known as 'CHSH') proposed an experiment similar to figure 8.7, in which two waves are created together at a source S and their polarisations are measured after they have propagated some distance. The alignment of the detectors could be changed in the period between emission and detection.

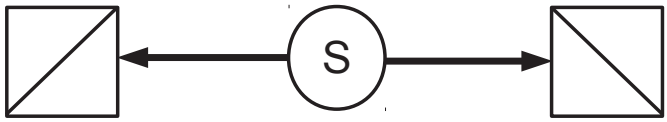

Figure 8.7: *Waves emanate from a source S and their polarisation is measured*

The polarisations were perfectly correlated when the waves are emitted, and the authors CHSH predicted the correlation between the polarisations when they are measured using the known equations of quantum mechanics. Their predictions were later confirmed experimentally by Alain Aspect and colleagues in experiments with light waves [52, 53].

After the alignment of the detectors was changed, there was not time for information, travelling at the speed of light, to reach both detectors. But the experiment showed a correlation which seemed to demand that the information travelled faster than light. More precisely, the observed correlation between the measurements would be impossible in an ordinary classical system provided that

(a) The polarisation is an intrinsic property of the waves

(b) Information can never travel faster than light

If you assume (a) is true, then the experiment indicates the existence of faster-than-light or backwards in time processes, or the creation of a new universe with each measurement. The reasoning is similar to that discussed in section 8.8. For more information see [45, 54].

The alternative possibility was raised in section 7.3. The polarisation of the waves in a fluid medium is not an intrinsic property of the waves themselves, but it depends on the phase alignment between the wave and the shear flows near the detectors. The experiment appears to indicate that there must be very long-range order in these shear flows. We will see the origin of this order in the next chapter.

8.10 Summary

Euler's equation for a barotropic fluid is scale invariant, that is, for every solution $\mathbf{u}(\mathbf{x}, t)$ there exists a larger or smaller solution, $\mathbf{u}(\alpha\mathbf{x}, \alpha t)$ where α is the scale factor. The Klein-Gordon equation for a quantum mechanical particle has the same symmetry.

When two scale invariant systems are drawn apart, they inflate in proportion to the distance between them so their overlap remains constant. This means they remain in contact and do not become independent of one another.

This behaviour is known in fluid mechanics, but it was first noticed in quantum mechanics in 1935, when Einstein, Podolsky and Rosen showed that the equations of quantum mechanics are inconsistent with the assumption that two systems always become spatially separated when they are carefully drawn apart. It is often believed that this is unique to quantum mechanics, but vortices in fluid mechanics behave in the same way. In quantum systems this behaviour is often interpreted as due to faster-then-light or backwards-in-time processes, or the creation of a new universe with each measurement, but these do not occur in fluid mechanics as far as we are aware.

8.11 Dialogue

On day 5 of their dialogue, Alice, Bob and Carol discuss the experiment proposed by John Bell [36], and argue as follows.

(a) Alice says that electrons can be created together with opposite spins and then drawn apart. If they remain 'entangled' it is not possible to change one spin without the other. If you do manage to change one spin, she concludes that the other must be affected instantaneously, which means information of a special sort must travel faster than light or backwards in time, or a new universe must be created at that instant.

(b) Bob says that vortices can be created together with opposite circulations and then drawn apart. If they remain coupled it is not possible to change the circulation of one without the other. If you do manage to change the circulation of one of them, he concludes that the other must be affected instantaneously, which means information of a special sort must travel faster than the speed of sound in the fluid or backwards in time, or a new universe must be created at that instant.

(c) Carol says Bob has made the mistake of assuming it is possible to change the circulation of a vortex by an instantaneous local process, such as using small paddles. The energy of a vortex extends out to very large distance, and so large paddles must be used, which span both vortices. Alice's ridiculous conclusions show that she must have made an equivalent mistake with electron spins.

Each of these approaches can be made consistent with all the relevant experiments. Argue in favour of each one in turn.

Chapter 9

Coherent motion

And it didn't stop being magic just because you found out how it was done

Terry Pratchett

In 1665 a letter from Cristiaan Huygens was read to the Royal Society of London about maritime clocks. It talked of 'an odd kind of sympathy perceived by him in these watches suspended by the side of each other'. [55, 56]. Huygens had mounted two pendulum clocks so they were weakly coupled by 'imperceptible movements' in the mounting. Whatever their initial configuration, after about half an hour the pendula always ended up swinging in opposite directions or 'antiphase' as in the lower photograph of figure 9.1.

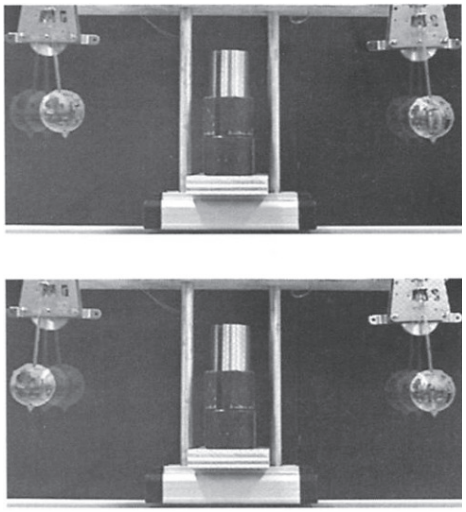

Figure 9.1: *Multi-exposure images of two pendulum clocks mounted on a movable cart so the mechanical coupling between them could be adjusted by weights at the centre. Even when they are started in-phase (upper image) they eventually oscillate stably antiphase (lower image). Courtesy Matthew Bennett [56].*

The coherent motion in Huygens's clocks is a simple example of a wider phenomenon: the spontaneous appearance of an intimate correlation between oscillators which are weakly coupled to one another. This correlation is seen in a wide range of systems, ranging from the flashing of fireflies at night, to the firing of neurons in the brain, to superfluids. In this chapter we will see that the same correlation is observed in bouncing droplets.

9.1 Minimising energy loss

In 1906, Diederik Korteweg, a Dutch mathematician, noticed that Huygens's clocks have spontaneously arranged themselves into a configuration that minimises energy loss into the environment via mechanical movements in the mounting [57].

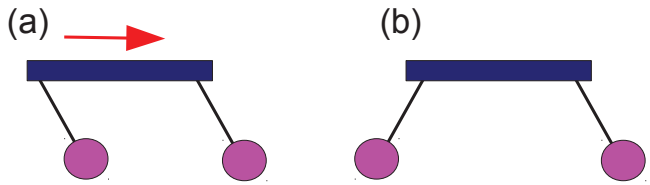

Figure 9.2: *Korteweg's explanation for the emergence of coherent motion in Huygens's clocks. (a) When the pendula oscillate in-phase with one another, they induce displacements in the mounting (red arrow) whose energy is eventually lost to friction. (b) When the pendula oscillate antiphase, they exert opposite forces on the mounting, so less energy is lost. The extra energy loss in (a) induces that mode to decay until (b) dominates.*

When the pendula oscillate in-phase with one another, as in figure 9.2(a), Korteweg reasoned, they will exert forces on the mounting which reinforce each other, causing small movements (red arrow) whose energy is eventually lost to friction. But when they are antiphase, as in (b), the two pendula exert opposite forces on the mounting and less energy is lost. This mechanism preferentially drains energy from the in-phase mode, which decays until the antiphase mode dominates. See Bennett [56] for further treatment in terms of nonlinear dynamics.

9.2 General solution for Huygens's clocks

When Huygens's clocks oscillate in their preferred antiphase mode, the difference in the angles is

$$\delta \;=\; \theta_1 - \theta_2 \;\propto\; \cos(\omega_o t)$$

where θ_1 and θ_2 are the angles of the pendula and ω_o is the angular frequency. Just as we saw in the previous chapter, it is convenient to extend this definition into the complex plane by writing

$$\delta \;=\; A_\delta \, e^{-i\omega_o t}$$

where it is understood that the imaginary component has no direct physical meaning and will be discarded at the end of the calculation. This representation has the advantage that an arbitrary phase (or origin of time) can be accommodated by choosing a complex value for the amplitude A_δ.

When the clocks swing in-phase with one another, their frequency is reduced, as shown in the next exercise.

Exercise 9.1 Two pendula swing in-phase with one another as in figure 9.2(a). The apparatus is on a strong spring so that the displacement of the mounting, shown by the red arrow, is proportional to the angle θ.

By considering the extra distance a bob must swing due to the displacement of the mounting, show that the in-phase mode has a slightly reduced frequency.

For the in-phase motion it is usual to define $\sigma = \theta_1 + \theta_2$ and extend it into the complex plane in the same way as above, $\sigma = A_\sigma\, e^{-i(\omega_o - \Omega)t}$ where Ω is the frequency difference.

We can immediately write down the general solution for Huygens's clocks, which is a sum of these two modes

$$\begin{aligned} 2\theta_1 &= \delta + \sigma &&= e^{-i\omega_o t}\,(A_\delta + A_\sigma\, e^{i\Omega t}) \\ -2\theta_2 &= \delta - \sigma &&= e^{-i\omega_o t}\,(A_\delta - A_\sigma\, e^{i\Omega t}) \end{aligned} \qquad (9.1)$$

This is illustrated in figure 9.3.

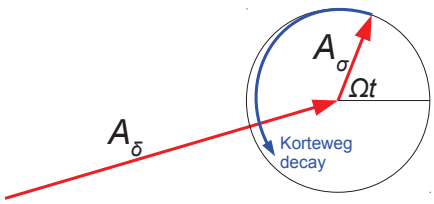

Figure 9.3: *Argand diagram showing the general solution for Huygens's clocks (equation 9.1 for θ_1, omitting the factor $e^{-i\omega_o t}$). The dominant mode has amplitude A_δ. It is perturbed by the in-phase mode (amplitude A_σ). The perturbation oscillates at the difference frequency Ω, and it slowly decays due to Korteweg's effect.*

Here the antiphase mode is dominant and given by A_δ. The in-phase mode, A_σ, can be regarded as an oscillatory perturbation which slowly decays due to the effect described by Korteweg.

9.3 Order parameter

There is a common factor in equations (9.1) for the two pendula, namely

$$\psi = e^{-i\omega_o t} \qquad (9.2)$$

This common factor is called an **order parameter**. There is a similar common factor, of the same origin, when there are many weakly coupled oscillators rather than just two. The associated patterns of synchronisation and resonance are studied in a branch of physics called **Kuramoto theory** after its Japanese founder, Yoshiki Kuramoto. This field has successfully tackled phenomena ranging from the flashing of fireflies at night through the oscillations of coupled Josephson junctions to the firing of neurons on the brain. A good reference is a survey article by Juan Acebrón, Luis Bonilla, Conrad Pérez Vicente, Félix Ritort and Renato Spigler [58].

9.4 Minimising energy loss into the environment

When multiple oscillators are phase locked by an order parameter, they readily exchange energy amongst themselves so the energy of the correlated motion becomes equilibrated.

There is another, equivalent, way to view the same phenomenon. Each oscillator radiates energy into the medium, so the sympathetic motion would die away if there were no other effect. The sympathy is maintained because the surrounding oscillators reflect the energy back with the correct phase to keep the synchronization alive.

This can be understood as a manifestation of Korteweg's effect, which we saw in the two pendula. Any modes where the energy is not reflected back with the right phase will decay away, leaving only those modes that minimise the escape of energy into the surrounding medium. This Darwinian-type mechanism is responsible for the appearance of an order in the oscillators, namely, that they spontaneously arrange themselves into the state that minimises energy loss into the environment.

9.5 Thermodynamic considerations

When an order parameter appears, the system is, obviously, more ordered. It has less entropy. For example, initially the pendula in Huygens's experiment are able to move in two different modes: in-phase or antiphase. But in the final state they can only move antiphase. The final state is therefore more ordered than the initial one.

The increase in order is made possible because energy and entropy are exchanged with the environment. The total entropy of the system plus its environment has not been reduced, of course. What has happened is that some of the modes have become stilled because their energy has escaped into the environment, leaving a smaller number of modes and a more ordered arrangement in the system, at the expense of greater entropy in the environment.

The same process occurs when a liquid slowly crystallizes as its latent heat escapes. If the energy lost is ΔE and the temperature is T, then the entropy of the system is reduced by $\Delta E/T$ and that of the environment is increased by the same amount. A spontaneous increase in order has occurred in the crystal.

This effect is observed in the bouncing droplets, which spontaneously form into crystal-like structures as photographed in figure 9.4.

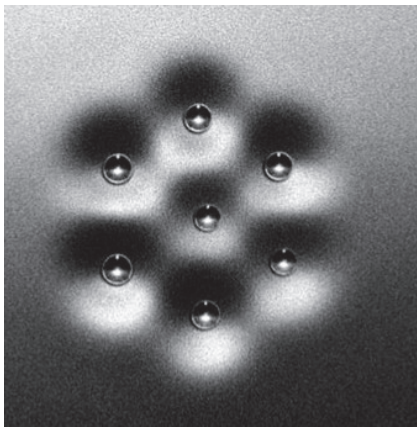

Figure 9.4: *Self-assembled cluster of droplets. (Courtesy Suzie Protière, Arezki Badaoud and Yves Couder) [11]*

Like Huygens's clocks, these droplets have aligned themselves into a configuration that minimises the escape of energy into the surrounding medium. They are approximately one wavelength apart. At this separation, the waves coming from the outer droplets reinforce at the centre, so the energy radiated by the central droplet is reflected back on to it. If the droplets were to move closer or further apart the reflection would be reduced and more energy would escape by radiation into the medium.

Another way to visualise the alignment in the photograph is that the outer droplets act as one layer of a **Bragg mirror**, reflecting outgoing radiation and minimising energy loss. (Bragg reflection was discussed in section 2.4). Adding further layers would further reduce the energy per droplet that is lost by radiation, which is one way to account for the appearance of very large crystal-like structures.

A third way to visualise the same effect is in terms of a sign reversal of the secondary Bjerknes force between two pulsating bubbles as they approach one another closely. See for example Ida [59] and references therein.

9.6 Perturbations to the order parameter

In addition to the correlated motion which is described by the crystalline structure or the order parameter, there may be other components which are of thermodynamic or mechanical origin. For example, in Huygens's clocks the other component is given by A_σ in figure 9.3. As the temperature increases, there comes a point where these perturbations disrupt the order parameter and a phase transition occurs. We will see this quantitatively in section 11.15 on the Thouless-Kosterlitz phase transition. For the present we are interested in systems that are below this transition temperature.

In figure 9.3, the perturbations to the order parameter have amplitude A_σ. They are oscillatory, or very nearly so. At low temperature, when the amplitude is small, these perturbations obey equations which are the same as those for a mass that is subject to a restoring force, such as a pendulum. The next exercise invites you to demonstrate this.

Exercise 9.2 A large number of oscillators are phase locked together and may be assumed to have a fixed angular frequency ω_o. One of the oscillators is perturbed so that its phase relative to the others is

$$\Delta\theta \quad = \quad \Delta\theta_o \, \cos(\Omega t)$$

This perturbation is illustrated in the Argand diagram in figure 9.3. Explain why this is a reasonable model when A_σ and the Korteweg decay are both small.

Show that the angular frequency of the perturbed oscillator is

$$\omega \quad = \quad \omega_o - \Omega \, \theta_o \sin(\Omega t)$$

and hence that

$$\frac{d^2\omega}{dt^2} \quad = \quad -\,\Omega^2 \omega$$

Show that a mass subjected to a restoring force, such as a pendulum, obeys an equation of the same form.

The foregoing analysis is for the case where the other oscillators are unaffected. This is not true if the interactions are local, since the perturbation will transmit to the nearby oscillators, by symmetry. In a wide range of circumstances when oscillatory motion is transmitted by purely local interactions, the motion obeys the wave equation (2.1) to first order. Examples include deep sea waves, shallow sea waves, waves determined by surface tension, longitudinal sound waves in the air and transverse waves in a solid.

We will be interested in the case where the perturbations to the order parameter, and hence the order parameter itself, obey the wave equation to first order.

9.7 Equations of coherent motion

With large number of locally coupled oscillators, such as the cluster of bouncing droplets in figure 9.4, we have seen that the order parameter is oscillatory and obeys the wave equation to first order.

The surface waves in the droplet experiments in chapter 6 are also oscillatory and obey the same equation. The analysis of that chapter can be applied, since the same equations have the same solutions.

Exercise 9.3 A set of locally coupled oscillators are correlated by an order parameter that is oscillatory and obeys the wave equation.

By apply the method of chapter 3, or otherwise, show that the order parameter must be Lorentz covariant with a characteristic speed equal to the speed of transmission c.

When it does not vary with position, the order parameter is given by $\psi = e^{-i\omega_o t}$. Show that this obeys

$$\frac{\partial^2 \psi}{\partial t^2} \quad = \quad -\omega_o^2 \, \psi$$

This equation does not take account of phase difference between locations. and it must be extended to a Lorentz invariant form in order to take them into account. By applying the method of chapter 6, show that , namely the Klein-Gordon equation

$$\frac{\partial^2 \psi}{\partial t^2} \; - c^2 \nabla^2 \psi \quad = \quad -\omega_o^2 \psi \tag{9.3}$$

Hence or otherwise show that the order parameter obeys Schrödinger's equation when the spatial variation is small.

In particular, the order parameter for the cluster of droplets photographed in figure 9.4 is Lorentz covariant with a characteristic speed equal to the speed of propagation, and it obeys the Klein-Gordon equation, which approximates to the Schrödinger equation at low velocity. It behaves like a 'field' in quantum mechanics.

If one of the droplets is accelerated horizontally, it will emit waves into the field. We saw in section 5.8 that these waves obey Maxwell's equations.

9.8 Superfluid

The appearance of an order parameter obeying the Klein-Gordon equation (9.3) is observed in a number of fluids at low temperature, called superfluids. In superconductors the order parameter is usually labelled δ, and in superfluid helium it is usually labelled ψ and called the wavefunction [60, 61]. Superfluids will be discussed in more detail in chapter 11.

9.9 Gauge symmetry

The equations governing classical oscillators are symmetrical under a transformation in which the phases of all the oscillators are advanced by an arbitrary amount. For instance, if they oscillate at the same frequency then the increase in phase corresponds merely to a change in the origin chosen for time.

Such systems are said to have **gauge symmetry**. To be more precise, the absolute phase cannot be measured by any expectation value (section 1.6).

Superfluids have the same gauge symmetry. This is usually explained as due to an underlying gauge symmetry of quantum mechanics, but we have seen that the same symmetry is exhibited by the classical motion of weakly coupled oscillators according to Newton's laws.

Even though absolute phase cannot be measured, the interactions between oscillators might depend on their relative phases. Relative phase can be measured. This subject was studied by Brian Josephson in superconductors. His analysis is set out in his highly readable thesis on his work for which he was awarded a fellowship at Trinity College Cambridge in 1962 [60], and, later, a Nobel prize.

The key to Josephson's analysis is a process called **spontaneous symmetry breaking**. A sphere of ferromagnetic material has the symmetry that it has no preferred direction in space. Nevertheless, the atoms prefer to align in the same direction as one another. In order to achieve this alignment, they must choose a specific direction, which is measured by the magnetic moment. Thus, the order parameter associated with the magnetic alignment breaks the overlying symmetry.

The order parameter in superconductors is associated with a similar spontaneous symmetry breaking. The elementary components in a bulk superconductor prefer to align themselves with the same phase, which requires that they choose a particular value. The absolute phase cannot be measured, but if two bulk superconductors are in weak contact then the interaction between them depends on their relative phases. This is the broken symmetry at the heart of the Josephson effect. We have seen that classical oscillators exhibit the same broken symmetry.

9.10 Summary

An isolated oscillator usually radiates its energy into the surroundings until its motion dies away. There is an exception when it is surrounded by other oscillators with which it is weakly coupled. The surrounding oscillators spontaneously align themselves as if conspiring to impede the energy loss. This was first explained in 1906 by Diederik Korteweg in the case of coupled pendula. There is a Darwinian-like selection process, where those modes whose energy loss is not impeded by nearby oscillators will die away, leaving a more ordered arrangement where the oscillators conspire collectively to reflect the energy back.

We saw that this phenomenon is responsible for the crystal-like clusters photographed in bouncing droplets. These structures are more ordered and have less entropy. Ordinary crystals likewise have less entropy when they are in their ordered arrangement, a phenomenon which is usually explained in terms of the postulates of thermodynamics rather than the motion of classical oscillators according to Newton's laws.

The same alignment phenomenon leads to the appearance of a so-called 'order parameter' in multiple coupled oscillators. There is a literature on this in

Kuramoto theory; see the survey article by Juan Acebrón, Luis Bonilla, Conrad Pérez Vicente, Félix Ritort and Renato Spigler [58]. When the coupling between the oscillators is weak and local, we saw that the order parameter obeys the Klen-Gordon equation, just like the order parameter that is observed in superconductors and in superfluid helium. Superfluids are usually explained in terms of the postulates of quantum mechanics rather than the motion of classical oscillators according to Newton's laws. They are the subject of chapter 11.

9.11 Dialogue

On day 6 of their dialogue, Alice, Bob and Carol discuss the spontaneous appearance of order in systems that are in contact with a low-temperature environment. They argue the following positions.

(a) Alice says that, in any group of interacting molecules, you can find an alignment that maximises their interaction energy. Any molecules that are out of alignment will have excess energy, which escapes into the environment as heat, coercing them back into alignment. This is why an order parameter emerges or they form into crystals.

(b) Bob says that, in any group of interacting oscillators, you can find an alignment that reflects energy back and minimises the rate at which they lose energy into the environment. Any modes of oscillation that are out of alignment will quickly lose energy, coercing them back into alignment. This is why an order parameter emerges or they form into crystal-like clusters.

(c) Carol says it is no coincidence that Alice's molecules and Bob's oscillators arrange themselves in the same way. It is known that molecules are oscillators with a frequency of order 10^{20} Hz. The mechanism Bob has described is the ultimate cause of the spontaneous alignment in both systems. Alice's implicit assumption, that heat always flows so as to maximise entropy, is superfluous.

Each of these approaches can be made consistent with all the relevant experiments. Argue in favour of each one in turn.

Chapter 10

Rotational motion

The world is full of magical things patiently waiting for our wits to grow sharper.

Bertrand Russel

We have so far only considered waves with circular and spherical symmetry. The photographs in figure 10.1 suggest we also have to think about solutions to the wave equation which depend on angle.

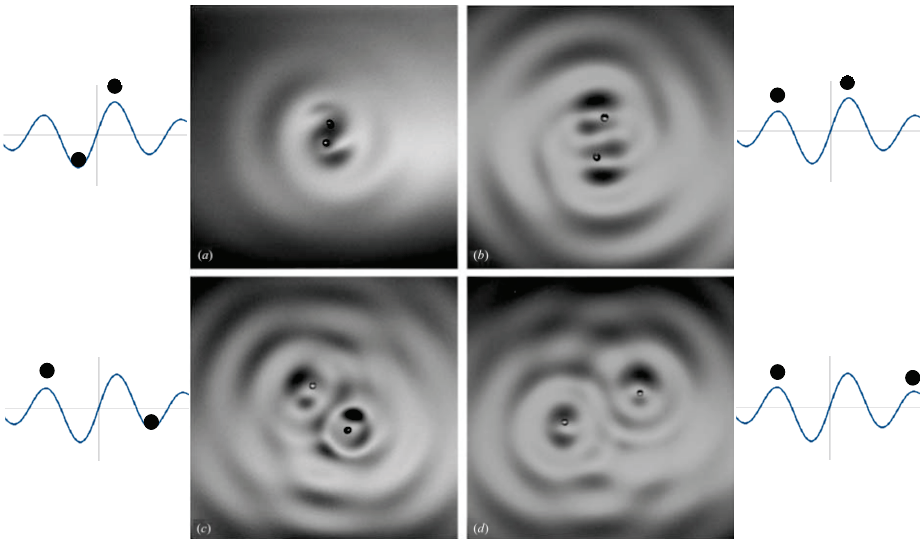

Figure 10.1: *The waves with two droplets. The side drawings show a Bessel function J_1, which is the lowest relevant component of the standing waves between the droplets. The bouncing is antiphase in (a) and (c) and in sympathy in (b) and (d). (Photograph courtesy Suzie Protière, Arezki Boudaoud and Yves Couder [11])*

In this experiment, the droplets orbit around one another with a period of

approximately 20 bouncing periods in (a), and longer in (b)-(d). Their velocity is approximately that of an ordinary walker driven with the same vertical acceleration, which is why the period increases with radius.

10.1 Harmonic solutions

The motion in the photographs can be described using the solutions to the wave equation in circular coordinates (r, θ), namely

$$h_m \;=\; h_o\ \cos(\omega_o t - m\theta)\ J_m(k_r r) \tag{10.1}$$

where J_m is a cylindrical Bessel function of the first kind, m is an integer whose sign is significant, and $\omega_o = c\ k_r$. The waves near the two droplets contain components with various values of m, but the main experimental results can be understood from the lowest order rotating components, with $m = \pm 1$. We neglect higher harmonics as well as J_o in (b) and (d).

Exercise 10.1 *Harder* A Bessel function is defined in (2.4) and, in circular coordinates, the wave equation is given by (2.3).

Show by direct substitution that (10.1) obeys the wave equation.

The drawings to the side of figure 10.1 shows the Bessel function J_1, which gives the wave height of the lowest rotating component on a line joining the droplets. As we have seen, the droplets prefer to land in the wave troughs, so they are in free flight over the crests, as shown. The rotating wave pattern is

$$\begin{aligned} h \;&=\; \tfrac{1}{2} h_0\ [\cos(\omega_o t + \Omega t - \theta)\ J_1(k_1 r)\ +\ \cos(\omega_o t - \Omega t + \theta)\ J_1(k_2 r)] \\ &\approx\; h_o\ \cos(\omega_o t)\ \cos(\Omega\ t - \theta)\ J_1(k_r r) \end{aligned} \tag{10.2}$$

where $ck_1 = \omega_o + \Omega$ and $ck_2 = \omega_o - \Omega$. In the second expression we have used the identity $\cos(A + B) + \cos(A - B) = 2\cos A \cos B$, and have approximated $k_1 \approx k_2 \approx k_r$, which is valid at small r and Ω. This can be regarded as a standing wave that rotates with the droplets at angular frequency Ω.

The factor $\cos(\Omega t - \theta)$ vanishes on the node line $\theta = \Omega t \pm \frac{1}{2}\pi$. On either side of this line, its sign reverses; we see in the photographs in figure 10.1(b) – (d) that the crests turn into troughs and the troughs crests. The node line is nearly normal to the line joining the droplets, indicating that they are bouncing close to the angle with the largest wave amplitude. The pattern is not so evident in (a), due to the greater angular velocity and the presence of higher-order components.

The Bessel function J_1 gives the amplitude of the standing waves on a line joining the droplets, and it is drawn to the side in figure 10.1. As we have already seen, the droplets prefer to land in the wave troughs, so they are in free flight over the crests. The modes (a)-(d) are the result.

10.2 Flux

Figure 10.2 shows how the wave height h_1 in (10.1) varies with angle at fixed radius. The wave propagates in the $+\theta$ direction.

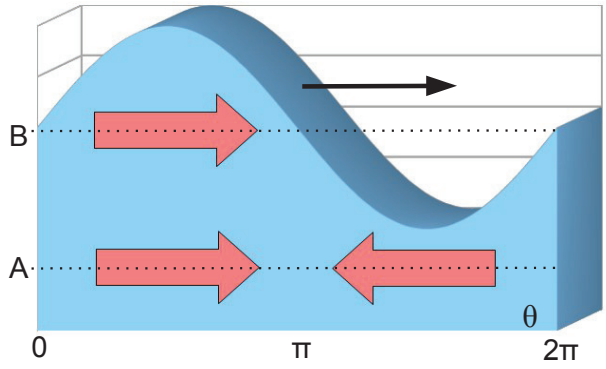

Figure 10.2: *The wave h_1 in (10.1) at fixed radius at the instant $\omega_o t = \pi/2$. The red arrows show the flow speed, which is proportional to the wave height.*

There is an integer number n of wavelengths in the diagram (which shows the case where $n = 1$). An equivalent way to express this condition is in terms of the phase of the wave, S, which must advance by $2n\pi$ when going around the centre,

$$\oint \nabla S.d\mathbf{l} \quad = \quad 2n\pi$$

The advance of phase around a loop can also be seen in the experiment of Michael Berry and colleagues in which water waves propagate past a vortex (figure 10.3. As the strength of the vortex increases, more wavelengths appear on one side of the vortex than the other, so that $\oint \nabla S.d\mathbf{l} \neq 0$ where S is the phase of the wave. For example, there is one flux quantum ($n = 1$) in the photograph labelled 1.

An analogous phase change also occurs in a quantum mechanical interaction with a magnetic field, called the Aharonov-Bohm effect, and the authors also showed that the water waves exhibited an analogue of this effect.

The same condition is associated with the quantisation of magnetic flux in superconductors and the quantisation of angular momentum in superfluid helium, where S is the phase of the order parameter (see section 9.8).

10.3 Irrotational vortex

Returning to the solution to the wave equation h_1 shown in figure 10.2, the flow velocity $\mathbf{u}$ is irrotational ($\oint \mathbf{u}.d\mathbf{l} = 0$) when the path of integration $d\mathbf{l}$ is on the

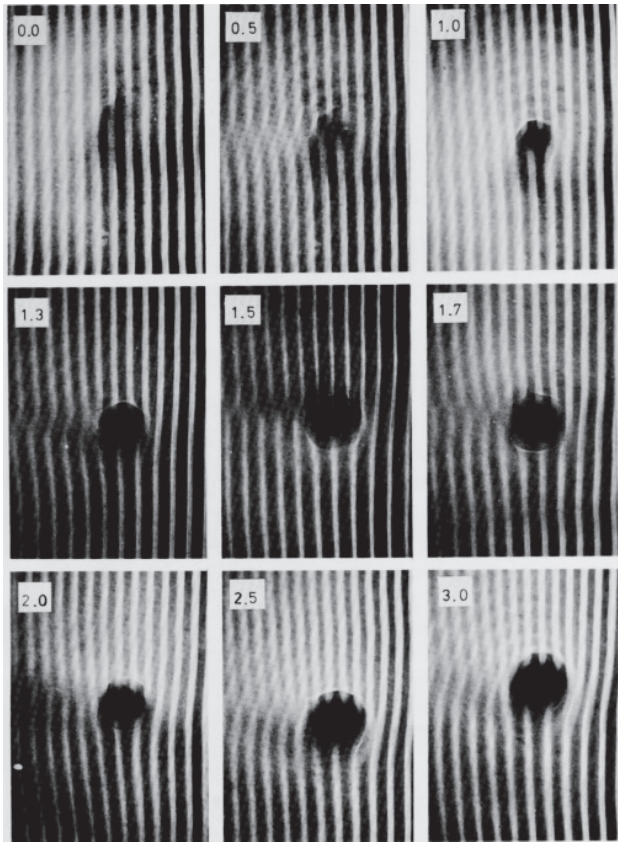

Figure 10.3: *Water waves near a vortex (Courtesy Michael Berry [5]*

submerged line A, as we would expect from Kelvin's circulation theorem (section 1.2). This can also be seen from the symmetry of the figure. Nevertheless the wave is quantised in the angular direction. Such a wave field is called an 'irrotational vortex'.

The vanishing of the circulation on the submerged line A does not mean the wave has no angular momentum, since the circulation does not vanish at B, a line which is not wholly submerged and to which Kelvin's circulation theorem does not apply. Physically, the elevations carry extra fluid around the centre.

In fact, at large radius, the net flow around the centre approximates to that of a vortex when averaged over a period and a wavelength. This is because the Bessel function in (10.1) approximates to a standing wave in the radial direction, whose amplitude reduces as $A \sim r^{-\frac{1}{2}}$. The flow speed is $u \propto A$ so the net flow is proportional to $uA \sim r^{-1}$, which is the same as a vortex.

At small radius the flow diverges from that of a vortex, and in particular there is no singularity. It is illustrated in figure 10.4.

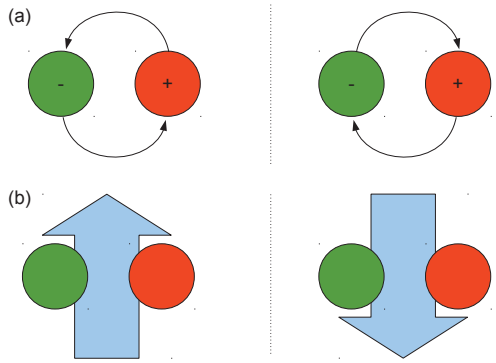

Figure 10.4: *(a) Schematic drawing of the rotating droplet pair photographed in figure 10.1(a), and its image in the boundary. At the instant drawn, the green circles are the wave troughs (where the droplet lands) and the red circles are crests. (b) The fluid flow due to the rotational motion. The trough has negative volume and contributes to the flow in the same Cartesian direction as the crest.*

10.4 Attraction to the boundary

If two vortices of opposite circulations are held so their centres cannot move, they will attract one another because their flows reinforce in the region between them, giving a reduced Bernoulli pressure. Rotating pairs of bouncing droplets will similarly be attracted towards their images in the boundary, which rotate in the opposite direction as illustrated in figure 10.4.

In the 19th century, Bjerknes had found that like bubbles (with the same phase) attract and unlike ones (with opposite phases) repel, as shown in figure 7.2. Inconveniently, this appeared to have the opposite sign to the electromagnetic forces he was attempting to model. But the forces between rotating droplets have the same sign as the forces between electrons, namely that unlike circulations attract and like ones repel. What of their fine structure constant?

We saw that individual droplets are repelled from the boundary by an inverse square force (chapter 5). This static force obeys the equations of electrostatics, with a fine structure constant of order 1. We also saw evidence for a motion-dependent force which obeys the same equations as magnetism, in which a droplet and its image in the boundary are attracted towards one another when they both move in the same direction parallel to the boundary.

Turning to a pair and its image in the boundary, the static forces nearly cancel out, since if one droplet of a pair is attracted to the image then the other, being antiphase, will be repelled. However, the motion-dependent force is always attractive. For example, consider the interactions with the wave crest marked in red on the left of figure 10.4. It is moving in the same direction as the (green) trough in the image, an alignment which we saw produces a force of attraction (section 5.9). The crest in the image (red) moves in the opposite direction and with the opposite phase. Each of these individually reverses the direction of the interaction, so the combination leaves the sign unchanged.

The ratio of the moving to the static forces is v^2/c^2 (the same as the ratio of the magnetic to the electrostatic forces for particles moving at velocity v). The force on each droplet is doubled, since there are two images, but it must be averaged over a rotation, giving a factor of $\frac{1}{2}$. The fine structure constant of the interaction is thus

$$\alpha_2 \;=\; \frac{v^2}{c^2}\,\alpha_1 \tag{10.3}$$

where α_1 is the fine structure constant for the static force between individual droplets. The strength of the interaction depends on the rotational speed, which can be varied in the experiment. A typical value might be $v = \frac{1}{4}c$ and $\alpha_1 \sim 0.3$ giving $\alpha_2 \sim 1/50$.

Our model predicts that an orbiting droplet pair will be attracted towards the boundary with this reduced fine structure constant. This phenomenon has been noted by the experimenters; orbiting pairs that approach a submerged boundary at a shallow angle can stick to it and then move along it, playing 'hopscotch' as each droplet takes it in turn to leapfrog the one in front. However an experiment with precise measurements has not yet been performed.

10.5 The emergence of spin-half behaviour

The rotating waves in (10.1) can be treated as independent because they are orthogonal in the sense that

$$\int_0^{2\pi} h_m\, h_n\, d\theta \;=\; 0 \qquad\qquad (m \neq n) \tag{10.4}$$

Exercise 10.2 By direct substitution into (10.1), show that this is true.

We have seen that the angular momentum of the wave h_1 in (10.1) is in the $+z$ direction (vertically upwards), and it is in the $-z$ direction for h_{-1}. The photograph in figure 10.1 shows the case where the waves have nearly equal amplitude. What if the amplitudes are not equal?

It simplifies the analysis to consider 'degenerate' solutions, that is, solutions that have the same energy. (Solutions of arbitrary energy can be obtained by scaling the wave height.) The degenerate solutions are

$$h \;=\; \cos(\alpha)\, h_1 \;+\; \sin(\alpha)\, h_{-1} \tag{10.5}$$

where α is a real parameter. This is a solution to the wave equation because it is a sum of solutions. Its energy is proportional to $\cos^2\alpha + \sin^2\alpha$, which is constant, so the waves are degenerate. The angular momentum is

$$\begin{aligned} L &= L_o(\cos^2\alpha - \sin^2\alpha) \\ &= L_o\cos(2\alpha) \end{aligned} \tag{10.6}$$

where L_o is the angular momentum of h_1. The angular momentum and the wave pattern h vary continuously with the parameter α, as shown in the table below

α	L/L_o	h
0	1	h_1
$\frac{\pi}{4}$	0	$\frac{1}{\sqrt{2}}(h_{-1}+h_1)$
$\frac{\pi}{2}$	-1	h_{-1}
$\frac{3\pi}{4}$	0	$\frac{1}{\sqrt{2}}(h_{-1}-h_1)$
π	1	$-h_1$

As we can see in the table, the wave field reverses sign after the direction of the angular momentum has gone through a complete cycle. Two cycles are needed to return to the starting position.

Fermions are like these waves, in that their wavefunctions reverse sign if the direction of their angular momentum is rotated through 360°. It is commonly believed that this behaviour cannot emerge from classical mechanics. However the rotating droplets show that this belief is wrong.

In fact, double symmetry is already known in systems that contain two harmonic sub-systems. Leroy, Bacri, Hocquet and Devaud provided another example in 2006 when they showed that two weakly coupled pendula with nearly the same frequency also have this symmetry [62].

10.6 Bloch sphere

The elementary waves in (10.1) are the real part of

$$\xi_m \;=\; A\, e^{-i(\omega_o t - m\theta)}\; J_m(k_r r) \tag{10.7}$$

where A is the amplitude. This can be factored as before into

$$\begin{aligned} \xi &= \psi\,\chi \\ \psi &= e^{-i\omega_o t} \\ \chi &= A\, e^{im\theta}\; J_m(k_r r) \end{aligned} \tag{10.8}$$

In chapter 6 we showed that ψ obeys Schrödinger's equation. Now let us examine the factor χ.

When the wave height in (10.5) is extended into the complex plane as in (10.8), we get a simple way to provide an arbitrary origin of time for each of the two components

$$\chi = e^{iS}\left[\cos\left(\tfrac{1}{2}\beta\right)\chi_1 + e^{i\varphi}\;\sin\left(\tfrac{1}{2}\beta\right)\chi_{-1}\right] \tag{10.9}$$

where S is an arbitrary overall phase, φ is the relative phase of the two components, and we have defined $\beta = 2\alpha$.

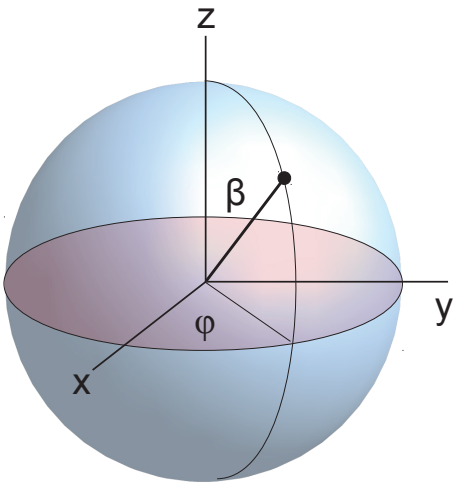

Figure 10.5: *A Bloch sphere.*

The parameters in this equation can be represented on a sphere as shown in figure 10.5. The angular momentum normal to the surface (in the z direction) is proportional to $\cos\beta$. When $\beta = \frac{1}{2}\pi$, the angular momentum vanishes and there are standing waves whose amplitude is greatest at angle φ to the x axis. However, this diagram should not be over-interpreted. It would be wrong to conclude that the system is physically oriented in the direction indicated in the figure. The existence of a simple geometrical way to picture the parameters in (10.9) should not blind us to the fact that we are describing ordinary surface waves which cannot rotate out of the plane of the surface.

Nonetheless, equation (10.9) is the same as that of a spin-half particle whose wavefunction is χ where χ_1 is the spin-up state and χ_{-1} the spin-down state, which is usually represented on the 'Bloch sphere' in figure 10.5. By inspection, the sign of χ reverses when β increases by 2π, which is characteristic of spin-half systems.

10.7 Pauli spin matrices

The mapping of the wave height near a droplet onto the Bloch sphere can be shown more formally by writing (10.9) as a dot product of two vectors $\mathbf{a}$ and $\boldsymbol{\chi}$

$$\chi \;=\; \mathbf{a}.\boldsymbol{\chi} \;=\; (a_1, a_2).(\chi_1, \chi_{-1})$$

where the values of a_i are obtained from (10.9). The angular momentum of the first component is proportional to $|a_1|^2$, and that of the second component is proportional to $-|a_2|^2$, so the normalised total is

$$\sigma_z \;=\; \frac{|a_1|^2 - |a_2|^2}{|a_1|^2 + |a_2|^2} \tag{10.10}$$

This can also be written

$$\sigma_z \quad = \quad \frac{\mathbf{a}^*.\ \widehat{\sigma}_z\,\mathbf{a}}{\mathbf{a}^*.\mathbf{a}} \tag{10.11}$$

where $\widehat{\sigma}_z = \left(\begin{smallmatrix} 1 & 0 \\ 0 & -1 \end{smallmatrix}\right)$ is the same as the Pauli spin matrix for the z direction.

As in quantum mechanics, we can extend this as follows. The Pauli matrices are $\widehat{\sigma}_x = \left(\begin{smallmatrix} 0 & 1 \\ 1 & 0 \end{smallmatrix}\right)$, $\widehat{\sigma}_y = \left(\begin{smallmatrix} 0 & -i \\ i & 0 \end{smallmatrix}\right)$, $\widehat{\sigma}_z = \left(\begin{smallmatrix} 1 & 0 \\ 0 & -1 \end{smallmatrix}\right)$, and spin projections σ_i are defined by

$$\sigma_i \quad = \quad \frac{\mathbf{a}^*.\ \widehat{\sigma}_i\,\mathbf{a}}{\mathbf{a}^*.\mathbf{a}}$$

where i can be x, y or z. The eigenvectors of $\widehat{\sigma}_i$ are

β	φ	(a_1, a_2)	$(\sigma_x, \sigma_y, \sigma_z)$	Eigenvector of
$\frac{1}{2}\pi$	0	$\frac{1}{\sqrt{2}}(1,1)$	$(1,0,0)$	$\widehat{\sigma}_x$
$\frac{1}{2}\pi$	$\frac{1}{2}\pi$	$\frac{1}{\sqrt{2}}(-i,i)$	$(0,1,0)$	$\widehat{\sigma}_y$
0	0	$(1,0)$	$(0,0,1)$	$\widehat{\sigma}_z$

It will be noticed that $(\sigma_x, \sigma_y, \sigma_z)$ correspond to the Cartesian coordinates of a unit vector at the spherical angle (β, φ) in figure 10.5. This is the basis of the Bloch sphere, which maps between the two representations. The mapping is a double covering because χ reverses sign when β increases by 2π. The same mathematics is used to describe fermions in quantum mechanics.

10.8 Antisymmetry

When the driving amplitude is reduced, the rotation speed of the droplets photographed in figure 10.1 slows to zero. Figure 10.6 is a schematic of two droplet pairs near each other. A is a solution to (10.9) with $(\beta, \varphi) = (\frac{1}{2}\pi, 0)$ and B has $(\frac{1}{2}\pi, \frac{1}{2}\pi)$.

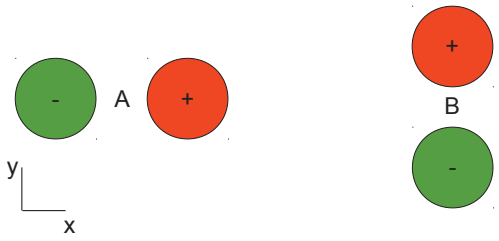

Figure 10.6: *Schematic of two droplet pairs near each other. Elevations are marked red and depressions green.*

The droplets in B have opposite phases, so one will attract the other pair whilst the other repels and the net forces cancel. However, there is still an effect

involving orientation. One droplet in A is closer to B than the other, which will cause B to rotate anticlockwise. This prediction might be tested experimentally.

After B has rotated into the preferred alignment, the solutions will be oriented in the x direction and the wave height is the real part of

$$\xi \;=\; \xi_a(\mathbf{x}, t) \;-\; \xi_a(\mathbf{x} - \mathbf{d}, t) \tag{10.12}$$

where ξ_a is the wave due to A and $\mathbf{d}$ is the separation of the pair, $B - A$.

Equation (10.12) is antisymmetric, and, in particular, exchanging A and B reverses the sign of the wave field. This may be compared to the principle, formulated by Wolfgang Pauli in 1925, that the total wave function for two identical fermions is anti-symmetric with respect to exchange of the particles.

10.9 Summary

We have seen photographs of circular solutions to the wave equation on the surface of a liquid. The waves are described by a parameter β. As this parameter advances, the wave changes continuously and reverses sign, whilst its angular momentum goes through a complete cycle and returns to its starting value. Two complete cycles of the direction of the angular momentum are needed to return to the starting state.

The same mathematics that describes these waves is also used for spin-half particles in quantum mechanics.

10.10 Dialogue

On day 7 of their dialogue, Alice, Bob and Carol argue for the following propositions

(a) Alice says electrons reverse sign when you rotate their angular momentum vectors through 360°. She concludes they cannot be modelled as classical systems, which are unchanged after rotation through a complete circle.

(b) Bob says waves on the surface of a liquid reverse sign when you rotate their angular momentum vectors through 360°. He concludes they cannot be modelled as classical waves, which are unchanged after rotation through a complete circle.

(c) Carol says the waves do not physically rotate with their angular momentum vectors. Alice and Bob have wrongly assumed the contrary.

Each of these approaches can be made consistent with all the relevant experiments. Argue in favour of each one in turn.

Chapter 11

Superfluids

Perhaps, if a more complicated wavefunction were tried, some special linear combination representing a kind of microscopic vortex ring or one with intrinsic angular momentum has in fact a lower energy.

Richard Feynman in 1954 [63]

The phenomena we have seen so far are governed by Euler's equation for a fluid, with viscous losses replenished by an external driving mechanism. We now turn to superfluids, where there are no viscous losses and external driving is superfluous.

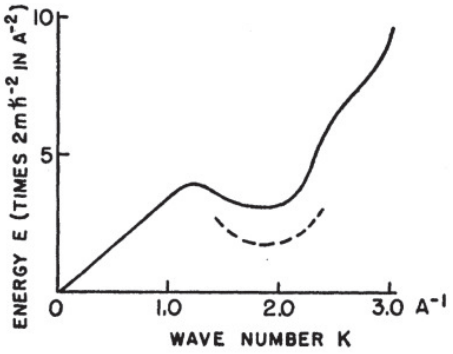

Figure 11.1: *The energy as a function of wavevector in superfluid helium from neutron scattering data, calculated neglecting compressibility (solid line), and from specific heat capacity data (dotted line) [63].*

In 1953 and 1954, Richard Feynman proposed a model of superfluid helium that neglected its compressibility [63–65]. He showed (figure 11.1) that his model did not agree with the experimental data, and he concluded there must be unidentified low-energy excitations in the fluid, which he presumed to be 'a kind of microscopic vortex ring or one with intrinsic angular momentum' [63]. He called these presumed excitations **rotons**, a term first introduced by Landau.

We will see that there has since emerged ample experimental evidence for rotons, but their precise nature remains unknown.

In this chapter we will treat superfluid helium as an ordinary compressible fluid that obeys Euler's equation. The helium atom is spherically symmetric, so it has no rotational modes into which energy can be dissipated, and there is no contribution to the viscosity. By applying what we have learnt from the droplet experiments, we will find excitations that have many features in common with what is observed for rotons.

11.1 Introduction to superfluid helium

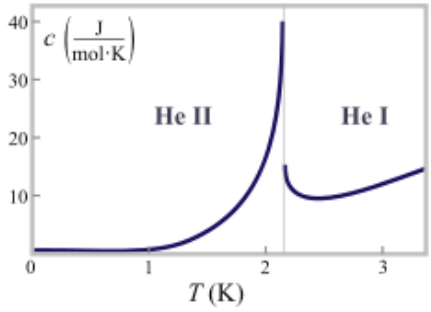

Figure 11.2: *The specific heat capacity of liquid helium as a function of temperature.*

In 1937, Pyotr Kapitsa, Jack Allen and Don Misener discovered that when ^{4}Helium is cooled below about 2.17K it becomes superfluid, with zero viscosity in certain limited respects. The normal fluid is often called He I and the superfluid He II. The onset of superfluidity is characterised by a second-order phase transition, with a discontinuity in the specific heat capacity of the liquid (figure 11.2). With some imagination this graph looks like the Greek letter lambda (λ), so it's called the 'lambda point'.

Below the transition temperature it was believed for many years that there was a mixture of He I and He II, with the proportion of the latter increasing as the temperature falls, until below about 1.1K it behaves almost entirely as a superfluid. The superfluid component will pass through small capillaries where viscosity would prevent normal flow (in a 'superleak'), and it will creep over the surface of vessels while the other component will not.

The superfluid phase is compressible, as evidenced by the fact that it supports sound waves like those in the air. These waves are called 'first sound,' and they propagate at about 230 m s^{-1} at low temperature and atmospheric pressure.

If helium flows at more than about 4 cm s^{-1} then it can acquire some viscosity. This is usually thought to be due to the creation of vortices which carry energy away, but this model is unsatisfactory in a number of respects, in particular there is a difficulty with the conservation of vorticity in the fluid. See for

example Seth Putterman's textbook [61].

The modern view is that liquid helium below the lambda point consists of a superfluid, plus excitations that are of thermal or mechanical origin (instead of the normal fluid with viscosity which was previously supposed). These excitations are thought to be the rotons originally suggested by Feynman in the 1950's, but their precise nature remains mysterious. Experimentally, they bounce off surfaces and so they cannot easily pass through apertures smaller than a few microns. Above about 1.1K there are enough of them that they collide with one another, so their mean free path becomes shorter than the size of the container. In this regime they behave collectively like a gas or a normal fluid, whose pressure can be observed experimentally. This gas supports compression waves, called 'second sound', whose propagation speed is typically an order of magnitude slower than first sound.

11.2 Wave equation

Superfluid helium is a compressible fluid, like the air, and so it supports sound waves (first sound) that obey the wave equation (section 1.9).

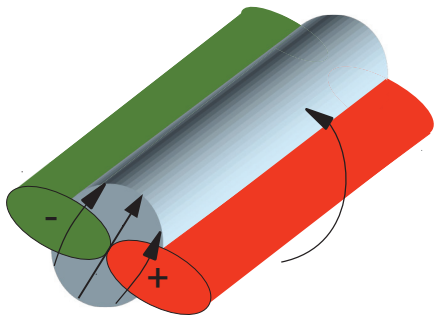

Figure 11.3: *The simplest rotating solution in a superfluid, given by* (11.1) *with* $m = 1$. *The regions of compression (red, schematic and near-field only) and rarefaction (green) rotate anticlockwise. They both contribute in the same direction to the flow* $\mathbf{u}$ *(arrows in the cross-section).*

Systems that obey the same equations have the same solutions. In particular, the rotating solution (10.1) photographed in the previous chapter has a superfluid twin. In cylindrical coordinates (r, θ, s)

$$\frac{\rho_m}{\rho_o} \;=\; 1 \;+\; A\, \cos(m\theta - \omega_o t)\; J_m(k_r r) \tag{11.1}$$

where ρ_o is the ambient density of the fluid. We will refer to this solution as an 'eddy.' Figure 11.3 is a schematic drawing of the $m = 1$ case, and figure 11.4 is a cross-section.

Just as with surface waves, we can get a more convenient and concise description of an eddy by extending the excess density into the complex plane. The imaginary part is purely for mathematical convenience and is discarded at

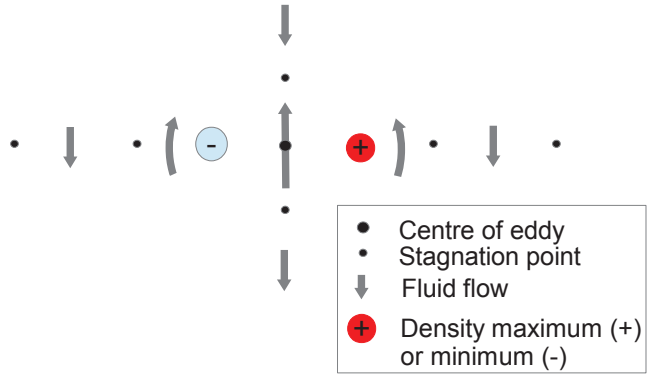

Figure 11.4: *Cross-section of the flow near an eddy. The entire flow pattern rotates around the centre, as if it were rigid, with angular speed* ω_o.

the end of the calculation. The usual convention in fluid mechanics is to define

$$\frac{\rho - \rho_o}{\rho_o} \;=\; \Re(\xi)$$

where $\Re$ means the real part. The excess density in (11.1) is thus the real part of

$$\begin{aligned} \xi &= \psi\,\chi \\ \psi &= e^{-i\omega_o t} \\ \chi &= A\; e^{im\theta}\; J_m(k_r r) \end{aligned} \tag{11.2}$$

You will notice that this is exactly the same as equation (10.8) for the wave near a rotating pair of droplets. It should be no surprise that the two solutions can be written in the same way, since they obey the same equations.

11.3 Energy and angular momentum of an eddy

We saw in the previous chapter that the flow *underneath* the rotating wave in (10.1) is irrotational, but if the entire wave is included then there is a net flow around the centre. At large distance, averaged over a wavelength and a period, the flow reduces to that of a vortex. This was illustrated graphically in figure 10.2.

The same holds for an eddy, as can be seen by replacing the wave height h by the density ρ. As we saw in the previous chapter, the flow is irrotational, $\oint \mathbf{u}.d\mathbf{l} = 0$, but the angular momentum L depends on $\oint \rho\, \mathbf{u}.d\mathbf{l}$, which does not vanish because ρ and $\mathbf{u}$ are correlated. If the frequency of the eddy and its amplitude are kept constant, then the angular momentum inside a large cylinder of fixed length and radius R centred on the eddy is the same as that of a vortex, namely $L \propto R^2$. This is shown explicitly in the advanced material below.

† *Track 2* *This material may be skipped on a first reading*

Here we explicitly translate the treatment of the rotating waves near a droplet (chapter 10 to the case of an eddy. The principal difference is that the wave height h is replaced by the density ρ.

The flow velocity near an eddy is proportional to the excess density. Expanding the Bessel function in (11.1) at large radius gives

$$u \approx \cos(m\theta - \omega t)\ u_o \sqrt{\frac{r_o}{r}}\ \cos\left(r + \frac{\pi}{4}\right)$$

where u_o is the maximum tangential velocity at some radius r_o where the Besssel function has a maximum or a minimum.

Inside a cylinder of radius R and length l centred on the eddy, the kinetic energy is

$$KE = \int_o^R \tfrac{1}{2}\rho u^2 . 2\pi r\ l\ dr$$

This must be doubled to get the total energy, since the potential energy is the same as the kinetic energy over a cycle. After substitution, this expression evaluates to

$$E \approx \tfrac{1}{2}\rho u_o^2\ R r_o l$$

where we have replaced each of the cosine terms by their average over a cycle, $\frac{1}{2}$.

Similarly, from the momentum $p = E/c$, the angular momentum inside the cylinder is

$$L = \frac{1}{2\pi c}\int_o^R \rho u^2 . 2\pi r^2\ l\ dr$$

which evaluates, after substitution, to

$$L \approx \tfrac{1}{8}\rho u_o^2\ R^2 r_o l$$

Angular momentum is conserved in a superfluid, so it follows that eddies must be created and destroyed in pairs (or larger groups), or at the boundary – which contains an image of opposite angular momentum and thus is a natural place for creation and annihilation events. In the absence of annihilation events, the lifetime of an eddy is infinite.

11.4 Comparison with a vortex

We have seen that an eddy and a vortex are both long, linear structures which are created in pairs and have infinite lifetime in the absence of annihilation events. In both cases the flow speed is elevated near the centre. Fluid is physically transported around the centre in the direction of rotation, with average velocity proportional to $1/r$ at large r, and the angular momentum increases as R^2 in both cases.

In an ordinary viscous fluid, viscous losses eventually suppress the oscillatory motion. The surviving features are those of a vortex. In this sense, a vortex can be thought of as a 'classical' approximation to an eddy. The principal difference between the two is that an eddy is well-behaved everywhere, but the $1/r$ behaviour of a vortex cannot apply very near the centre, where there is a singularity.

There is one further correspondence which will be relevant. A vortex has what is called a 'tension' along its length, as if it were a stretched rubber band. The tension can be seen by supposing it is terminated on two surfaces. There is a negative Bernoulli pressure near the centre, where the flow velocity is greater, so the surfaces will be attracted towards one another due to the reduced pressure [1]. An eddy is similar: the pressure is reduced when averaged over a cycle.

11.5 Quantization

An eddy is characterised by an integer m, given by

$$m = \frac{1}{2\pi} \oint \frac{-i}{\xi} \frac{\partial \xi}{\partial \theta} \, d\theta \tag{11.3}$$

This can be seen by direct substitution into (11.2). At its heart, this equation tells us that the phase θ increases by $2m\pi$ on any loop around the centre.

There is another way to write this equation. The following representation is less intuitive, and arguably it is unnecessarily complicated, but it is mathematically equivalent.

We *define* a quantity (which we will call 'momentum') by

$$\mathbf{p} = -i\hbar \frac{\nabla \xi}{\xi} \tag{11.4}$$

With this definition, (11.3) becomes

$$m = \frac{1}{2\pi\hbar} \oint \mathbf{p}.d\mathbf{l} \tag{11.5}$$

as may be verified by direct substitution and choosing a path of constant radius.

An eddy is a completely classical phenomenon, but equations (11.4) and (11.5) are precisely the same as those used in the quantum mechanical theory of superfluid vortices. In that formalism, there is an 'order parameter' δ (for superconductors) or a 'wavefunction' ψ (for superfluid helium). The momentum is defined, axiomatically, by $\mathbf{p}\,\psi = -i\hbar\,\nabla\psi$ (or $\mathbf{p}\,\delta = -i\hbar\,\nabla\delta$ for a superconductor), which is the same as in (11.4) with ψ or δ in place of the complex excess density ξ. The quantization condition for a superfluid vortex is exactly the same as (11.5). Note that the constant $\hbar$ cancels out when the definition of $\mathbf{p}$ is substituted. For further information see a textbook on quantum mechanics such as Alastair Rae's [66], or Brian Josephson's original and very clear treatment of the quantum mechanical phase of a superconductor [60].

It follows that the eddies in a classical compressible fluid obey the same equations of quantization as vortices in a superfluid. The principal difference is that an eddy is well-behaved everywhere but the conventional equations of superfluid motion break down at the centre of a vortex due the high flow speeds. It is usual to explain this difficulty by asserting that the order parameter or wavefunction must vanish near the centre.

It is usually thought that ^{4}Helium at low temperature is a 'Bose-Einstein condensate,' an inherently quantum mechanical state of matter predicted by Satyendra Nath Bose and Albert Einstein in the mid-1920s. However, see Adrian Wyatt's review of the evidence for this, which he says is less clear cut than usually supposed [67]. The principal reason for this belief is vortex quantization. We have seen that the same equations of quantization emerge naturally from the motion of a classical compressible fluid obeying Euler's equation.

11.6 Simple eddy ring

Vortices are easily distorted into rings, such as smoke rings, which can be energetically favourable by reducing their length. Eddies are similar. Figure 11.5 shows a simple eddy ring. The flow pattern erupts from the centre, carrying material with it.

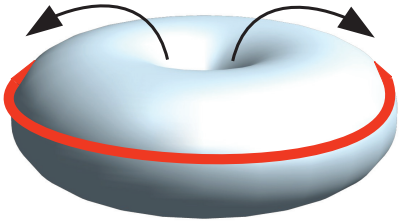

Figure 11.5: *A ring based on the eddy in figure 11.4. The red line is a region of compression; the rarefaction opposite it is not visible as it is inside the ring. This eddy ring will be written* ξ_{10}.

An eddy ring will collapse to microscopic size under the influence of the natural tension along its length discussed in section 11.4. As it collapses, the conservation of energy means the flow speed near the centre will increase until it approaches the speed of sound, c, where there would be a large negative Bernoulli pressure. The collapse halts at this point since it is not sustainable for the total pressure to become negative due to cavitation.

† *Track 2* *This material may be skipped on a first reading*

A vortex ring, such as a smoke ring, does not collapse in this way. A moving vortex experiences a Magnus force, like the lift of an aircraft wing. As the ring moves forward theough the fluid, this lift prevents it from collapsing under the natural tension along the length of the vortex [1].

An eddy is irrotational and so its collapse cannot be opposed by Magnus forces, which require rotational motion.

When describing an ordinary vortex ring in fluid mechanics, it is usual simply to ask the reader to imagine the s axis curved into a ring. The above eddy ring can be described in this way, in which case it is given by the real part of (11.2). We will refer to the spatial factor as χ_{mo} for reasons that will soon become clear.

There is an equivalent description in terms of spherical Bessel functions that is easier to work with. Suppose an eddy ring has radius R_o, so that $ds = R_o d\varphi'$ where φ' is the angle around the ring. The eddy ring is a sum of spherical solutions to the wave equation, given by the real part of

$$\begin{aligned} \xi &= \psi\, \chi_{mo} \\ \psi &= e^{-i\omega_o t} \\ \chi_{mo} &= \int_0^{2\pi} e^{-im\theta'} j_m(k_r\sigma) k_r R_o d\varphi' \end{aligned} \tag{11.6}$$

where j_m is a spherical Bessel function of the first kind.

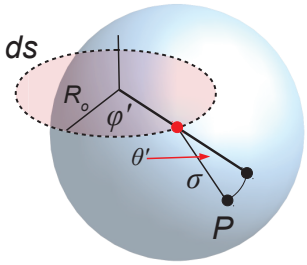

Figure 11.6: *The integral at the point P in* (11.6) *is a sum of spherical solutions to the wave equation, one of which is indicated by the sphere. The centre of each solution (red) follows the path of integration (dotted).*

This integral is illustrated in figure 11.6. Each element of the integrand is a solution to the wave equation, and the integral is a sum of them, so it must be a solution too. By inspection it has the required topology. See [46] for a more detailed mathematical treatment.

By symmetry, these simple eddy rings have no angular momentum and therefore they might not have to be created in pairs.

11.7 Rotons

The precise nature of rotons has remained a mystery. Many physicists assume they are to do with local circulation and vorticity, with Feynman having described them as 'a ghost of a vanishing vortex ring'. There have been other proposals; in 2004 Philippe Nozières described the roton as a 'beautiful theoretical challenge' and proposed that it is the ghost of a Bragg spot [68]. But no-one has so far come up with a concrete model that fits the data.

When writing about the missing low-energy excitations in liquid helium in the original paper on the subject [63, p267], Feynman suggested

> Perhaps, if a more complicated wavefunction were tried, some special linear combination representing a kind of microscopic vortex ring or one with intrinsic angular momentum has in fact a lower energy.

An eddy ring has these properties, and it relies on the compressibility terms Feynman had neglected. The eddy ring drawn above has no net angular momentum, from the symmetry, but we will shortly see there are higher-order rings which do have intrinsic angular momentum.

More generally, eddy rings are oscillatory quasiparticle solutions to Euler's equation for a fluid. We saw in chapter 3 that all expectation values for such solutions are Lorentz covariant with characteristic speed equal to the speed of sound in the medium.

Exercise 11.1 By reproducing the treatment in chapter 3, replacing the wave height h by the density ρ, show that all expectation values for the ring in (11.6) are Lorentz covariant.

Further, being solutions to Euler's equation, eddy rings obey the same equations as in chapter 6, and accordingly they will interfere and diffract like quantum mechanical particles with a modified value of Planck's constant. When coherent effects are not relevant, they obey the same equations of motion as classical relativistic particles, with a characteristic speed equal to the speed of sound rather than light.

Exercise 11.2 By reproducing the treatment in chapter 6, replacing the wave height h by the density ρ, show that an eddy ring obeys the Schrödinger-like equation (6.14) when averaged over a cycle.

11.8 Thermal conductivity

Superfluid helium is observed to have high thermal conductivity, and Feynman supposed that rotons and phonons (ordinary sound waves) together are responsible for the heat transport. Eddy rings will contribute as follows. There is a range of ring sizes for each topology, giving a spectrum of intrinsic energies

E_o for the non-walking solutions. More eddy rings will be created on hotter boundaries, where more energy is available, and they will preferentially be annihilated at cooler boundaries. From the Lorentz symmetry, their walking velocity through the fluid is given by $E = \gamma E_o$ where E is the total energy and γ is the acoustic Lorentz factor.

Exercise 11.3 By expanding the acoustic Lorentz factor γ, show that an eddy ring travels through the fluid at speed

$$v \;=\; c\sqrt{1-\frac{1}{\gamma^2}} \;=\; c\sqrt{\frac{E^2-E_o^2}{E^2}}$$

Suggest why most eddy rings created on the boundary will travel through the fluid at a speed of order the speed of sound.

Harder Taking a simplified model, the number of eddy rings of a given type with energy E is proportional to $e^{-E/KT}$ where K is Boltzmann's constant and T is the temperature. Estimate the distribution of velocities.

The large velocity means the eddy rings will carry energy efficiently from a hotter to a cooler region, making a significant contribution to the thermal conductivity.

11.9 Pressure

Feynman also suggested that the excitations might exert a pressure on the walls of the container and on the surface. The next exercise invites you to calculate this pressure in the case of an eddy ring.

Exercise 11.4 Show that the momentum of an eddy ring is

$$p \;=\; \frac{Ev}{c^2} \;=\; \frac{E}{c}\sqrt{\frac{E^2-E_o^2}{E^2}}$$

Estimate the pressure exerted by a single eddy ring with energy $E = KT \gg E_o$, assuming it is reflected specularly from the walls of a container 1cm across filled with liquid helium at 1K. The speed of sound in liquid helium is about 230m/s.

This pressure is confirmed rather spectacularly in the 'fountain effect': see Alfred Leitner's video online [69]. The apparatus is illustrated schematically in figure 11.7.

In the experiment, a glass tube protrudes into a bath of superfluid helium. It has a plug of jeweller's rouge at the bottom, which has gaps of about one micron through which He II can pass but eddy rings cannot. When the liquid in the tube is heated, the pressure of the eddy rings increases and the level of helium

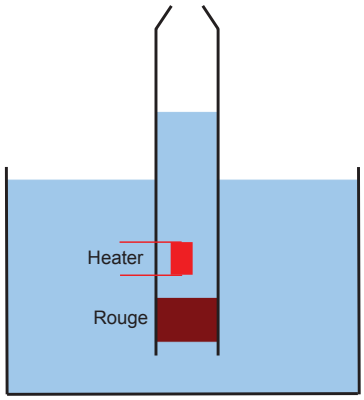

Figure 11.7: *The fountain effect in superfluid helium.*

rises above the surrounding bath. If the pressure is large enough, a fountain of liquid helium sprinkles out of the tube.

Eddy rings are non-linear near the centre, and so they will interact with one another when they approach close enough. As the temperature rises their density in the superfluid helium will increase until their mean free path becomes smaller than the size of the container. They can be modelled as an ideal gas, with the usual pressure and density relationship. Such a gas supports waves of compression, like sound waves. These are observed in 'second sound', which travels at about a tenth of the speed of ordinary pressure waves (first sound). Second sound is observed to transport heat and to reflect off the walls of the container, as we might expect.

11.10 Quantum-like phenomena

We saw single-slit and double-slit diffraction patterns in the bouncing droplet experiments. The excitations in a superfluid obey the same equations and so they should exhibit the same phenomena. We are not aware of systematic attempts to measure diffraction patterns in rotons.

Neither have there been systematic attempts to measure stationary states which are solutions to the Schrödinger-like equation (6.14), but they may have been observed in experiments with a different purpose. Recently Anssi Salmela, Juha Tuoriniemi, and Juho Rysti at Aalto university in Finland measured the resonant frequency of an electronic tuning fork which was coupled to second sound in a container of superfluid helium [70, 71]. They found unexplained variations in the resonant frequency of the tuning fork and in the width of the resonance, shown in figure 11.8. Note the spikes in the width Δf of the resonances. Wider resonances are usually associated with greater dissipation.

We hypothesise that the tuning fork excites eddy rings at its resonant frequency. Solving the Schrödinger-like equation for these species, they will have stationary states whose energies depend on the details of the apparatus. The

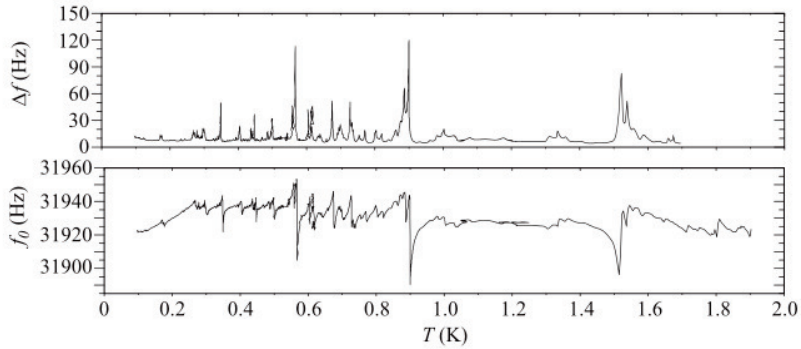

Figure 11.8: *The resonant frequency of an electronic tuning fork coupled to second sound in superfluid helium, as a function of temperature. The symmetry is because the speed of sound was a maximum at about 1.2K. Courtesy Juho Rysti [71]*

spikes in the experimental data correspond to conditions where these stationary states are excited. They drain energy into other modes, like in atomic absorption spectra, thereby increasing the width of the resonance. Further experimental work is indicated in this area.

11.11 Ejection of atoms by eddy rings

If an eddy ring encounters the surface of the liquid, as in figure 11.9(a), the high amplitude wave crests near the centre will crash into the surface, like a storm wave crashing onto a sea wall, and helium atoms may be ejected.

This was observed in 1984, when Adrian Wyatt and colleagues fired high energy rotons towards the surface of liquid helium from below, and found that atoms were ejected from the surface as a gas.

The intrinsic motion of an eddy ring can be in either direction. As illustrated in figure 11.9(b), the helium atoms will be ejected in the opposite horizontal direction if the intrinsic motion is reversed. The effect is indirect and would be expected to be a little weaker. This was observed in 1999. Mark Tucker and Adrian Wyatt created high energy rotons and arranged that they approached the surface at an angle. One type of roton (which they called the R^+ roton) induced atoms of helium to be ejected from the surface in the same horizontal direction as the direction of travel, and the other (the R^- roton) induced atoms to be ejected at an angle [72]. The reverse process was weaker, the helium atoms having a maximum energy about $\frac{3}{4}$ of that seen in the R^+ case.

The researchers suggested that the momentum of the R^- roton was in the opposite direction to its direction of travel. The analysis in chapter 6 suggests the fountain effect would be significantly reduced if half of all rotons had negative momentum. We hypothesise that the atoms were ejected only where the waves are powerful enough to overcome the latent heat of evaporation. To analyse this more completely, we will have to look more more closely at possible structures

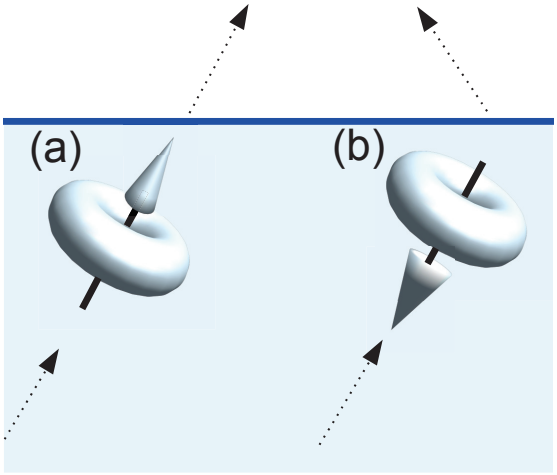

Figure 11.9: *(a) An eddy ring encounters the surface of the liquid. The high amplitude wave crests near the centre crash into the surface and eject helium atoms as a gas. (b) When the intrinsic motion is in the opposite direction, the atoms will be ejected in the opposite horizontal direction, by an indirect and weaker mechanism.*

for the eddy ring.

11.12 Chiral eddy

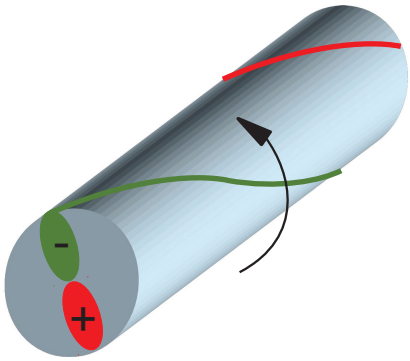

Figure 11.10: *Schematic drawing of a solution to the wave equation which varies along its length. The cross section is the same as in figure 11.4.*

Figure 11.10 is a schematic drawing of an eddy solution to the wave equation which varies along its length (in the s direction). The rotation resolves into motion in the $+s$ direction, away from the reader. The excess density is the real

part of

$$\begin{aligned} \xi &= \psi\,\chi \\ \psi &= e^{-i\omega t} \\ \chi &= A\,e^{i(m\theta+k_s s)}\,J_m(k_r r) \end{aligned} \tag{11.7}$$

Exercise 11.5 By applying a Lorentz transformation in the s direction to the eddy in (11.2), show that (11.7) is a solution to the wave equation when

$$\omega^2 = c^2(k_s^2 + k_r^2)$$

Harder Obtain the same result by direct substitution into the wave equation in cylindrical coordinates.

This eddy has both angular and linear momentum.

11.13 Chiral eddy rings

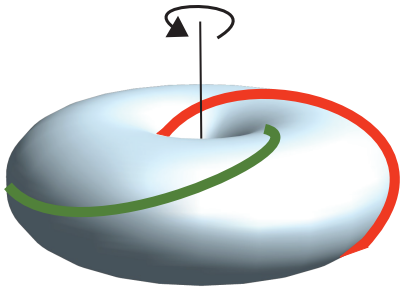

Figure 11.11: *A chiral eddy ring, ξ_{11}. The flow pattern erupting from the centre resolves into rotation around the axis of the ring.*

Figure 11.11 shows the simplest ring based on this eddy, in which there is one complete twist around the torus. Imagine the s axis of 11.10 curved into a ring; then the excess density is given by the real part of (11.7) with

$$\chi_{mn} = A\,e^{i(m\theta+n\phi)}\,J_m(k_r r)$$

where ϕ is the angle around the ring. We can give a fuller description in the coordinates in figure 11.6

$$\chi_{mn} = \int_0^{2\pi} e^{i(m\theta'+n\varphi')} j_m(k_r\sigma)\,k_r R_o d\varphi'$$

which reduces to equation (11.6) when $n = 0$.

This eddy ring has a wave propagating in the ϕ direction (around the axis of the ring). As we saw in section 11.4, such waves carry fluid with them and

thus have angular momentum. It follows that chiral eddy rings have intrinsic angular momentum. Like a classical vortex, the angular momentum of an eddy ring at the centre of a sphere of radius R is proportional to R^2, as shown in the next exercise.

11.14 Conservation rules

The creation and annihilation of chiral eddy rings are subject to a number of conservation rules.

First, angular momentum is conserved in a superfluid. So unlike achiral rings, chiral rings must be created in pairs (or in more complicated events). Their lifetimes are infinite in the absence of annihilation events.

It is usually not possible to create (or annihilate) a pair of eddy rings if they both have the same chirality, since the energy would have to be supplied by a wave or other process, which would not couple effectively to the motion unless it were itself chiral. It follows that chirality is conserved, at least at moderate energies.

One consequence of the conservation of chirality is that eddy rings with the same chirality but angular momentum in opposite directions, such as ξ_{11} and ξ_{-1-1}, shown in figure 11.12(a) and (d), co-exist and are unable to annihilate one another. As we saw in section 10.5 on spin-half symmetry, the degenerate states can be written

$$\xi \;=\; \cos(\alpha)\xi_{11} \;+\; \sin(\alpha)\xi_{-1-1}$$

where α is a real parameter. As α increases continuously by π, the angular momentum rotates through 360° and ξ reverses sign. It follows that chiral eddy rings have spin-half symmetry.

Exercise 11.6 By applying the treatment in section 10.5 onwards, write down the Bloch representation of a chiral eddy ring.

It is conceivable that a chiral eddy ring will be created or destroyed by its image in the boundary, which has the opposite chirality. However, such events appear to be very unlikely. Refer to figure 11.12, which shows the ξ_{11} eddy ring and its reflections in the boundary. It is not possible to create or annihilate the pair (a) and (c), since it is forbidden by the conservation of angular momentum. If the fluid is liquid helium, chiral eddy rings can be destroyed at the surface, where energy is taken out by the emission of helium atoms as in the experiment in figure 11.9.

Similar conservation rules have been observed experimentally in rotons. In 1976, David Allum, Roger Bowley and Peter McClintock showed that ions being drawn through liquid helium at a pressure of 25 bar and a temperature below 0.45K gave rise to the creation of pairs of rotons. There were additional complicated effects from the creation of ordinary vortex rings, and presumably from the creation of achiral rings as well [73]. This confirmed a hypothesis that rotons were created in pairs by Roger Bowley and Fred Sheard.

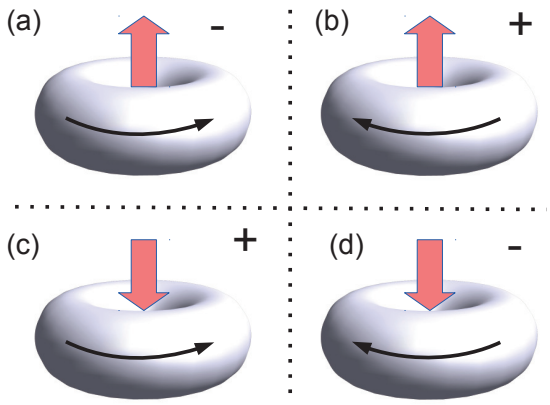

Figure 11.12: *(a) A ξ_{11} eddy ring. The − sign indicates its chirality and the red arrow indicates the flow erupting from the centre. The figure also shows its reflections in the boundary. (b) ξ_{1-1} (c) ξ_{-11} (d) ξ_{-1-1}.*

11.15 Phase transition

As the temperature continues to rise, the density of excitations continues to increase until they dominate and the fluid behaves as a normal fluid above the superfluid transition temperature. The relevant thermodynamics were first described in 1973 by Kosterlitz and Thouless [41]. They considered the simplified case where the excitations are vortices in two dimensions.

Kausterlitz and Thouless idealised a vortex as a core of radius a, with fluid flowing around it at speed $u = C/r$ where r is the radius and C is called the circulation. The kinetic energy density (per unit area) is proportional to $u^2 \propto r^{-2}$, and so if it is at the centre of a cylindrical container of radius R then the total kinetic energy is proportional to $\int u^2.2\pi r dr$, or

$$E = E_o \log\left(\frac{R}{a}\right) \tag{11.8}$$

where the energy E_o depends on the circulation and other details of the system.

The energy in (11.8) grows without limit as the container becomes large. This means that the vortex must be paired with another vortex of opposite circulation, so that their velocity fields are opposed at large distance and the total energy is limited, even in a very large container.

In the Kosterlitz-Thouless transition, this vortex-antivortex pairing is broken by the thermal motion. This occurs above a specific transition temperature, as outlined in the advanced material below.

† *Track 2* *This material may be skipped on a first reading*

Here we assume familiarity with the thermodynamic concept of free energy, which is minimised.

A vortex whose core is of size a could be placed in a container of radius R in of order $W = (R/a)^2$ different positions. Its entropy $S = K \log W$ is given by

$$S = 2K \log\left(\frac{R}{a}\right) \tag{11.9}$$

where K is Boltzmann's constant.

Substituting (11.8) and (11.9) into the free energy $F = E - TS$, where T is the temperature, gives

$$F = (E_o - 2KT)\ \log\left(\frac{R}{a}\right)$$

In thermodynamics, the free energy is minimised. At low temperature, the energy required to create an isolated vortex dominates, and so each vortex must be paired with an antivortex. However, there is a transition at the temperature $T_c = E_o/2K$. Above this temperature the entropy term dominates, irrespective of the size of the container, and unpaired vortices can be created at will. They will dominate the motion and swamp the superfluidity. This is the Kosterlitz-Thouless transition.

This method might be extended to three dimensions. In a full calculation, it would be necessary to take into account the full range of excitations, including vortices, eddies, vortex rings, and the multiple families of achiral and chiral eddy rings. It seems likely that computer simulation would be required for such a complex calculation.

Nevertheless, an upper estimate for the superfluid transition temperature in liquid ^{4}Helium can be obtained by noting that the flow speed in the fluid cannot much exceed the speed of sound, which is about 230 m s^{-1}, since otherwise the total pressure would become negative due to the Bernoulli effect. In the unrealistic case that all the fluid were moving at the speed of sound, the kinetic energy per helium atom would be $\frac{1}{2}Mc^2$ where M is the mass of the atom. Equating this to the thermal energy, KT, gives an upper estimate of the transition temperature of

$$T_c < \frac{Mc^2}{2K} \tag{11.10}$$

which gives an upper estimate of about 14K.

In practice the speed c will be approached only very near the cores of the excitations and the average speed will be smaller than c. The observed transition temperature of 2.17K gives $0.4c$.

11.16 Bose-Einstein gas

There is a second system which is believed to be a Bose-Einstein condensate (BEC): a dilute gas of bosons, typically alkali ions, cooled very close to absolute zero. Such a gas was first produced by Eric Cornell and Carl Wieman at the University of Colorado in 1995. Since then, there has been very rapid development. The system has a very low speed of sound, typically in millimetres per second, and the atoms in it can be photographed using phase-contrast imaging, providing us with a superfluid medium in which acoustic phenomena may be photographed.

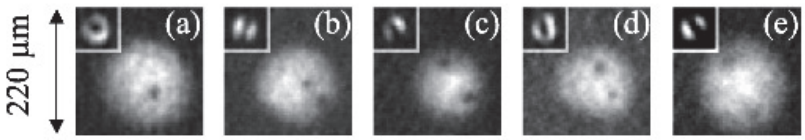

Figure 11.13: *Vortex pairs generated in a Bose-Einstein condensate gas of* ^{87}*Rb (courtesy Eric Cornell).*

In 2000, Wolfgang Ketterle and colleagues observed that a BEC gas sustained superfluid flow and measured a critical velocity for the onset of dissipation, which depends on density [74]. They measured a rate of heating that was less than half of that expected from the conventional theory, but which was consistent with the creation of vortices, according to a model of vortex creation in superfluids by Thomas Frisch, Yves Pomeau and Sergio Rica [75]. In 2001, Eric Cornell and colleagues injected energy into a BEC gas of ^{87}Rb and photographed pairs of vortices that resulted, as can be seen in figure 11.13 [76].

Like superfluid ^{4}Helium, a BEC gas is usually modelled as two fluids, one being a superfluid and the second a normal fluid made up of excitations; see the book by Christopher Pethick and Henrik Smith for a detailed review of the subject [77].

11.17 Summary

We wrote down low-energy excitations in superfluid helium which are solutions to the wave equation in an ordinary classical fluid without viscosity. The linear solutions (eddies) are quantized in the same way as superfluid vortices. When they are curved into eddy rings, they appear to be the rotons which Richard Feynman predicted. These rings obey the Schrödinger-like equation (6.14), which may account for unexplained spikes in resonance widths which have recently been seen experimentally.

Achiral eddy rings can be created on a hot boundary and destroyed on a cold boundary, contributing to the observed high thermal conductivity of superfluid helium. At greater temperatures they form a virtual gas, through which second sound is observed to travel. Second sound transmits heat, and reflects from container walls.

There are also higher-order eddy rings, which are chiral. They are subject to a number of conservation rules, in particular conservation of chirality. They have spin-half symmetry. Similar conservation rules have been observed experimentally. They are also created and annihilated in pairs. Vortex pair creation has been observed in liquid helium and photographed in a Bose-Einstein condensate.

11.18 Dialogue

On day 8 of their dialogue, Alice, Bob and Carol argue for the following propositions

(a) Alice says it has been established that particles were much closer and hotter in the early universe. Extrapolating back in time, she concludes there was a singularity, where the laws of physics might not apply and at which space itself was created.

(b) Bob says it has been established that particle-like excitations in superfluid helium were much closer and hotter just after the superfluid condensed in a refrigerator. Extrapolating back in time, he concludes there was a singularity, where the laws of physics might not apply and at which space itself was created.

(c) Carol says Alice and Bob have made the same mistake. There only seems to be a singularity when you extrapolate from a low temperature region towards a phase transition.

Each of these approaches can be made consistent with all the relevant experiments. Argue in favour of each one in turn.

Bibliography

[1] T. E. Faber. *Fluid dynamics for physicists*. Cambridge University press, Cambridge, UK, 1995.

[2] George Forbes. Hydrodynamic analogies to electricity and magnetism. *Nature*, 24:360–361, 1881.

[3] Daniel Bernoulli. *Danielis Bernoulli... Hydrodynamica, sive De viribus et motibus fluidorum commentarii. Opus academicum ab auctore, dum Petropoli ageret, congestum*. Sumptibus Johannis Reinholdi Dulseckeri, 1738.

[4] F. Dubois, E. Duceau, F. Maréchal, and I. Terrasse. Lorentz transform and staggered finite differences for advective acoustics. *arXiv:1105.1485v1*, 2011.

[5] MV Berry, RG Chambers, MD Large, C Upstill, and JC Walmsley. Wavefront dislocations in the aharonov-bohm effect and its water wave analogue. *European Journal of Physics*, 1(3):154, 1980.

[6] LD Landau. Oscillations in a fermi liquid. *SOVIET PHYSICS JETP-USSR*, 5(1):101–108, 1957.

[7] Y Lee, TM Haard, WP Halperin, and JA Sauls. Discovery of the acoustic faraday effect in superfluid 3he-b. *Nature*, 400(6743):431–433, 1999.

[8] A. Henri, R. McGough, and B. Patten. *The Mersey Sound*. Penguin UK, 2007.

[9] J. Walker. Drops of liquid can be made to float on the liquid. What enables them to do so? *Sci. Am*, 238(6):123–129, 1978.

[10] Y. Couder, S. Protière, E. Fort, and A. Boudaoud. Dynamical phenomena: Walking and orbiting droplets. *Nature*, 437(7056):208–208, 2005.

[11] S. Protière, A. Boudaoud, and Y. Couder. Particle-wave association on a fluid interface. *Journal of Fluid Mechanics*, 554(10):85–108, 2006.

[12] J. Moláček and J. W. M. Bush. Drops bouncing on a vibrating bath. *Submitted to J. Fluid Mech.*, 2013.

[13] T. B. Benjamin and F. Ursell. The stability of the plane free surface of a liquid in vertical periodic motion. *Proc. Roy. Soc. London. A.*, 225(1163):505–515, 1954.

[14] A. Eddi, E. Sultan, J. Moukhtar, E. Fort, M. Rossi, and Y. Couder. Information stored in faraday waves: the origin of a path memory. *Journal of Fluid Mechanics*, 674:433, 2011.

[15] Y. Couder and E. Fort. Single-particle diffraction and interference at a macroscopic scale. *Phy. Rev. Lett.*, 97(15):154101, 2006.

[16] E. Fort, A. Eddi, A. Boudaoud, J. Moukhtar, and Y. Couder. Path-memory induced quantization of classical orbits. *Proceedings of the National Academy of Sciences*, 107(41):17515–17520, 2010.

[17] Y. Couder. television programme. `https://www.youtube.com/watch?v=W9yWv5dqSKk#t=14`, cited January 2014.

[18] J. Moláček and J. W. M. Bush. Drops walking on a vibrating bath: towards a hydrodynamic pilot-wave theory. *Submitted to J. Fluid Mech.*, 2013.

[19] G. F. Fitzgerald. The ether and the Earth's atmosphere. *Science*, 13:390–390, 1889.

[20] A. Einstein. Ether and the theory of relativity. *The Genesis of General Relativity*, pages 1537–1542, 2007 (*originally 1920 – out of copyright and available online – search for the title*).

[21] D. Bohm. A suggested interpretation of the quantum theory in terms of 'hidden' variables. *Physical Review*, 85(2):166, 1952.

[22] E Madelung. Eine anschauliche deutung der gleichung von schrödinger. *Naturwissenschaften*, 14(45):1004–1004, 1926.

[23] Guido Bacciagaluppi and Antony Valentini. *Quantum theory at the crossroads: reconsidering the 1927 Solvay conference*. Cambridge University Press, 2009.

[24] A. Eddi, E. Fort, F. Moisy, and Y. Couder. Unpredictable tunneling of a classical wave-particle association. *Physical review letters*, 102(24):240401, 2009.

[25] S Perrard, M Labousse, M Miskin, E Fort, and Y Couder. Self-organization into quantized eigenstates of a classical wave-driven particle. *Nature Communications*, 5, 2014.

[26] C. A. Bjerknes. *Hydrodynamische Fernkräfte [collected papers on hydrodynamic action at a distance]*. Ostwald's Klassiker der exacten Wissenschaften, nr.195, 1915.

[27] J. C. Maxwell. On physical lines of force. *Philosophical Magazine*, 21, 23(4), 1861.

[28] HA Lorentz. The theory of electrons and the propagation of light. *Nobel Lectures: Physics 1901–1921*, 1902.

[29] A. A. Michelson and Morley E. The relative motion of the earth and the luminiferous ether. *American Journal of Science*, 34(201):333–345, 1887 (*out of copyright and available online: search for the title*).

[30] H. Lorentz. The relative motion of the earth and the aether. en.wikisource.org/wiki/Translation:The_Relative_Motion_of_the_Earth_and_the_Aether, 1892. English translation, accessed February 2014.

[31] A. Einstein. On the electrodynamics of moving bodies. *Annalen der Physik*, 17(891):50, 1905 (*out of copyright; English translation available online – search for the title*).

[32] C. Barceló, S. Liberati, and M. Visser. Analogue gravity. *Living Reviews in Relativity*, 14(3), 2011.

[33] W. G. Unruh. Experimental black-hole evaporation? *Physical Review Letters*, 46(21):1351–1353, 1981.

[34] O. Lahav, A. Itah, A. Blumkin, C. Gordon, S. Rinott, A. Zayats, and J. Steinhauer. Realization of a sonic black hole analog in a Bose-Einstein condensate. *Physical review letters*, 105(24):240401, 2010.

[35] G. E. Volovik. *The Universe in a Helium Droplet*. Clarendon Press, Oxford, 2003.

[36] J. S. Bell. On the Einstein-Podolsky-Rosen paradox. *Physics*, 1(3):195–200, 1964.

[37] M Sierpiński. Sur une courbe dont tout point est un point de ramification. *Compte Rendus hebdomadaires de l'Académie des Science de Paris*, 160:302–305, 1915.

[38] Benoit B Mandelbrot. How long is the coast of britain. *Science*, 156(3775):636–638, 1967.

[39] RM Brady and RC Ball. Fractal growth of copper electrodeposits. *Nature*, 309:225–229, 1984.

[40] D. Howard and L. (ed.) Miller. 'Nicht sen kann was nicht sein darf': or The prehistory of EPR: 1909-1935, in Sixty two years of uncertainty: historical, philosophical, & physical inquiries into the foundations of quantum mechanics. *NATO ASI series B*, 226:61 – 111, 1990 (*online*: http://www3.nd.edu/∼dhoward1/Sixty-Two Years of Uncertainty.pdf).

[41] J. M. Kosterlitz and D. J. Thouless. Ordering, metastability and phase transitions in two-dimensional systems. *Journal of Physics C: Solid State Physics*, 6(7):1181, 1973.

[42] A. Einstein, B. Podolsky, and N. Rosen. Can quantum-mechanical description of physical reality be considered complete? *Physical review*, 47(10):777, 1935 (*out of copyright and available online: search for the title*).

[43] J. G. Cramer. The transactional interpretation of quantum mechanics. *Reviews of Modern Physics*, 58(3):647, 1986.

[44] H. Everett. *The Everett interpretation of quantum mechanics: Collected works 1955-1980 with commentary*. Princeton University Press, 2012.

[45] J. S. Bell. *Speakable and Unspeakable in Quantum Mechanics: Collected papers on quantum philosophy*. Cambridge University Press, 2004.

[46] R. M. Brady. The irrotational motion of a compressible inviscid fluid. *ArXiv 1301.7540*, 2013.

[47] R. M. Brady and R. J. Anderson. Violation of bell's inequality in fluid mechanics. *arXiv:1305.6822*, 2013.

[48] D. K. Ferry and L. B Kish. Noise and bell's inequality. *Fluctuation and Noise Letters*, 9(04):423–426, 2010.

[49] D. K. Ferry. Probing bell's inequality with classical systems. *Fluctuation and Noise Letters*, 9(04):395–402, 2010.

[50] W. A Hofer. Elements of physics for the 21st century. *arXiv preprint arXiv:1311.5470*, 2013.

[51] J. Christian. Disproof of bell's theorem by clifford algebra valued local variables. *arXiv preprint quant-ph/0703179*, 2007.

[52] John F Clauser, Michael A Horne, Abner Shimony, and Richard A Holt. Proposed experiment to test local hidden-variable theories. *Physical Review Letters*, 23:880–884, 1969.

[53] A. Aspect, J. Dalibard, and G. Roger. Experimental test of Bell's inequalities using time-varying analyzers. *Physical review letters*, 49(25):1804–1807, 1982.

[54] M Redhead. Incompleteness, non-locality and realism, clarendon press, 1987.

[55] T. Birch. The history of The Royal Society of London for improving of natural knowledge, in which the most considerable of those papers communicated to the Society, which have hitherto not been published, are inserted in their proper order, as a supplement to the Philosophical Transactions. *Phil. Trans. Roy. Soc.*, 2:19, 21, 23–24, 1756 (reprint 1968, London: Johnson).

[56] M. Bennett, M. F. Schatz, H. Rockwood, and K. Wiesenfeld. Huygens's clocks. *Proc. Roy. Soc. A*, 458:563–579, 2002.

[57] DJ Korteweg. Les horloges sympathiques de huygens. *Archives Néérlandaises, Série II, tome XI*, pages 273–295, 1906.

[58] J. A. Acebrón, L. L. Bonilla, C. J. P. Vicente, F. Ritort, and R. Spigler. The kuramoto model: A simple paradigm for synchronization phenomena. *Reviews of Modern Physics*, 77(1):137, 2005.

[59] M. Ida. Alternative interpretation of the sign reversal of secondary bjerknes force acting between two pulsating gas bubbles. *Physical Review E*, 67(5):056617, 2003.

[60] B. D. Josephson. *The relativistic shift in the Mössbauer effect and coupled superconductors. Fellowship dissertation thesis*. Trinity College, Cambridge http://dspace.cam.ac.uk/handle/1810/243916, 1962.

[61] S. Putterman. *Superfluid Hydrodynamics*. American Elsevier Pub. Co, 1974.

[62] V. Leroy, J. C. Bacri, T. Hocquet, and M. Devaud. Simulating a one-half spin with two coupled pendula: the free larmor precession. *European journal of Physics*, 27(6):1363, 2006.

[63] R. P. Feynman. Atomic theory of the two-fluid model of liquid helium. *Physical Review*, 94(2):262, 1954.

[64] R. P. Feynman. Atomic theory of liquid helium near absolute zero. *Physical Review*, 91(6):1301, 1953.

[65] R. P. Feynman. Atomic theory of the λ transition in helium. *Physical Review*, 91(6):1291, 1953.

[66] A. I. M. Rae. *Quantum mechanics, fifth edition*. Taylor and Francis, 2008.

[67] A. F. G. Wyatt. Evidence for a Bose–Einstein condensate in liquid ^{4}He from quantum evaporation. *Nature*, 391(6662):56–59, 1998.

[68] P. Nozières. Is the roton in ^{4}He the ghost of a Bragg spot? *Journal of Low Temperature Physics*, 137:45–67, 2004.

[69] A. Leitner. The fountain effect. `https://www.youtube.com/watch?v=YVMuI_shltE`, 1963. Accessed September 2013.

[70] A Salmela, J Tuoriniemi, and J Rysti. Acoustic resonances in helium fluids excited by quartz tuning forks. *Journal of Low Temperature Physics*, 162(5-6):678–685, 2011.

[71] J. Rysti. Microscopic and macroscopic studies of liquid and solid helium mixtures. *PhD dissertation*, 2013.

[72] M. A. H. Tucker and A. F. G. Wyatt. Direct evidence for R^- rotons having antiparallel momentum and velocity. *Science*, 283:1150–1152, 1999.

[73] D. R. Allum, R. M. Bowley, and P. V. E McClintock. Evidence for roton pair creation in superfluid ^{4}He. *Physical Review Letters*, 36(22), 1976.

[74] R. Onofrio, C. Raman, J. M. Vogels, J. R. Abo-Shaeer, A. P. Chikkatur, and W. Ketterle. Observation of superfluid flow in a Bose-Einstein condensed gas. *Physical Review Letters 85, 11*, 2000.

[75] T. Frisch, Y. Pomeau, and S. Rica. Transition to dissipation in a model of superflow. *Physical Review Letters*, 69(11):1644–8, 1992.

[76] B.P Anderson, P.C. Haljan, C.A. Regal, D.L. Feder, L. A. Collins, C. W. Clark, and E. A. Cornell. Watching dark solitons decay into vortex rings in a bose-einstein condensate. *Physical Review Letters 86, 14*, 2001.

[77] C. J. Pethick and H. Smith. *Bose-Einstein condensation in dilute gases*. Cambridge University Press, 2008.